Accommodating a High Penetration of Plug-in Electric Vehicles in Distribution Networks

by

Mostafa Shaaban

A thesis
presented to the University of Waterloo
in fulfillment of the
thesis requirement for the degree of
Doctor of Philosophy
in
Electrical and Computer Engineering

Waterloo, Ontario, Canada, 2014

AUTHOR'S DECLARATION

I hereby declare that I am the sole author of this thesis. This is a true copy of the thesis, including any required final revisions, as accepted by my examiners.

I understand that my thesis may be made electronically available to the public.

Abstract

The last few decades have seen growing concern about climate change caused by global warming, and it now seems that the very future of humanity depends on saving the environment. With recognition of CO_2 emissions as the primary cause of global warming, their reduction has become critically important. An effective method of achieving this goal is to focus on the sectors that represent the greatest contribution to these emissions: electricity generation and transportation. For these reasons, the goal of the work presented in this thesis was to address the challenges associated with the accommodation of a high penetration of plug-in electric vehicles (PEVs) in combination with renewable energy sources.

Every utility must consider how to manage the challenges created by PEVs. The current structure of distribution systems is capable of accommodating low PEV penetration; however, high penetration (20 % to 60 %) is expected over the next decades due to the accelerated growth in both the PEV market and emission reduction plans. The energy consumed by such a high penetration of PEVs is expected to add considerable loading on distribution networks, with consequences such as thermal overloading, higher losses, and equipment degradation. A further consideration is that renewable energy resources, which are neither exhaustible nor polluting, currently offer the only clean-energy option and should thus be utilized in place of conventional sources in order to supply the additional transportation-related demand. Otherwise, PEV technology would merely transfer emissions from the transportation sector to the electricity generation sector.

As a means of facilitating the accommodation of high PEV penetration, this thesis proposes methodologies focused on two main themes: uncontrolled and coordinated charging. For uncontrolled charging, which represents current grid conditions, the proposal is to utilize dispatchable and renewable distributed generation (DG) units to address the high PEV penetration in a way that would not be counterproductive. This objective is achieved through three main steps. First, the benefits of allocating renewable DG in distribution systems are investigated, with different methodologies developed for their evaluation. The benefits are defined as the deferral of system upgrade investments, the reduction in the energy losses, and the reliability improvement. The research also includes a proposal for applying the developed methodologies for an assessment of the benefits of renewable DG in a planning approach for the optimal allocation of the DG units. The second step involves the development of a novel probabilistic energy consumption model for uncontrolled PEV

charging, which includes consideration of the drivers' behaviors and ambient temperature effect associated with vehicle usage. The final step integrates the approaches and models developed in the previous two steps, where a long-term dynamic planning approach is developed for the optimal allocation of renewable and dispatchable DG units in order to accommodate the rising penetration of PEV uncontrolled charging. The proposed planning approach is multi-objective and includes consideration of system emissions and costs.

The second theme addressed in this thesis is coordinated PEV charging, which is dependent on the ongoing development of a smart grid communication infrastructure, in which vehicle-grid communication is feasible via appropriate communication pathways. This part of the work led to the development of a proposed coordinated charging architecture that can efficiently improve the performance of the real-time coordinating PEV charging in the smart grid. The architecture is comprised of two novel units: a prediction unit and an optimization unit. The prediction unit provides an accurate forecast of future PEV power demand, and the optimization unit generates optimal coordinated charging/discharging decisions that maximize service reliability, minimize operating costs, and satisfy system constraints.

Acknowledgements

All praise is due to Allah almighty, who is the source of all knowledge in this world and whose countless bounties have enabled me to complete this thesis successfully.

I would not have been able to finish my dissertation without the guidance of my committee members, help from friends, and support from my wife and family.

I gratefully acknowledge the data and the analysis provided by the Toronto Parking Authority and the London offices of the UK Department for Transport

I would like to express my deepest gratitude to my advisor, Professor E. El-Saadany, for his guidance, care, and patience and for providing me with such a wonderful atmosphere for conducting research. In addition to my advisor, I also wish to thank the rest of my thesis committee for their encouragement and insightful comments: Professor Osama A. Mohammed, Professor K. Bhattacharya, Professor R. El Shatshat, and Professor S. Lambert.

My sincere thanks go to Dr. Mohamed Sadek for his great support during my PhD journey. Special thanks also go for Dr. Yasser Attwa for guiding my research and helping me to develop my background.

I also offer my gratitude to my father and my mother. My research would not have been possible without their help, their constant support and encouragement, and their never-failing good wishes.

Finally, I would like to thank my wife Sarah, my son Omar, and my daughter Maryam for always standing by me through both the good times and the bad.

Dedication

To my beloved father, Farouk ,

To my dear mother, Nabila,

To my beloved wife and life partner, Sarah,

To my dearest son Omar, and sweet daughter Maryam,

in recognition of your endless love, support, and encouragement.

Table of Contents

List of Figures

List of Tables

Nomenclature

Acronyms

A/C	Air conditioner
ADN	Active distribution network
AER	All-electric range
ARMA	Autoregressive moving average
BCD	Battery charge depletion
BCS	Battery charge sustaining
CDF	Cost of damage function
CMS	Cost minimization stage
CVC	Central vehicle controller
DEMS	Delivered energy maximization stage
DG	Distributed generation
DM	Decision maker
EV	Electric vehicle
EENS	Expected energy not served
FCFS	First come first served
FFICE	Fossil-fuel internal combustion engine
FOR	Forced outage rate
GA	Genetic algorithm
GHG	Greenhouse gas
HEVs	Hybrid electric vehicles
HT	Heater
IP	Internet protocol
LDC	Local distribution company
LDF	Light duty fleet
MCS	Monte Carlo simulation
NDSGA	Non-dominated sorting GA
NGDG	Natural gas dispatchable DG
NPV	Net present value

pdf	Probability density function
PEV	Plug-in electric vehicle
PHEV	Plug-in hybrid electric vehicle
PLC	Power line carrier
PVDG	Photo-voltaic based DG
RTS	Reliability test system
SOC	State-of-charge
SRTCS	Smart real-time coordination system
SRTCS-C	Smart real-time coordination system with charging only
SRTCS-C/D	Smart real-time coordination system with charging/ discharging
SUVs	Sports utility vehicle
UNCR	Uncoordinated
V2G	Vehicle-to-grid
V2V	Vehicle-to-vehicle
VID	Vehicle identity
WDG	Wind based DG units

Constants

$N_{day(m)}$	Number of days in a month m
$z_{1(q)}$	Vector of length N_q consisting of zeroes except for the q^{th} element, which is 1
$z_{2(m)}$	Vector of length 12 consisting of zeroes except for the m^{th} element, which is 1
$z_{3(d)}$	Vector of length 7 consisting of zeroes except for the d^{th} element, which is 1
$z_{4(h)}$	Vector of length 24 consisting of zeroes except for the h^{th} element, which is 1

Functions

$[(\cdot)]_{\mathrm{IB}}$	Iverson bracket
$CDF_{6(q)}^{-1}$	Inverse of the cumulative density function, which describes the probability of a trip of purpose q to be less than a specific distance
$f_{(\cdot)}^{CH}$	Function of the battery charging characteristics
$f_{(\cdot)}^{DCH}$	Function of the battery discharging characteristics
$f_w(v)$	Weibull pdf

$OF_{(\sigma)}(\cdot)$	Objective function σ required to be optimized
Γ	Gamma function operator

Indices

a	Index of aggregators
$b_{(r)}, t, u$	Indices of time segments
$ch_{(\cdot)}$	Index of chargers in parking lot $(\cdot)$
d	Index of days
g	Index of scenarios
h	Index of hours
i, j	Indices of load points
m	Index of months
r	Index of request events
s	Index of system states
s_c	Index of commercial load states
s_{ev}	Index of PEV load states
s_g	Index of NGDG states
s_i	Index of industrial load states
s_l	Index of normal load states
s_{pv}	Index of PVDG states
s_r	Index of residential load states
s_w	Index of WDG states
y	Index of years

Parameters

$AER_{(vh)}$	AER for vehicle vh, mi
$B_{(r)}$	Number of time segments in the prediction interval
c	Scale parameter of a Weibull pdf, m/sec
C_{kWh}^{AVG}	Average cost of energy, $/kWh
c_d	Peak demand charges, $/kW
c^{ENG}	Price signal representing the cost of energy, $/kWh

$C_{kWh(y)}$	Vector representing the hourly energy price for the 8760 hours for year y, \$/kWh
d	Discount rate
d'	Effective discount rate
$D_{mi/kWh}^{AVG}$	Average distance travelled per kWh, mi/kWh
e	Inflation rate
$E_{BAT}(ch)$	Battery capacity of a vehicle connected to charger ch, kWh
$E_{kWh(y)}^{PEV}$	Annual energy consumption for a 100 % PEV penetration, kWh
h_1	Meteorological mast height, m
h_2	Turbine hub height, m
$H_{(p_{(i,a)})}^{MAX}$	Capacity of parking lot $p_{(i,a)}$ under the jurisdiction of aggregator $a \in \mathcal{A}$
H_{total}	Total number of the PEVs served over the period under study
k	Shape parameter of Weibull pdf
$\mathrm{K}_{CO2/mi}$	Equivalent CO_2 emissions from the conventional vehicles, kg/mi
K_{CO2}^{Grid}	Carbon footprint for the energy purchased from the grid, kg/kWh
K_{CO2}^{NGDG}	Equivalent CO_2 emissions from the NGDG, kg/kWh
$M_{trip(q)}^{Annual}$	Annual number of trips for purpose q
M_{trip}^{AVG}	Average annual trips per vehicle
$M_{trip/day(q,m,d)}^{AVG}$	Mean value of the number of daily trips per vehicle
$M_{trip(q,m,d)}^{day}$	Total number of purpose q trips in month m and day d
$M_{trip(q,m,d,h)}^{hour}$	Total number of purpose q trips in month m, day d, and hour h
$M_{trip(q,m)}^{month}$	Total number of purpose q trips in month m
M_{NGDG}^{Limit}	Maximum number of NGDG units installed in the system
M_{PVDG}^{Limit}	Maximum number of PVDG units installed in the system
M_{WDG}^{Limit}	Maximum number of WDG units installed in the system
N_{AG}	Number of aggregators in the system
N_l	Number of system lines
N_{MCS}	Number of scenarios generated by MCS
N_s	Number of system states
N_{sg}	Number of the NGDG output states

N_{sl}	Number of the load states
N_{sw}	Number of the WDG output states
$N_{(m,d)}^{trip/vh}(tr)$	Number of vehicles with daily trips tr in month m and day d
N_{vh}	Total number of vehicles
N_y	Planning period in years
$OWS_{(t)}$	Observed wind speed at hour t, m/sec
$\mathbb{p}_{(\cdot)}$	Probability of occurrence of state $(\cdot)$
$\mathbb{p}_{(t,\cdot)}$	Probability of occurrence state $(\cdot)$ in time segment t
$P_{Load(i,t)}^{Actual}$	Actual load power at time t for load point i, pu
P_{CONT}^{AC}	Power consumed by A/C during continuous operation, kW
P_{ST}^{AC}	Power consumed by A/C during starting, kW
$P_{Load(i)}^{AVG}$	Average demand power of load point i, pu
$P_{rating(vh)}^{Charger}$	Charger continuous rating connected to vehicle vh, kW
P_{CH}	Charger transferred power limit to/from the battery, kW
$P_{DG(i,b_{(r)})}$	DG generated active power at bus i and time instant $t_{(b_{(r)})}$, pu
$\mathbb{p}_{trip(q,d)}^{day}$	Probability of a trip of purpose q to be in day d
$pf_{L(i)}$	Power factor of the normal load on bus $i \in \mathcal{I}$
pf_{NGDG}	Power factor of the NGDG
pf_{PVDG}	Power factor of the PVDG
pf_{WDG}	Power factor of the WDG
$\mathbb{p}_{trip(q,h)}^{hour}$	Probability of a trip of purpose q *to* be in hour h
P_{CONT}^{HT}	Power consumed by the HT during continuous operation, kW
P_{ST}^{HT}	Power consumed by the HT during starting, kW
$P_{DG(i)}^{limit}$	Maximum limit of the connected DG capacity at bus i
$P_{NL(i,s,y)}$	Original normal load at bus i in year y corresponding to state s, pu
$P_{IL(s)}^{NORM}$	Fraction of the peak demand corresponding to state s for the industrial loads
$P_{CL(s)}^{NORM}$	Fraction of the peak demand corresponding to state s for the commercial loads
$\mathbb{p}_{trip(q,m)}^{month}$	Probability of a trip of purpose q to be in month m

$P_{NGDG(s)}^{NORM}$	Generated active power corresponding to state s as a fraction of the NGDG capacity
$P_{PEV(s)}^{NORM}$	Fraction of the peak PEV demand corresponding to state s
$P_{PVDG(s)}^{NORM}$	Generated active power corresponding to state s as a fraction of the PVDG capacity
$P_{RL(s)}^{NORM}$	Fraction of the peak active power demand corresponding to state s for residential load
$P_{WG(s)}^{NORM}$	Generated active power corresponding to state s as a fraction of the WDG capacity
$P_{NL(i,y)}^{Peak}$	Peak active power demand for normal loads on bus i in year y, pu
$P_{PEV(i,y)}^{Peak}$	Peak active power demand for PEVs at 100 % penetration, pu
$P_{PEV0(i)}^{Peak}$	Peak demand on bus i at the beginning of the planning period for the PEV charging load, pu
$P_{NL0(i)}^{Peak}$	Peak active power demand on bus i at the beginning of the planning period for the normal loads, pu
P_{WT}^{rated}	Rated power of a wind turbine
P_{MAX}^{Rev}	Allowable limit of the reverse power flow at the substation, pu
P_{NGDG}^{Step}	Discretized step of the NGDG capacity, pu
P_{PVDG}^{Step}	Discretized step of the PVDG capacity
P_{WDG}^{Step}	Discretized step of the WDG capacity, pu
$\mathbb{P}_{(m,d)}^{trip/vh}(tr)$	Probability of having daily trips tr per vehicle in month m and day d
$P_{WT}(v)$	Output power of the wind turbine corresponding to wind speed v, pu
$Q_{DG(i,b_{(r)})}$	DG generated reactive power at bus i and time instant $t_{(b_{(r)})}$, pu
RF	Risk factor, h
rn	Random number between zero and one
S_{base}	Base power for the per unit system, kW
$SOC_{(ch,b_{(r)})}^{Initial}$	Initial SOC for the PEV connected to charger ch at $t_{(b_{(r)})}$, %
SOC^{MIN}	Minimum SOC level for the predicted PEV arrivals, %
$SOC_{(ch,r)}^{Target}$	Target SOC, %

$t_{prk(p_{(i,a)},w)}^{AVG}$	Mean parking time, min
tr	Number of the daily trips per vehicle
v_1	Measured wind speed at meteorological mast height, m/sec
v_2	Wind speed at the hub height, m/sec
$v_{mile/h(q)}^{AVG}$	Average vehicle speed for purpose q, mi/h
v_{in}	Cut-in speed of the wind turbine, m/sec
v_{out}	Cut-out speed of the wind turbine, m/sec
v_{rated}	Rated speed of the wind turbine, m/sec
Y	Magnitude of the Y-bus matrix admittance, pu
z_0	Roughness factor, m
α_{AR}	AR model parameter
$\beta_{PEV(y)}^{MIN}$	Allowable minimum PEV penetration in year y
$\beta_{PEV(y)}^{MAX}$	Allowable maximum PEV penetration in year y
Δt	Time step, min
ϵ	Prediction error probability
η_A	Efficiency of the accessory load
η_{BT}	Efficiency of the battery
η_{CH}	Efficiency of the charger
η_M	Efficiency of the motor
η_{PE}	Efficiency of the onboard power electronics
θ	Angle of the Y-bus matrix admittance, rad
$\theta_{MA(u)}$	MA model parameter
Θ_{AC}	Average threshold for the A/C operation, ^{o}C
Θ_{HT}	Average threshold for the HT operation, ^{o}C
Θ_{max}	Maximum temperature limit for the battery usage in BCD mode, ^{o}C
Θ_{min}	Minimum temperature limits for the battery usage in BCD mode, ^{o}C
$\lambda_{(p_{(i,a)},w)}$	Arrival rate of a Poisson process, vehicle/min
$\mu_{V(p_{(i,a)},w,b_{(r)})}$	Mean number of vehicles for a Poisson process
$\sigma_{trip/vh}$	Standard deviation of daily trips per vehicle
$\tau_{(vh)}$	Average tractive effort required per mile by vehicle vh, kWh/mi

Sets

$\mathcal{A}$	Set of aggregators
$\mathcal{CH}_{(i,p_{(i,a)})}$	Set of chargers in parking lot p on bus i under the jurisdiction of aggregator a
$\mathcal{CH}^{ON}$	Set of active chargers
$\mathcal{CV}_{(t)}$	Set of vehicles required to be charged at hour t
$\mathcal{D}_{(r)}$	Set of periods in prediction interval
$\mathcal{FS}$	Set of feasible solution vectors
$\mathcal{I}$	Set of system load buses
$\mathcal{I}_{(a)}^{AGG}$	Set of buses under jurisdiction of aggregator a
$\mathcal{I}_{(a)}^{AGG}$	Set of system buses under the jurisdiction of aggregator a
$\mathcal{I}_{CL}$	Set of commercial load buses
$\mathcal{I}_{IL}$	Set of industrial load buses
$\mathcal{I}_{NGDG}$	Set of candidate buses for NGDG
$\mathcal{I}_{PEV}$	Set of PEV load buses
$\mathcal{I}_{PVDG}$	Set of candidate buses for PVDG units
$\mathcal{I}_{RL}$	Set of residential load buses
$\mathcal{I}_{WDG}$	Set of candidate buses for WDG
$\mathcal{L}$	Set of system lines
$\mathcal{O}$	Set of objectives required to be minimized
$\mathcal{OS}$	Set of optimal solution vectors
$\mathcal{PL}_{(i,a)}$	Set of parking lots on bus i under the jurisdiction of aggregator a
$\mathcal{Q}$	Set of trip purposes
$\mathcal{RN}$	Set of uniformly distributed random number between 0 and 1
$\mathcal{RQ}$	Set for the CVC information request events
$\mathcal{S}_{CL}$	Set of load power states for commercial customers
$\mathcal{S}_{eff(l)}$	Set of all considered system states that contribute to the upgrade of line l
$\mathcal{S}_{EV}$	Set of PEV consumption power states
$\mathcal{S}_{IL}$	Set of load power states for industrial customers
$\mathcal{S}_{L}$	Set of load power states

$\mathcal{S}_{NGDG}$	Set of states for the NGDG units
$\mathcal{S}_{PVDG}$	Set of states for the PVDG units
$\mathcal{S}_{RL}$	Set of load power states for the residential customers
$\mathcal{S}_{sys}$	Set of states for the NGDG units
$\mathcal{S}_{WDG}$	Set of wind based DG output power states
$\mathcal{T}$	Set of time intervals that covers the 24 hours of the day
$\mathcal{Z}_{(i)}$	Set of interruption events for load i

Variables

$a_{NGDG(i)}$	Integer variables indicating the installed NGDG size as a multiple of a fixed step
$a_{PVDG(i)}$	Integer variables indicating the installed PVDG size as a multiple of a fixed step
$a_{WDG(i)}$	Integer variables indicating the installed WDG size as a multiple of a fixed step
$\mathcal{b}_{NGDG(i)}$	Binary variables indicating the decision of installing NGDG units at bus i
$\mathcal{b}_{PVDG(i)}$	Binary variables indicating the decision of installing PVDG on bus i
$\mathcal{b}_{WDG(i)}$	Binary variables indicating the decision of installing WDG units at bus i
$bt_{(vh,t)}$	Battery available charge for vehicle vh at the end of hour t, kWh
$BT_{(t,g)}^{SOC}$	Vector representing the SOC of the batteries of an LDF of PEVs at the end of each hour t for scenario g, %
$C_{loss(y)}^{Annual}$	Cost of annual energy losses for year y, \$
$CDF\left(t_{OUT(z)}\right)$	Outage cost corresponding to interruption event z with outage duration $t_{OUT(z)}$, \$
$C_L\left(\tau_{sys(r)}^{PRD}\right)$	Cost of losses during period $\tau_{sys(r)}^{PRD}$, \$
$C_{OUT(y,i)}$	Outage cost of the load point i in year y, \$
$C_P\left(\tau_{sys(r)}^{PRD}\right)$	Peak demand charges during period $\tau_{sys(r)}^{PRD}$, \$
$C_{UP(l)}$	Cost of the reinforcement for line l, \$
$D_{(q,m,d,h,g)}^{mile}$	Distance of finished trip for purpose q in month m and day d at hour h for scenario g, mi
$DS_{(\sigma)}(\Omega^*)$	Dissatisfaction associated with any operating point Ω^* on the Pareto frontier
$E_{AC(vh,t,g)}$	Energy consumed by the A/C during the trip finished by vehicle vh in scenario g at the end of hour t, kWh

$EC_{(g)}$	Vector representing the consumed power during each hour by an LDF of PEVs for scenario g, kW
$ec_{(t,g)}$	Average consumed power by an LDF of PEVs during hour t in scenario g, kW
$E^{Cons}_{1(vh,t,g)}$	Total tractive energy required to overcome the vehicle inertia, the road resistance, and the aerodynamics drag for the trip finished by vehicle vh in scenario g at the end of hour t, kWh
$E^{Cons}_{2(vh,t,g)}$	Energy required to maintain the cabin temperature comfortable for the vehicle driver and the passengers during the trip finished by vehicle vh in scenario g at the end of hour t, kWh
$E^{Cons}_{total(vh,t,g)}$	The consumed energy for each finished trip by vehicle vh in scenario g at the end of hour t, kWh
$E_D(ch, b_{(r)})$	The delivered energy during $t_{(b_{(r)})}$ to $t_{(b_{(r)}+1)}$, for a PEV connected to charger ch, kWh
$E_{D(vh)}$	Delivered energy for PEV vh, kWh
E^{DG}_{CO2}	Equivalent CO2 emissions due to the DG units, kg
E^{Grid}_{CO2}	Equivalent CO2 emissions due to the energy purchased from the grid, kg
$E_{HT(vh,t,g)}$	Energy consumed by the HT during the trip finished by vehicle vh in scenario g at the end of hour t, kWh
E^{PEV}_{CO2}	Equivalent CO2 emissions reduction due to the PEVs, kg
$E_{R(vh)}$	Required energy for PEV vh, kWh
$H_{(p)}\left(t_{(b_{(r)})}\right)$	Number of existing PEVs in parking lot p at time instant $t_{(b_{(r)})}$
$\widetilde{H}_{1(p)}\left(t_{(b_{(r)})}\right)$	Number of PEVs in parking lot p that will stay till the end of the periods in $\mathcal{D}_{(r)}$
$\widetilde{H}_{2(p)}\left(t_{(b_{(r)})}\right)$	Predicted number of the new PEV arrivals by the end of period $D_{(b_{(r)})}$ In parking lot p
$I_{(l,b_{(r)})}$	Current through line l at time instant $t_{(b_{(r)})}$, pu
NPV_{INT}	NPV of the cost of interruptions, \$
NPV_{Loss}	NPV of the cost of energy losses, \$
$P^{Annual}_{loss(y)}$	Vector of the system power loss for year y, pu
$P_{G(i,b_{(r)})}$	Active generated power at bus i and time instant $t_{(b_{(r)})}$, pu

$P_{G(i,s,y)}$	Active generated power at bus i corresponding to state s and year y, pu
$P_{L(i,b_{(r)})}$	Active power demand at bus i and time instant $t_{(b_{(r)})}$, pu
$P_{L(i,s,y)}$	Active power demand at bus i corresponding to state s and year y, pu
$P_{Loss(b_{(r)})}$	Total power loss of the system at time instant $t_{(b_{(r)})}$, pu
$P_{loss(s)}$	Total power loss in the system corresponding to state s, pu
$P_{loss(s,y)}$	Total power loss in the system corresponding to state s and year y, pu
$\tilde{P}_{max}(\tau_{sys(r)}^{PRD})$	Target peak grid power value during period $\tau_{sys(r)}^{PRD}$, pu
$P_{max}(\tau_{sys(r)}^{PRD})$	Maximum incurred total load power during $\tau_{sys(r)}^{PRD}$, pu
$P_{NGDG(i,y)}$	Capacity of connected NGDG on bus i in year y, pu
$P_{0(i)}^{NGDG}$	Capacity of the installed NGDG units on bus i, pu
$P_{NL(i,b_{(r)})}$	Active power consumed by the normal load at bus i and time instant $t_{(b_{(r)})}$, pu
$P_{L(i,b_{(r)})}^{PEV}$	Active power consumed by the PEV charging load at bus i and time instant $t_{(b_{(r)})}$, pu
$P_{L(i,s,y)}^{PEV}$	PEV load at bus i in year y corresponding to state s, pu
$P_{PVDG(i,y)}$	Capacity of the connected PVDG units on bus i in year y, pu
$P_{0(i)}^{PVDG}$	Capacity of the installed PVDG units on bus i, pu
$\mathbb{P}_{T(p,b_{(r)})}$	Probability that a PEV arriving at the parking lot p during $(t_{(r)}, t_{(b_{(r)})}]$ is still present at time $t_{(b_{(r)})}$
$P_{WDG(i,y)}$	Capacity of the connected WDG units on bus i in year y, pu
$P_{0(i)}^{WDG}$	Capacity of the installed WDG units on bus i, pu
$Q_{G(i,b_{(r)})}$	Reactive generated power at bus i and time instant $t_{(b_{(r)})}$, pu
$Q_{G(i,s,y)}$	Reactive generated power at bus i corresponding to state s and year y, pu
$Q_{L(i,b_{(r)})}$	Reactive power demand at bus i and time instant $t_{(b_{(r)})}$, pu
$Q_{L(i,s,y)}$	Reactive power demand at bus i corresponding to state s and year y, pu
$SOC_{(ch,b_{(r)})}^{Final}$	Reached SOC at time instant $t_{(b_{(r)}+1)}$, %
$t_{CH(vh,t,g)}$	Required charging time to fully charge the battery of vehicle vh at time t in scenario g, h

$t_{prk(p,w)}$	Residence duration of the PEVs in parking lot p and time interval $T_{(w)}$, min
$\mathrm{t}_{trip(vh,t,g)}$	Duration of the trip finished by vehicle vh in scenario g at the end of hour t, min
$V_{(i,b_{(r)})}$	Magnitude of the voltage at bus i and time instant $t_{(b_{(r)})}$, pu
$V_{(i,s,y)}$	Magnitude of the voltage at bus i corresponding to state s and year y, pu
$v_{(u)}$	Sample speed for u^{th} time segment, m/sec
$\mathbb{X}$	Charging decision as a percentage of the allowable charging power
$Y_{(i,j,y)}$	Magnitude of the Y-bus matrix admittance, pu
$Y_{(i)}^{NGDG}$	Year of placing the NGDG units on bus i
$Y_{(i)}^{PVDG}$	Year of placing the PVDG units on bus i
$Y_{UP(l)}$	Year in which upgrade of line l is required
$Y_{(i)}^{WDG}$	Year of placing the WDG units on bus i
$\beta_{PEV(y)}^{PEN}$	Optimal PEV penetration in year y
$\delta_{(i,b_{(r)})}$	Angle of the voltage at bus i and time instant $t_{(b_{(r)})}$, rad
$\delta_{(i,s,y)}$	Angle of the voltage at bus i corresponding to state s and year y, rad
$\theta_{(i,j,y)}$	Angle of the Y-bus matrix admittance, rad
$\tau_{(a,r)}^{PRD}$	Prediction interval of the aggregator a, min
$\tau_{sys(r)}^{PRD}$	Unified prediction interval for the aggregators, min
Ω^{*}	Solution vectors on the Pareto frontier
$\Omega_{(\sigma)}^{*MAX}$	Optimal solution vector corresponding to the maximum value for objective σ
$\Omega_{(\sigma)}^{*MIN}$	Optimal solution vector corresponding to the minimum value for objective σ

Chapter 1
Introduction and Objectives

Over the last few decades, a growing body of evidence has shown that global temperatures are rising due to the accumulation of greenhouse gases (GHG), which will result in severe climate changes and rises in sea levels. Such predictions have made the reduction of gas emissions a vital necessity, and governments around the globe are taking action to minimize their emissions. More than 140 countries have reacted to global warming, and in 1997 they agreed on the implementation of the Kyoto protocol for reducing emissions [1]. Canada's Kyoto target was a 6 % total reduction of 1990 GHG emission levels by 2012. Despite the measures implemented, by 2011 Canada's GHG had actually increased by 18.8 % compared to 1990 levels [2], as shown in Figure 1.1. In 2010, Canada therefore submitted a revised emissions reduction target under the Copenhagen Accord: a reduction 17 % compared to 2005 emission levels.

A key component in the reduction of CO_2 emissions is to shift to low- or zero-emission vehicles for transportation because the transportation sector is responsible for the largest share of Canadian GHG: almost 24 %, as shown in Figure 1.2. To this end, the electrification of vehicles has become the best option for reducing transportation emissions, given that the electric power system is best positioned to provide the requisite infrastructure for these vehicles.

Concerns about emissions coupled with developments in plug-in electric vehicle (PEV) technology have led to the expectation that PEV penetration[1] will rise rapidly over the next few decades. Some countries have created a target of up to 7.9 million of PEVs by 2030, as reported by the International Energy Agency [3]. The targets of a selection of countries are listed in Table 1.1.

However, insufficient research is available to enable verification of the impact on distribution networks. Even with low PEV penetration (5 % to 10 %), the PEV charging process has been shown to create potential risk to the electric power system [4, 5], due mainly to the expectation that PEVs will likely be clustered in specific geographical areas, resulting in higher penetrations (40 % to 60 %) in some territories. Such concentrations can lead to significant stress on local power distribution systems. If not managed effectively, the additional load imposed by high PEV penetration is expected to have severe consequences, such as feeders' thermal limit violation, phase imbalance, transformer

[1] PEV penetration is defined as the percentage of the total population of vehicles in the system represented by the PEVs.

degradation, and fuse blowouts [4]. The accommodation of high PEV penetration in distribution networks thus requires further study and analysis.

With high PEV penetration, two main scenarios are expected: uncontrolled charging and controlled charging. An uncontrolled charging scenario, which represents the current practice for charging PEVs, includes no communication between the grid and the vehicles, and the vehicles start charging as soon as they are plugged in. Managing the uncontrolled charging scenario requires the development of uncontrolled PEV charging load models that can facilitate appropriate planning in the distribution system infrastructure so that the excess load can be accommodated. An additional factor is the expectation that renewable energy resources will play an important role in supplying energy to the transportation sector because delivering the required energy from conventional generation units will have the effect of shifting the emissions to the electric energy sector rather than reducing them. Renewable resources are characterized by highly variable and uncertain output power that is dependent on wind speed and solar irradiance, and distribution networks were not originally designed to accommodate such energy sources. Planning for PEV accommodation must therefore include consideration of these renewable distributed generation (DG) units.

The uncontrolled charging is the current practice for PEV charging and is expected to persist in the near future to enable a transition period for the PEV penetration to be significant, hence it paves the way for the coordinated charging, which is the second expected scenario. For this scenario, a coordinated charging system should be developed under the smart grid paradigm. This system must be able to deal with real-time measurements and parking lot dynamics through the utilization of the two-way smart grid communication infrastructure. The primary target of such a coordinated charging system is the best use of smart grid resources so that the PEV load can be shifted to optimal periods during the PEV parking duration in order to maximize customer satisfaction without jeopardizing system equipment.

The research presented in this thesis was focused primarily on these two scenarios. The work presented can thus be described as consisting of two phases: with the first addresses uncoordinated charging and the second deals with coordinated charging. These two phases are described in detail in the next section.

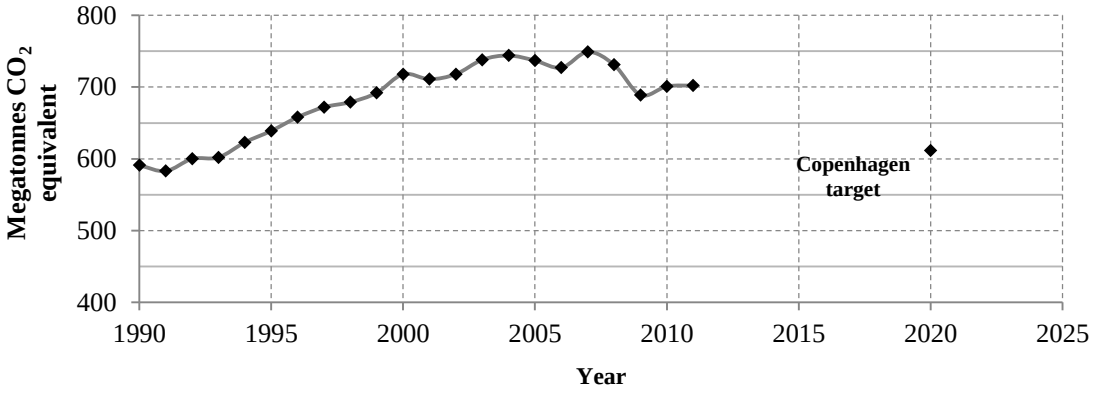

Figure 1.1 National greenhouse gas emissions, Canada, 1990 to 2011 [2]

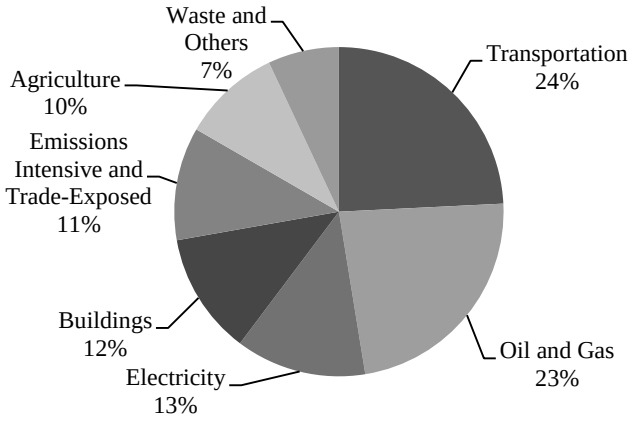

Figure 1.2 Canada's emissions breakdown by sector for 2011 [2]

Table 1.1 Announced national PEV targets

Country	Target [3]
Canada	2018: 500 000
Denmark	2020: 200 000
France	2020: 2 000 000
Ireland	2020: 230 000
Spain	2020: 2 500 000
Sweden	2020: 600 000
United Kingdom	2030: 7 900 000
United States	2015: 1 000 000

1.1 Research Objectives

As mentioned in the previous section, high PEV penetration can be managed through two scenarios: uncontrolled charging and coordinated charging. In the first scenario, the excess load due to uncontrolled PEV charging can be managed through the installation of DG units and/or the upgrading of the network infrastructure [5]. On the other hand, the coordinated charging scenario relies on the two-way communication infrastructure inherent in a smart grid paradigm as a means of optimally coordinating PEV charging requirements [6]. The research was therefore based on five main objectives related to these two scenarios, as shown in Figure 1.3 and outlined below.

1.1.1 Uncontrolled PEV charging scenario

To accommodate a high penetration of uncontrolled PEV charging, which entails the vehicles starting to charge as soon as they are plugged in, the utility can upgrade its distribution system infrastructure and/or deploy DG units to supply the extra load [5]. For this scenario, the research resulted in the development of a proposed long-term multi-objective planning approach to accommodate the rising penetration of uncontrolled PEV charging. The completion of this task was guided by the definition of three objectives, as shown in Figure 1.3.

1.1.1.1 Objective (1): DG allocation in distribution networks

For this objective, the task was to develop methodologies for evaluating the economic benefits of dispatchable and renewable DG, which are defined as the deferral of system upgrade investments, the reduction in the cost of energy losses, and the reduction in the cost of interruptions. The developed methodologies were also used for evaluating the benefits of renewable DG in a planning approach for the optimal allocation of these units. A number of scenarios were considered with respect to two types of DG units: natural gas dispatchable DG (NGDG) units and wind-based DG (WDG) units.

1.1.1.2 Objective (2): Modeling of uncontrolled PEV charging load

For the second objective, the research was focused on the development of a probabilistic energy consumption model for uncontrolled PEV charging. It was assumed that the batteries of the vehicles start charging as soon as they are plugged into the charger. The proposed model includes consideration of the uncertainty and variability associated with vehicle usage as well as ambient temperature effect.

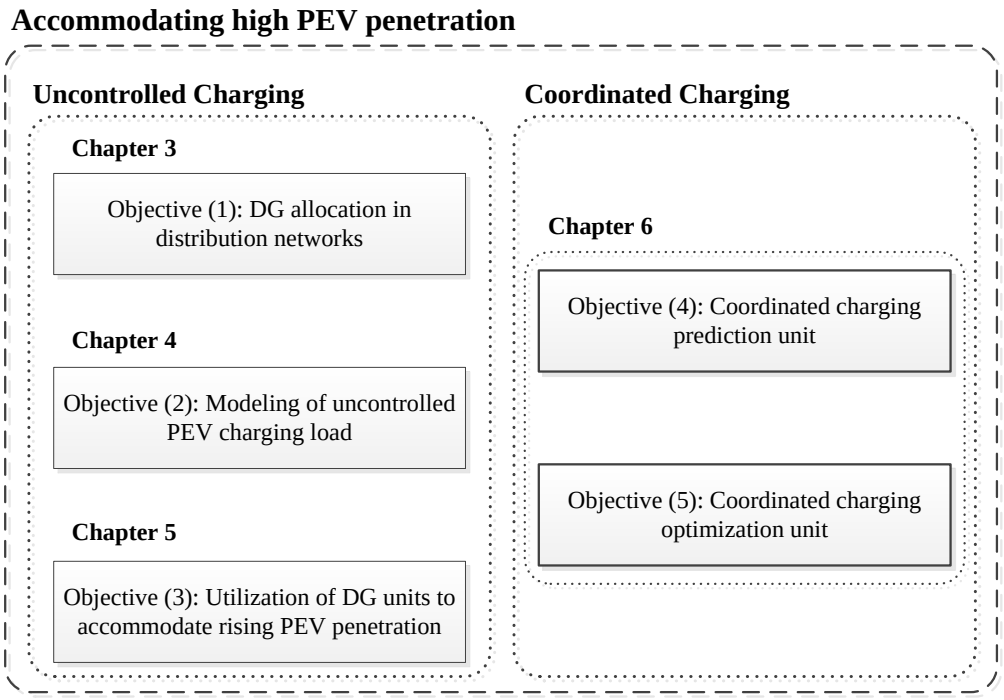

Figure 1.3 Research objectives

1.1.1.3 Objective (3): Utilization of DG units to accommodate high PEV penetration

For this objective, the models and methodologies developed as a result of the previous two objectives were utilized. The aim was to develop a long-term dynamic planning approach to accommodate rising PEV penetration through the utilization of renewable and dispatchable DG units to mitigate the impact of PEVs in the distribution networks. Higher penetration limits would thus be permitted under the uncontrolled charging scenario. In addition to the economic benefits in objective (1), the work also incorporated an equivalency factor for CO_2 emission. In addition to facilitating the use of DG units to reduce system costs the proposed methodology can thus enable the accommodation of high PEV penetration and the reduction of emissions through a multi-objective planning approach.

1.1.2 Coordinated PEV charging scenario

The proposed coordinated charging architecture consists of three main units: data collection and storage, prediction, and optimization [7]. The data collection and storage unit collects information related to current PEV charging demands, the current state-of-charge (SOC) of the PEV batteries, and the demand for normal loads. The prediction unit estimates the normal and PEV charging load for a short time horizon, and the optimization unit computes the optimal charging decision. The research

resulted in the development of two novel proposed prediction and optimization units for managing the dynamics of coordinated PEV charging in real-time, as indicated in Figure 1.3 and described below.

1.1.2.1 Objective (4): Coordinated charging prediction unit

Meeting this objective entailed the development of the PEV prediction unit, which estimates the number of PEVs that will be simultaneously present in the parking lots under the jurisdiction of a specific aggregator. This unit must include consideration of the dynamics of PEV arrivals and departures in the parking lots, and the unit is incorporated into the PEV coordination architecture as a means of enhancing the PEV coordination mechanism.

1.1.2.2 Objective (5): Coordinated charging optimization unit

This objective is related to the development of an optimization methodology for determining the optimal coordination of PEV charging in a distribution network. The proposed solution relies on the ongoing development of the smart grid communication infrastructure, which can efficiently mitigate the impact of uncontrolled PEV charging through smart coordination. The outcome of meeting this objective will be an improved smart grid performance under high PEV penetration.

1.2 Thesis outline

The remainder of the thesis is organized as shown in Figure 1.3. The details of each chapter are as follows:

Chapter 2 provides a brief review of the background topics and associated literature pertinent to this research.

Chapter 3 presents the proposed approach for renewable DG allocation along with related simulation results.

Chapter 4 explains the proposed uncontrolled PEV charging load model.

Chapter 5 introduces the proposed long-term multi-objective planning approach for the accommodation of rising penetration of uncontrolled PEV charging in distribution networks.

Chapter 6 describes the proposed architecture for the coordinated charging mechanism.

Chapter 7 summarizes the research and its contributions and offers suggestions for future work.

Chapter 2
Background and literature review

2.1 Introduction

This chapter provides an introduction to and background information about DG modeling and electric vehicles (EVs), followed by a discussion of previous research. Finally, the drawbacks with respect to DG allocation, uncontrolled PEV charging load modeling, and coordinated PEV charging are highlighted in the summary.

2.2 DG modeling

The IEEE definition of DG is "*the generation of electricity by facilities that are sufficiently smaller than central generating plants as to allow interconnection at nearly any point in a power system*." DG units can be categorized according to the interface, output power, and energy source. The classification based on energy source is illustrated in Figure 2.1. With respect to output power, they can be classified as dispatchable or non-dispatchable resources. The next two subsections discuss common techniques described in the literature for modeling dispatchable and non-dispatchable DG systems.

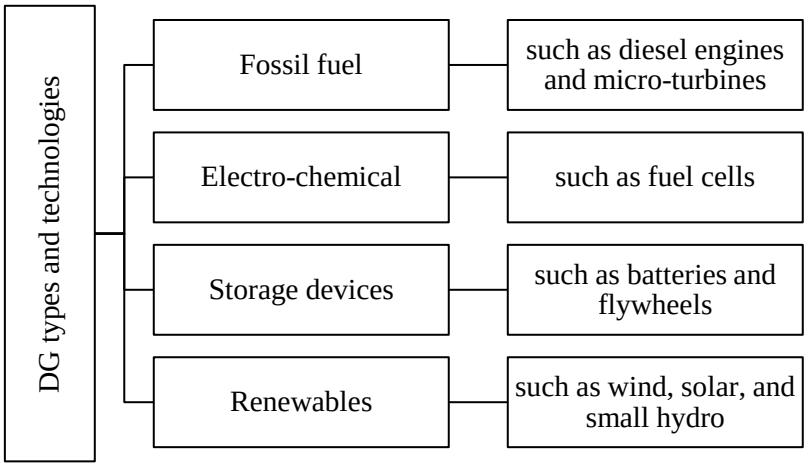

Figure 2.1 DG classification based on energy source [8]

2.2.1 Modeling of dispatchable DG

Dispatchable DG units can be divided into two groups: synchronous machine based, such as biomass and NGDG, and inverter based, such as fuel cells and micro turbines. The output of these DG units is assumed to be constant in normal operating mode. However, during islanding mode, the output is assumed to be varied in order to manage the active and reactive power balance. For studies that require analysis of a snapshot of the system, these types of DG are usually treated as a constant power source, as in [9-11]. For long-term planning studies, the DG model must take into account internal failures or scheduled maintenance, so a two-state model is used to represent the operation of these DG units [12], as shown in Figure 2.2. The up state indicates that the DG unit is in an operating state and the down state implies that the element is inoperable due to a failure or a scheduled off period. This type of model can be used in a Monte Carlo simulation (MCS) to produce artificial operating scenarios for each dispatchable DG unit.

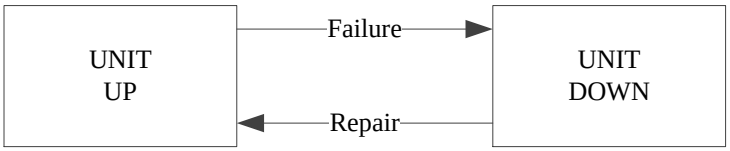

Figure 2.2 Two-state model [12]

2.2.2 Modeling of non-dispatchable renewable DG

Because renewable resources are characterized by a high degree of uncertainty and variability, no unique model exists for them. Different models are therefore used to describe the output of these types of DG units: probabilistic analytical models that use an appropriate probability density function (pdf), probabilistic chronological models that employ an MCS, and time-series models. Although only models of WDG units are described in this chapter, the same concepts can be applied for photovoltaic-based DG (PVDG).

Time-series models are generally used for short-term studies involving periods of a few hours or a few days ahead, such as unit commitment and storage scheduling. On the other hand, probabilistic analytical and chronological models are suitable for long-term studies representing a few years to a few decades. Time-series modelling, probabilistic modelling, and MCS modelling are explained in the following subsections with respect to wind speed, followed by a description of the output power characteristics of WDG units.

2.2.2.1 Time-series modeling

A time series is a set of time-ordered observations of a phenomenon at uniform time intervals. Time-series models are used to predict data points before they are measured based on known past observations. Because time-series models reflect the fact that observations close together in time are more closely related than observations further apart, these models are suitable for the analysis of short periods ranging from a few hours to few days. The autoregressive moving-average (ARMA) technique is one of the most popular for wind-speed time-series modeling. As reported in [13-16], it has been used for modeling wind turbine output power for the purposes of adequacy assessment, storage analysis, and the unit commitment problem. A typical ARMA model for wind speed is described in [17].

2.2.2.2 Analytical probabilistic modelling using an appropriate pdf

A Weibull pdf $f_w(v)$ is the pdf most commonly used to represent wind variability [18]. Its formula [19], which describes the probability of the wind speed v, is given in (2.1). In [18, 20, 21], it is used to model wind speed variability for the purposes of site matching, capacity factor estimation, energy loss calculations, and the assessment of supply adequacy.

$$f_w(v) = \frac{k}{c}\left(\frac{v}{c}\right)^{k-1} exp\left(-\left(\frac{v}{c}\right)^{k}\right) \tag{2.1}$$

This formula is dependent on two parameters for the fitting of the distribution function to the measured wind speed values. The parameters are calculated using the mean wind speed $\bar{v}$ and the standard deviation σ [19], as in the following equations:

$$k = \left(\frac{\sigma}{\bar{v}}\right)^{-1.086} \tag{2.2}$$

$$c = \frac{\bar{v}}{\Gamma(1+\frac{1}{k})} \tag{2.3}$$

$$\bar{v} = \frac{\sum_{u=1}^{N} v_{(u)}}{N} \tag{2.4}$$

$$\sigma = \sqrt{\frac{\sum_{u=1}^{N}(\bar{v} - v_{(u)})^2}{N-1}} \tag{2.5}$$

where

k is the shape parameter;

c is the scale parameter;

$v_{(u)}$ is the sample speed for the u^{th} time segment;

Γ is a gamma function operator.

Reference [18] describes a typical analytical probabilistic wind speed model, in which historical wind speed data are utilized for modeling the output power of the WDG units. The entire year is first divided into clusters (seasons or months). Historical data for each cluster are then used for generating the frequency distribution of the wind speed measurements for a typical day, as a representation of each cluster. The day corresponding to each cluster is further subdivided into time segments, usually hourly. From these data, the mean and standard deviation for each time segment are calculated and used in order to generate the Weibull pdf for each hour, based on (2.2) to (2.5). The entire range of wind speeds is then discretized into a definite number of states. The final step is to convert these wind speed states into output power, as explained in subsection 2.2.2.4.

2.2.2.3 Chronological probabilistic modelling using MCS

MCS is a computerized mathematical technique that allows the building of virtual models of possible scenarios involving phenomena that entail significant uncertainty. The use of MCS is reported in [21-23] for the modeling of the random output of renewable resources, load variation, and the availability of system components. A typical MCS wind model is described in [21]: the period under study is divided into time segments (usually hourly), and the system state is then examined in each segment to enable the evaluation of the reliability indices. To generate the MCS model for wind speeds, virtual simulated scenarios of wind speeds are first generated using the inverse of the Weibull cumulative distribution function [24] for each time segment, as defined in (2.6), where an appropriate stopping criterion is adopted to insure accuracy of the simulation. The wind speeds in the model are then converted into output power based on the wind turbine power-speed characteristics, as explained in the next subsection. In the final step, the forced outage rate (FOR) of the WDG is utilized in order to generate an artificial two-state availability model, which is convolved with the previously generated virtual scenarios.

$$v_{(t,g)} = c(-\ln(1 - rn_{(g)}))^{\frac{1}{k}} \qquad \forall rn \in \mathcal{RN} \tag{2.6}$$

where $\mathcal{RN}$ is the set of uniformly distributed random numbers between 0 and 1.

2.2.2.4 Wind turbine output power states

The wind speed outcomes from any of the three previously mentioned models are converted to output power using the wind turbine characteristics [18], as in (2.7). These characteristics are also illustrated in Figure 2.3.

$$P_{WT}(v) = \begin{cases} 0 & \forall\ 0 \le v < v_{in} \\ P_{WT}^{rated} . \left(\dfrac{v - v_{in}}{v_{rated} - v_{in}} \right) & \forall\ v_{in} \le v < v_{rated} \\ P_{WT}^{rated} & \forall\ v_{rated} \le v < v_{out} \\ 0 & \forall\ v_{out} \le v \end{cases} \tag{2.7}$$

where

$P_{WT}(v)$ is the wind turbine output corresponding to wind speed v;

$v_{in}, v_{rated},$ and v_{out} are the cut-in, rated, and cut-out speeds of the utilized wind turbine, respectively;

P_{WT}^{rated} is the rated power of the wind turbine.

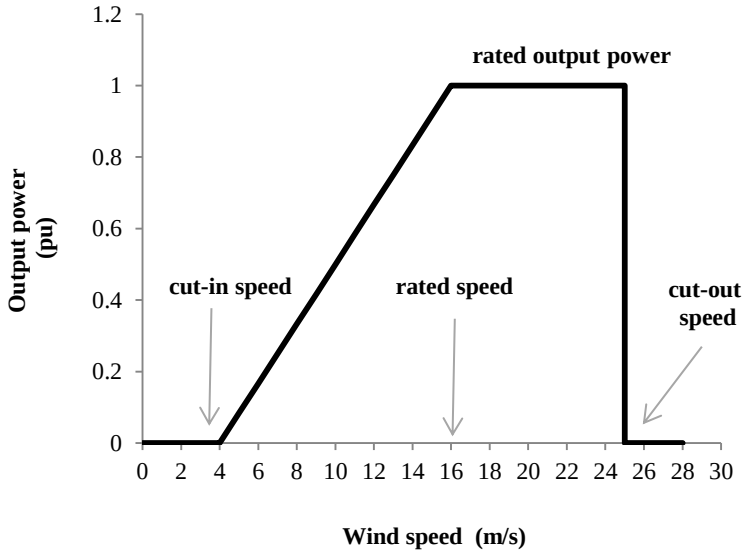

Figure 2.3 WDG output power [18]

2.3 Optimal allocation of DG

Given the challenges currently associated with electricity generation and the recent restructuring of energy systems, renewable DG has become a vitally important option. As mentioned, renewable energy resources are the key to a sustainable energy supply infrastructure because they are neither exhaustible nor polluting [18]. Both the local distribution company (LDC) and its customers can derive numerous technical and economic benefits from the installation of DG units [25-29]:

- Deferral of upgrade investments
- Reduced energy losses
- Reduced emissions
- Improved voltage profile
- Enhanced reliability
- Improved power quality
- Increased energy security

However, installing renewable DG units in the distribution system has a significant impact, given that the system was originally designed to be passive, i.e., to have a single supply structure. When DG units are incorporated, a distribution system ceases to be passive and becomes designated as an active distribution network (ADN). Improper allocation of DG units in the system might have detrimental effects, including violation of voltage technical limits, overloading of system equipment, increase in system power losses, and/or failure of the protective equipment. The proper allocation of DG units into an existing distribution system is thus a very important aspect of DG operational planning. As well, the intermittent nature of renewable DG units such as wind and PV also introduces additional technical and economic challenges to the planning problem.

Many researchers have addressed the problem of DG allocation in ADNs, yet previously proposed solutions have focused primarily on three main benefits.

The first benefit is the relief of congestion in network feeders and the deferral of previously required system upgrades. With respect to system upgrades for addressing load growth and security issues, DG can provide a superior planning alternative for utilities, which can be the most valuable contribution [30] of DG installation. In [10], a multi-year multi-period optimal power flow is suggested for the optimal allocation of DG units in ADNs in order to minimize system upgrades, taking into consideration the effect of distribution network operators' regulations for DG ownership, whereby each year in the planning period is divided into four loading periods: peak, normal, medium,

and minimum. However, that study considered only non-intermittent DG, which offers a firm supply of energy and failed to account for the effect of DG on protective equipment. In [31, 32], different methodologies are presented for evaluating the effect of DG with respect to reinforcing the deferral of investments; however, the researchers considered only dispatchable DG units that have predefined sizes and locations. A multi-objective approach to DG allocation based on a genetic algorithm (GA) is presented in [33]: grid upgrades and the cost of losses are considered as objectives; however, only dispatchable DG with fixed output power is considered. The work described in [9] is based on a long-term dynamic multi-objective DG allocation methodology, whereby emissions and a variety of system costs, such as purchased energy and reinforcement costs, are minimized, but the effect of DG on energy losses or reliability is not taken into account. The studies presented in [9, 10, 31-33] included consideration of dispatchable DG units only.

Some research, however, has included consideration of renewable DG, such as in [34], in which the system peak load and the capacity credit of WDG units are utilized in the planning problem. A multi-objective GA-based approach is introduced in [35] as a means of minimizing losses and upgrade costs, taking into consideration emissions constraints. However, the work presented in both of these studies ignores the stochastic nature of WDG units. The variability and uncertainty associated with renewable DG is an important factor that has a significant effect on system upgrade investments and that has not been fully considered in any of the research mentioned above.

The second benefit of installing DG units in the distribution network is the reduction in energy losses. Some researchers have proposed the optimal placement of DG units as a technique for minimizing power losses in the system. The DG allocation algorithm presented in [36] was developed with the goal of improving the voltage profile and reducing power losses on radial feeders in the case of a non-uniformly distributed load; however, the algorithm includes consideration of only dispatchable DG units with fixed output power. In [37] an approach is presented for determining the optimal allocation of dispatchable DG with the goal of minimizing power loss; however, load variability is not taken into account. A method of minimizing system power loss by establishing the optimal size and power factor for four types of dispatchable DG units is proposed in [38]. While all four units are dispatchable, they differ with respect to their ability to inject active or reactive power. In [39], the researchers describe a multi-objective approach based on a GA, in which a variety of objectives are introduced: improved voltage profile, reduced power loss, increased spinning reserve, and reduced power flow in critical lines. Again, only dispatchable DG units are considered. In [40], the authors present a heuristic approach to optimal investment in DG units so that distribution

companies can meet their load growth. The objective in this case is to minimize DG capital and operating costs, the cost of purchasing power, and the cost of system losses. The report discusses only fixed output power DG and ignores the effect of DG on system upgrades, which can have a major impact. As a means of minimizing power loss, a new optimization approach for DG allocation based on an artificial bee colony algorithm is presented in [41]; however, the suggested solution fails to include the effect of load variability. In [42], the authors introduce a multi-objective technique for optimal DG allocation that factors in system losses and voltage profile; however, consideration of load variability is once more omitted. The work presented in [36-42] is based only on conventional DG units with dispatchable output power.

In [11], time-varying loads and DG power are factored into the determination of the optimal DG allocation on a radial feeder. Consideration of WDG units is included, but the modeling of the wind turbines is based on only a single day's worth of historical data for variable output power: the effects of the variability and uncertainty of wind speeds are thus neglected. The uncertainty associated with renewable DG units is addressed in the work presented in [18]. The authors propose an approach for minimizing energy losses through the optimal placement of renewable DG, taking into consideration both the variability and uncertainty associated with renewable DG resources. However, the focus is on reducing energy losses regardless of the time at which the loss occurred, rather than on the cost of the energy losses, which would provide a better representation of utility requirements. In [43], the researchers compared the calculation of optimal DG penetration using different technologies by examining how changing the penetration level affects annual energy losses. However, the locations of the DG units are assumed to be fixed, and the capacities of the DG units are all varied linearly together until the optimum sizes are reached, which does not guarantee optimal penetration because different penetration levels at system buses for the installed DG units may result in better outcomes with respect to the sizing problem. In [44], the effect of renewable DG unit allocation on the minimization of energy losses is demonstrated through a technique based on a multi-period AC optimal power flow, taking into consideration smart control schemes. A multi-objective approach is presented in [45] for the optimal allocation of variable and controllable DG units in the system with the goal of minimizing different objectives, including line losses and CO_2 emissions. A multi-objective approach to allocating WDG based on a GA is proposed in [46]; the objectives considered are the maximization of energy exports, the minimization of losses, and the minimization of short-circuit levels. However, all of these studies focus on reducing either the power loss or the annual energy losses, neither of which provides an accurate representation of LDC requirements because the

most important factor is the cost of the annual energy losses. As well, in addition to energy losses, another key aspect that should be included in the planning problem is the effect of DG on system upgrades because it can have greater significance than system losses.

The third benefit is the enhancement of the reliability of the power supply for different customers. DG power can affect system reliability only if islanding is allowed. While current policies prohibit the connection of DG units to the system in the case of islanding, in the next few years, given the government-supported trend toward smarter grids, it is expected that DG units will be allowed to operate in islanding mode. DG units will thus be able to supply customers during main supply failures. Most of the previously mentioned studies do not include investigation of the impact of DG units on system reliability. However, some research has been conducted in this area, as in [47], for example, which presents a multi-objective approach based on a GA for optimal DG allocation. The method developed includes consideration of the benefits of DG connection, such as those related to upgrades, losses, and reliability. An algorithm for determining an optimum DG operating strategy is described in [48]; it incorporates the evaluation of the reliability value of a distribution system, in order to minimize the cost of customer interruption. However, the authors of both of these studies based their work on an assumption of conventional dispatchable DG. In contrast, in [49], a method for determining the optimal placement of renewable DG units for maximum system improvement is proposed; however, considering reliability as a single objective in the allocation problem may result in a negative impact on other system costs, such as upgrades and losses.

2.4 Background information about EVs

Due to increased emission rates over the last few decades, which are a major factor in global warming, interest in zero- or low-emission vehicles has increased substantially, and such vehicles are now considered essential [50]. Therefore, a key element in future propulsion strategies for many vehicle manufacturers around the world is the replacement of gasoline with alternative clean energy source. Due to the recent development of renewable energy sources and the almost universal availability of electric power systems, the electrification of vehicles is now considered an effective solution that will reduce fuel consumption and emissions as well as increase energy security through the diversification of available energy sources [51]. The electric energy generated from low-emission renewable resources will play a vital role in supplying the transportation sector with the electric energy required and will also address concerns about shifting emissions from the transportation sector to the electricity generation sector.

The history of EVs began a hundred years ago in the early 1900s, when more electric than fossil-fuel vehicles were on the roads, and EVs outsold their gasoline counterparts [52]. However, due to the limitations of battery technology and the lack of power electronics technologies, the speed and range of EVs were limited. Gasoline engines offered superior performance, which led to the decline of the EV industry by the late 1930s. Recently, however, EVs have begun to reappear as a result of new developments in battery and power electronics technologies that make possible speeds and ranges comparable to those of fossil-fuel vehicles.

With the support of many governments, vehicle manufacturers are now racing to develop EVs; challenges related to size, weight, cost, and driving range have been effectively resolved over the last few years. EVs have now become a reality and are commercially available in many sizes and ranges, with thousands on the roads in many countries in North America, Europe, and Asia. Some governments have initiated incentive programs to increase the EV market share. In Canada, beginning in July 2010, the Ontario government established a rebate of up to $8,500 CAD for the purchase or lease of a new EV [53], and the goal for 2020 is for one of every 20 vehicles driven in Ontario to be electric. This program constitutes part of the government's climate change plan for reducing both gas emissions and the province's carbon footprint. In the U.S., the government is providing a $2.4 billion USD fund for the development of the next generation of PEVs and advanced battery components that will increase the efficiency and driving range of these vehicles [54]. This fund will provide a tax credit of up to $7,500 USD for the purchase of any new PEV as part of the government's plan to have more than 1 million EVs on the roads by 2015.

The next subsections include a description of the different types of EVs, followed by a detailed discussion of PEV operation, chargers, and communication as well as the associated impact on the grid.

2.4.1 EV types and modes of operation

An EV is any vehicle whose driving torque is produced by any type of electric motor. Three main types of EVs are currently available:

- Hybrid EVs (HEVs): These vehicles have an electric propulsion system in conjunction with a FFICE. However, as with conventional vehicles, the only source of energy is the fossil fuel. Due to the efficiency-improving technologies incorporated into these vehicles, such as regenerative braking, which reduces fuel consumption and emissions, they produce fewer emissions and provide greater efficiency than FFICE vehicles.

- PEVs: Two types of PEVs are available in the markets:
    - Plug-in hybrid EV (PHEV) or extended-range EV: The construction of these vehicles is almost the same as that of HEVs, except that they use higher-capacity batteries that can be recharged through connection to an external electric power source. They can therefore operate as pure EVs as long as the battery charge is not depleted. This type of vehicle offers greater efficiency than an HEV and also produces fewer emissions.
    - Plug-in pure EV: These vehicles can be considered to be special case of the PHEV with zero-emission because they rely only on energy stored in the battery and are not equipped with a conventional fossil-fuel internal combustion engine (FFICE). As needed, their batteries can be plugged into a source of electric energy to restore their charge or exchanged with fully charged battery, but the market for them is very limited due to the high initial cost, and the limited availability of charging stations.
- Fuel cell EVs: These vehicles utilize fuel cell technology to power the motor by converting chemical energy from the fuel to electric energy. Hydrogen is used as the fuel for these vehicles, which are considered to be zero-emission vehicles. The driving range of this type of vehicle is acceptable and is comparable to that of conventional fossil-fuel vehicles. The only limitation with respect to this type of vehicle is the hydrogen transmission infrastructure, which is very expensive, a factor that keeps hydrogen suppliers from constructing such infrastructures without an adequate market for fuel cell EVs in their territory. On the other hand, users will not purchase these vehicles unless a satisfactory hydrogen supply is available in their driving region.

2.4.2 PEVs

The most promising of these types of EVs is the PEV, whose operating modes can be generally classified as either battery charge depletion (BCD) or battery charge sustaining (BCS) [50]. In BCD mode, the energy stored in the battery is used to supply the motor with power. The total distance that can be traveled in this mode starting with fully charged batteries is defined as the all-electric range (AER) of the vehicle. When all of the battery energy has been used, or when the energy stored in the battery must be reserved for any reason, the vehicle enters the BCS mode, in which it operates as a conventional fossil-fuel-consuming vehicle. Accordingly, pure electric plug-in vehicles operate in

BCD mode all the time. Common PEV architectures are shown in Figure 2.4 [55]. The two basic designs are the parallel and series configurations illustrated in Figure 2.4 (a) and (b). In a series configuration, the output of the engine is converted to electricity via a generator. This electricity can be used either to charge the battery or to supply the motor that propels the wheels. In a parallel configuration, the engine and the battery can propel the wheels separately because the electric motor and the engine are coupled through clutches to the transmission system. In both configurations, regenerative braking is applied to increase system efficiency: any excess energy generated during braking is fed back to add to the battery charge. Other configurations designed to improve system efficiency, such as a series/parallel configuration, are also available.

2.4.3 Charger ratings

Three main types of chargers are commonly used for PEV charging. The specifications [56] for each type are listed in Table 2.1. The charger most often used in Canada is the level 2_R charger, which is recommended by vehicle manufacturers [57].

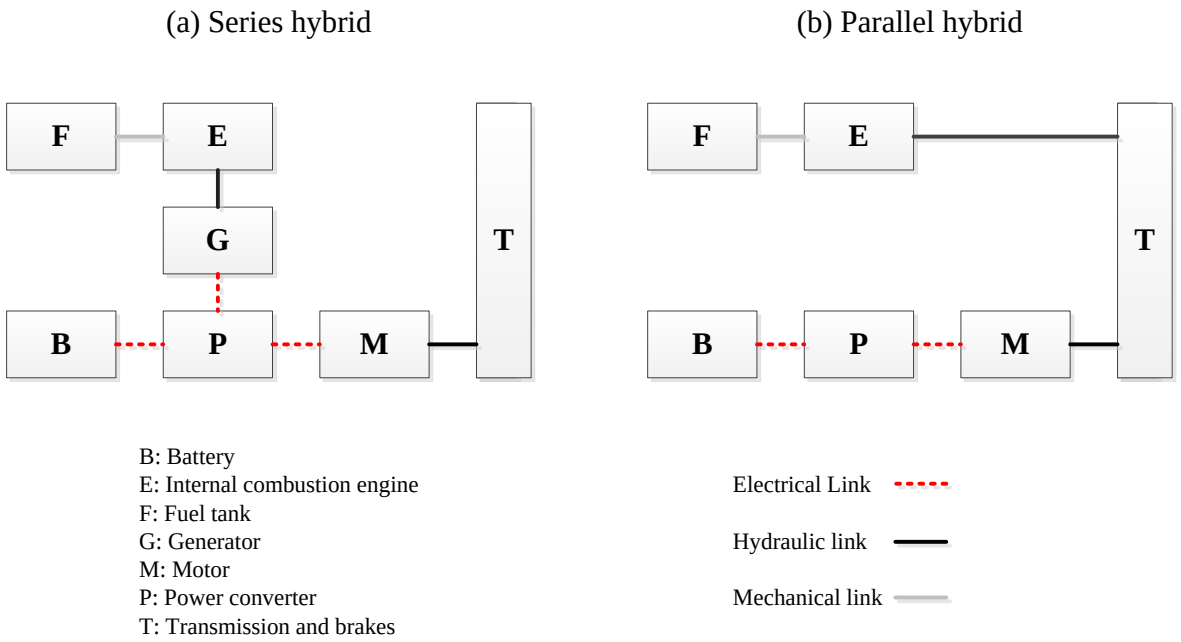

Figure 2.4 Common architectures of a typical PEV [55]

Table 2.1 PEV charger ratings

Type	Specifications
Level 1_R	• 110/120 V, AC, 15 -20 amp • Does not require installation and can use standard 120 V electrical outlet • Typical charge times: 8-12 hours
Level 2_R	• 208-240 V, AC, 15-30 amp • Requires special installation • Typical charge times: 3-8 hours
Level 3_R	• Known as "DC fast charging" • 440 V, DC, 125 amp, 55 kW or higher • Requires special installation • Typically returns 50 % of PEV battery charge in under 30 min

2.4.4 Communication and control

Any communication between the grid and a vehicle is likely to be executed through the charger because it is fixed in place. Sending information to the grid about the location of the vehicle when it is plugged in is therefore unnecessary. However, customers who install level 2_R charging or higher must give advance notice to the electric utility [56]. Vehicles chargers are equipped with different levels of communication and control capabilities. Table 2.2 shows the capabilities of each level, as stated in [58].

Since standards for vehicle-grid communication have not yet been fully developed, several pathways [59, 60] for communication between the chargers and the grid are possible:

- Wireless network: In this method, a transceiver is installed at each charger location. Since the scheduling of the charging is not a critical operation and the rate of data to be sent is relatively low (9.6 to 56 kb/s) [61], time division multiple access can be used for sharing the communication medium among customers in the same region, thus enabling the use of a lower bandwidth.
- Power line carrier (PLC): Power lines were originally designed to transmit electric power at frequencies ranging from 50 Hz to 60 Hz. For requirements related to protection, PLC was

used primarily for the transmission of data over power lines. Due to the high levels of noise and signal fading in power lines, standards are in force to limit data transfer rates to 14 Mb/s [62]. This rate is more than sufficient for PEV control and home energy management. However, issues associated with reliability and vulnerability require additional investigation.

- Over internet protocol (IP): This method may be the cheapest and simplest. A local area network circuit is built inside the charger, which connects it to the internet through cables or a wireless modem. Each user has an individual account and can monitor his or her vehicle charging from a personal computer or mobile device. However, communication over IP also has drawbacks: the need of an internet service provider wherever there is an EV, the reliability of the service is not guaranteed, and the system is vulnerable.

Table 2.2 Control and communication levels

Charger control and communication level	**Capabilities**
Level 0_{cc}	• Only charges the vehicle: discharging not allowed • Controls the charging current and voltage of the battery pack in the vehicle, which should match the battery specifications • Supplies electric energy to the vehicle battery directly as soon as it is plugged in
Level 1_{cc}	• Includes the features of level 0_{cc} • Includes time delay circuitry so the vehicle owner can control the starting time and possibly the finish time for charging the vehicle
Level 2_{cc}	• Includes the features of level 0_{cc} • Enables two-way communications with the electric utility • Receives on or off enabling signal from the electric utility • Reports vehicle identification to the electric utility upon connection to the vehicle
Level 3_{cc}	• Includes the features of level 2_{cc} • Includes bidirectional power flow to enable vehicle discharge to the grid

2.4.5 Potential impact of uncontrolled PEV charging on distribution systems

Because battery charging takes hours for level 1_R and 2_R, it is unlikely to be achieved at charging stations; instead, the majority of PEVs are expected to be charged at home, in parking lots, or in public locations. Studies show that level 1_R charging does not have a significant impact on a distribution system [56]. However, if not managed properly, level 2_R charging can pose a potential risk to the system even if PEV penetration is low (5 % to 10 %) [4, 5]. The risk is associated with the expectation that PEVs will likely be clustered in specific geographical areas, which can be a source of significant additional stress on local distribution equipment, especially with multiple residential customers.

A high PEV penetration (20 % to 60 %) [3] is expected in the next few decades. The energy consumed by these PEVs is anticipated to add considerable loading to the distribution networks. According to [4, 50, 51, 56, 63], if not managed effectively, PEV charging can have severe consequences: increased power losses, phase imbalance, power quality problems, violations of feeder thermal limits, transformer degradation, and fuse blowouts.

2.5 Load modeling of uncontrolled PEV charging

This section presents a discussion of the work published with respect to PEV modeling. In [50], it is assumed that a specific percentage of PEVs will be operated as pure EVs in BCD mode; however, this percentage is entirely dependent on travel patterns and can change from day to day. In [64], a specific daily mileage is assigned to all vehicles, and a single charge per day is assumed. The reality is that vehicle mileage varies from one vehicle to another, and some vehicles may charge more than once per day or not at all. In the study reported in [65], all battery charging is assumed to have the same start time and duration. The work presented in [66, 67] involves a rigid recharging schedule, based on which vehicles are plugged in at a specific time and left until fully charged. Energy consumption is assumed to be constant for any recharging event, whereas in the real world, charging could occur at any time during the day, with different amounts of energy consumption, depending on the available charge in the battery.

Some authors, such as in [66-69], have assumed same AER for all vehicles, which does not reflect the different ranges available in the market. In [68, 69], the percentage of annual trips under the AER is assumed to be the same percentage of all vehicle miles driven in electric mode. This assumption is questionable for two reasons. First, for trip distances greater than the vehicle AER, the battery is still used until depleted, and gasoline then powers the remainder of the trip. Secondly, the

gasoline engine could be used for trips less than the vehicle AER due to insufficient stored energy in the battery because not all vehicles begin a trip with a fully charged battery. This assumption therefore results in inaccurate estimations of the energy consumed by the PEVs. A remarkable study is reported in [70] with respect to quantifying the benefits of smart metering and demand side management in a distribution system. The work includes consideration of the control of PEV charging; however, drivers' travel patterns are not taken into account, and all trips shorter than 100 miles are assumed to be powered by the batteries, which may lead to inaccurate results, as explained above. The authors of [71] discuss different charging scenarios, including a controlled charging scenario based on the minimization of the charging costs. A one-day charging pattern is considered in this work; however, even within a single week, charging patterns vary because weekend charging differs from weekday charging, and the charging pattern is also different according to the month. Conclusions based on a one-day charging pattern may thus be misleading because alternative days can exhibit severe peaks in load or PEV charging demand, which must be taken into account.

The PEV charging model presented in [72] assumes one charging event per day after the last trip, and also ignores seasonal variations throughout the year. The entire consumption is modeled based on two days only: weekday and weekend. A methodology is presented in [73] for the modeling and optimal coordination of PEV charging so that energy losses and voltage deviations on a radial distribution feeder are minimized. The results reveal the effectiveness of the methodology with respect to reducing system energy losses, but the study is based on assumed fixed battery capacities and identical charger ratings for all vehicles. In addition, the proposed methodology is based on a two-day model: one to represent summer, and the other to represent winter. The PEV energy-consumption model presented in [74] excludes consideration of any variability in usage associated with the PEV charging. In [75], all PEVs are assumed to have the same charging duration as well as a rigid starting time. An investigation of the impact of PEV charging on power system and gas emissions is described in [76] with respect to four different charging scenarios: uncontrolled at home, uncontrolled at any location, delayed, and controlled. However, one charging event per day and a fixed percentage of daily miles driven in electric mode are assumed. The work conducted in [77] is based on different battery capacities, but all vehicles are assumed to consume and charge all their batteries each day, which does not account for variable usage.

Notable work is reported in [66] with respect to investigating the potential impact of PEV charging in different U.S. regions. The methodology developed, in this study, involves the generation of an annual PEV energy consumption model, which is then added to the normal load model for each

region. However, the research was based on the assumption that the vehicles are plugged in at a fixed time during the day and remain plugged in until fully charged, an assumption that neglects the variability inherent in PEV charging.

In [74], the impact of PEV charging on the expected life of distribution transformers is examined. The model developed is based on the average daily energy consumed by a light duty fleet (LDF) of PEVs, which may be misleading because PEV energy consumption is dependent on the habits of drivers, which on some days can result in significant peaks in system demand and which must be taken into consideration.

2.6 Coordinated PEV charging

The literature provides two categories of solutions that have been proposed in order to accommodate the PEV charging in distribution networks. The first involves uncoordinated PEV charging, which is possible either through upgrades to the power system infrastructure or through the deployment of DG units to meet the excess power demand [78]. The second category targets coordinated PEV charging or charging/discharging, which relies on a two-way communication infrastructure under a smart grid paradigm [6]. Coordinated smart PEV charging and discharging is known to be overall more beneficial for electric grid operators and customers than uncoordinated operation [79].

The literature includes reports of a number of studies related to the problem of coordinated PEV charging and discharging in a smart grid. This work can be divided into two categories of solutions: The first includes myopic solutions, in which the charging and discharging decisions are based solely on the current information in the grid [80-84]. The second category includes forecast-based solutions, in which future power demands in the grid are considered during the determination of the charging and discharging decisions [85-90].

In [80], a real-time coordinated PEV charging strategy is proposed, which takes into account the time-varying energy process and the charging time and zone preferred by the PEV owner. PEV demand side management is presented in [81], with the goal of providing dynamically configurable dispersed energy storage during peak power demand and outage conditions. An autonomous distributed vehicle-to-grid (V2G) control system is suggested in [82] as a means of satisfying the requirements for scheduled charging. In [83], the development of a framework is for V2G ancillary service modeling and operation is described. An optimal PEV charging model that responds to the time-of-use price in a regulated market is proposed in [84]. The authors in [91] presented a new PEV battery energy management mechanism based on cloud computing networks, which reduces PEV

interactions with parking lots and the grid. The energy management mechanism is useful for massive implementations of PEVs and other smart devices that require direct communication with the grid. However, the work fails to include consideration of the utility benefits and the distribution system constraints. Since the studies mentioned are based on myopic solutions, the effect of current and future PEV charging and discharging decisions on the power grid is not considered. The feasibility of such decisions is thus not guaranteed, which means that achieving the target SOC level for PEVs can jeopardize distribution system equipment.

In [85], a probabilistic method is proposed for the estimation of the amount of power that can be delivered from PEVs to the grid. The charging coordination strategy presented in [86] is based on solving a global problem that optimizes day-ahead charging decisions and a local problem that optimizes the real-time connection of the vehicles to the grid. In [87], the researchers introduce a PEV charging coordination methodology based on day-ahead and/or real-time markets. Another study [88] led to the development of an intelligent unit commitment model for V2G that optimizes power system costs and emissions. Stochastic unit commitment models for PEV operation with volatile wind power generation are proposed in [89, 90]. The work described in [92] resulted in fuzzy logic controllers for managing PEV charging/discharging in real time. The authors of [93] developed a dual PEV coordination mechanism that operates on two different levels: market operation and real-time operation. While these existing studies deal with coordinated decisions based on forecast data, they fail to include a method of forecasting the PEV load and are not based on real-time measurements and short-term predictions. The system response to short-term fluctuations in PEV load has thus not yet been examined.

2.7 Summary

The brief literature review included in this chapter reveals that a number of studies have been conducted in the areas of DG allocation and the accommodation of PEV charging. Despite the amount of research undertaken, major drawbacks are still unresolved and have provided the impetus for the work presented in this thesis. With respect to the DG allocation methodologies described in the literature, these drawbacks can be summarized as follows:

- No accurate method has been proposed for evaluating the upgrade requirements in ADNs with renewable DG units connections.
- Most of the work involves single-objective optimization, which may result in a negative impact on other objectives. On the other hand, some studies incorporated multi-objective

optimization using a weighted sum, but identifying weighting factors for a planning problem a priori is usually questionable and can result in misleading outcomes.

- The work related to the minimization of system losses was based on consideration of either the system power loss or the average energy cost of the energy loss. In fact, the cost of energy losses cannot hinge on the average cost of the energy because the effect of renewable DG on energy losses is not uniform during the day and can be concentrated during periods of low or high energy prices.

It is also clear from the discussion in section 2.5 that the research published in the area of the modeling of uncontrolled PEV charging loads is insufficient. The primary drawbacks exhibited by the models presented in the literature can be summarized as follows:

- The variability and uncertainty inherent in vehicle usage are ignored, which can lead to inaccurate results that cannot be relied upon to accurately quantify the effects of PEVs on distribution networks.
- When the effect of ambient temperature on PEV energy consumption is not considered, the results may be misleading because extreme temperatures could dramatically reduce a vehicle's AER [94].

The charging coordination methodologies presented in the literature are characterized by the following drawbacks:

- Feasible charging decisions are not guaranteed. In general, the formulation of PEV charging coordination described in the literature is based on either single-objective or multi-objective optimization. Single-objective approaches are aimed at minimizing the charging cost or system losses. In the absence of appropriate coordination, the inclusion of the customer target SOC in the problem constraints may result in infeasible decisions during cases involving extreme peak load levels. An additional objective is to maximize the SOC of the PEV batteries, which, however, might be achieved at the expense of higher system operating costs. In multi-objective optimization, the objective function is to balance the operating cost with customer satisfaction. In fact, customer satisfaction and the reliability of the PEV charging service should have higher priority than the system operating cost. Some research also fails to address power system constraints in the problem formulation, e.g., [81, 84, 86]. The solutions proposed in the literature thus guarantee neither the feasibility of the charging and discharging decisions nor customer satisfaction.

- Previous research has failed to develop a charging coordination mechanism that is based on real-time measurements and that includes consideration of current and future information obtained from PEVs and the grid. The effect of current and future PEV charging and discharging decisions on the power grid has therefore not been considered.
- The literature contains no mention of a prediction scheme for PEVs. Previous work either ignores future information or assumes that the PEV load forecast data are perfect. Hence, the system response to short-term fluctuations in the PEV load has not been examined.

The research presented in this thesis was motivated by the above shortcomings. The next four chapters describe the work conducted to address these deficiencies and to develop useful methodologies that can benefit both utility operators and customers. Specifically, Chapter 3 focuses on the development of an optimal DG allocation approach, and Chapter 4 introduces a new method of modeling an uncoordinated PEV charging load. Chapter 5 presents the use of these models and methods in a planning approach for the accommodation of increased uncoordinated PEV penetration that utilizes DG units. Chapter 6 details a new charging coordination methodology that can accommodate real-time parking lot dynamics.

Chapter 3
DG optimal allocation

3.1 Introduction

This chapter presents an approach for evaluating the economic benefits of renewable DG. Also proposed is a long-term planning procedure for maximizing the benefits of DG allocation in ADNs. Due to the complexity of the long-term optimal DG allocation planning problem, a GA-based approach is utilized. The proposed approach addresses the drawbacks mentioned in Chapter 2 by taking into account the following:

- The uncertainty and variability associated with DG output
- The variable hourly cost of energy
- Load variability and type of customer sector
- Protection and metering equipment upgrades

The next two sections describe the problem and explain the modeling. The problem formulation, a sample case study, and concluding remarks are presented in the last three sections of this chapter.

3.2 Problem description

This work includes consideration of three economic benefits associated with DG allocation in distribution systems: deferral of system upgrade investments, reduced cost of energy losses, and reduced cost of interruptions. The following subsections provide details about these benefits:

3.2.1 System Upgrade Cost

In this work, system upgrade cost is considered to be the sum of the cost of upgrading the lines and the protection and metering equipment. The main substation transformers are assumed to be redundant, which is the common practice in Ontario, Canada. The costs considered are explained in the next subsections.

3.2.1.1 Line reinforcement costs

Increased loads may result in mandatory line or cable upgrades. Line upgrades can also be used as a means of avoiding voltage violation and increasing system security. If carefully planned, the

installation of DG units in a distribution system can relieve feeder congestion, which would have the effect of deferring such upgrades.

3.2.1.2 Protection and metering equipment upgrades

High DG penetration can cause reverse power flow at a substation, which would necessitate the upgrading of the metering equipment at that location. Installing DG units in the system also contributes to short circuit levels, with a consequent requirement to upgrade protective equipment.

3.2.1.3 Cost of energy losses

Installing DG units in a distribution network affects energy losses; however, due to the variations in the load, energy prices, and the DG units' output power, the cost of annual energy losses must be calculated hourly. This requirement translates into the necessity of performing the load flow analysis $8760 \times N_{MCS}$ times, where N_{MCS} is the number of scenarios generated by MCS, which is impractical. In this work, the proposed approach limits the iterations of the load flow analysis to the number of states of the combined load and the DG model.

The process of predicting electric energy price variations along the planning horizon is very complicated because of its dependency on so many factors. Energy price variations are therefore assumed as input for this study and are beyond the scope of the research. For these reasons, the 2010 hourly energy prices in Ontario, Canada, have been utilized to represent each year in the planning horizon. Using variable hourly energy prices is assumed to provide a better assessment of the effect of renewable DG on system losses because the effect can be concentrated during periods of low or high energy prices during the day.

3.2.1.4 Cost of interruptions

The distribution system is an important link between the transmission-generation systems and the customers. In most cases, these links are radial, which makes them susceptible to outages caused by the failure of a single element. Statistical analysis conducted by the Canadian Electrical Association indicates that almost 80 % of the outages experienced by Canadian utility customers arise from faults in the distribution system [95]. A system typically has two operating modes:

- Grid connected: The grid and the installed DG are supplying the load requirements. Both dispatchable and renewable DG units dump the power they generate into the system.
- Islanded system: A distribution network is fed from a transmission network, and when the connection to the transmission system is lost, the distribution network is islanded. According

to [96], DG units can supply system loads during scheduled or unscheduled outage events, which can improve system reliability.

The following assumptions are considered in the proposed approach for evaluating the cost of interruptions in distribution networks that include renewable DG connections:

- Islanding operating mode is assumed to be allowed [96], which benefits both the LDC and the customers.
- During islanded operating mode, sole reliance on renewable DG may cause stability problems with respect to voltage and frequency variations [97]. Dispatchable DG units are therefore typically allocated for the management of the power balance in the island between the generation (involving dispatchable and renewable DG units) from one side and the load from the other. Hence, if there is enough generated power, a minimum percentage of dispatchable DG must be assumed for successful islanding to be ensured. As given in [97], the threshold is assumed to be 60 % of the total DG units installed in the system. Below this threshold, renewable DG units must disconnect during islanding operating mode.
- For an island to be successful, the power generated from all DG units within the island must be higher than or equal to a specific percentage of the power required for the load. The success of an island is not dependent on the setting of an upper limit for the DG units because the communication signals are assumed to control the output of dispatchable DG units, and if required, to curtail the output of renewable DG units.

3.3 Generation and load modeling

This section introduces the generation and load models, which are utilized later in the proposed planning problem formulation. The generation models include both dispatchable and non-dispatchable DG units while the load model represents the normal load of the system.

3.3.1 Dispatchable DG unit modeling

NGDG are considered in this work both because they are known to produce the lowest level of emissions compared to other fossil-fuel DG [98] and because of the availability of natural gas networks. In normal operating mode, the output of these DG units is assumed to be fixed. However, during islanding mode, their output is considered to be variable in order to manage the active and reactive power balance. A two-state model has been used for modeling the operation of each DG, as

described in subsection 2.2.1. This model is employed in an MCS to produce an artificial annual operating scenario for each dispatchable DG unit.

3.3.2 WDG modeling

Due to the variability in the hourly cost of energy and the nonlinear cost damage function, for wind generation modeling, an MCS model is utilized for the determination of the cost of the energy loss and the cost of interruptions, while a probabilistic wind speed model is used for evaluating the cost of upgrades. A time series model is not used in the proposed long-term planning allocation problem because this type of model is unsuitable for use with time spans that cover decades. The principles of the two models are described in subsection 2.2.2. Before the output power of WDG units can be modeled, the wind speed measurements must be adjusted to the proper height. The heights of meteorological masts used for wind speed measurements are usually much lower than the hub height of wind turbines, so wind speed measurements must be adjusted to reflect the hub height. The hourly wind data provided by [99] was measured at a height of 10 m, which must be adjusted to the typical hub heights of modern wind turbines (50 m to 120 m). The correction can be determined based on the roughness factor, which is available for the measured historical data. Along with the data listed in Table 3.1, the following formula has been used to adjust the historical data to the hub height [100]:

$$v_2 = v_1.\left(\frac{\ln(\frac{h_2}{z_0})}{\ln(\frac{h_1}{z_0})}\right) \tag{3.1}$$

where

v_2 is the wind speed at hub height;

v_1 is the measured wind speed;

h_1 is the meteorological mast height;

h_2 is the hub height of the turbine;

z_0 is the roughness factor, which varies from 0.0002 to 1 [101], according to the terrain descriptions listed in Table 3.1.

Table 3.1 Roughness factor for different terrains [101]

Terrain Description	z_0 (m)
Open sea, fetch at least 5 km	0.0002
Mud flats, snow; no vegetation, no obstacles	0.005
Open flat terrain; grass, few isolated obstacles	0.03
Low crops, occasional large obstacles	0.10
High crops, scattered obstacles	0.25
Parkland, bushes, numerous obstacles	0.50
Normal large obstacle coverage (suburb, forest)	1.0
City centre with high- and low-rise buildings	≥ 2.0

After the wind speeds have been modified to correspond to the appropriate wind turbine hub height, three years of historical wind speed data are utilized for modeling the output power of the wind DG units. The entire year is then divided into 12 months, and the historical data for each month are used in order to generate the frequency distributions of the wind speed measurements for a typical day [102]. The day that represents each month is further subdivided into 24 hourly time segments. Thus, 288 time segments represent the year (24 for each month). Considering a month to be 30 days, each time segment then has 90 data points to indicate the wind speed level (3 years × 30 days per month). From these data, the mean and standard deviation for each time segment are calculated, from which a Weibull pdf is generated for each hour, using (2.2) to (2.5).

For each time segment, the entire range of wind speeds is discretized into a defined number of states $s_w \in \mathcal{S}_{WDG}$, where $\mathcal{S}_{WDG}$ is the set of WDG output power states. In this work, 14 states [18] have been chosen to represent the entire wind speed range for each hour. The number of states is a trade-off between accuracy and the complexity of the problem [18]. The values of these states have been selected based on the central centroid sorting process described in [103]. These states are described in Table 3.2, with each state having a probability corresponding to the Weibull pdf. The wind speed probabilities for each hour are converted to hourly output power probabilities. Hence, for a specific wind turbine, the output power for each state is calculated using (2.7). For each of the 14 states of wind speed, the average speed is used for the calculation of the power for that state. The

wind turbine utilized in the system under study is assumed to have the most common [104] cut-in, rated, and cut-out speeds: 4 m/s, 16 m/s, and 25 m/s, respectively.

In the final step, the wind turbine is modeled as a multi-state model for each of the 288 hours representing the year. This generated model is designated a probabilistic model. The same configuration of states is also used in order to convert the MCS speed model to an output power multi-state model, as explained in subsection 2.2.2.

3.3.3 Load modeling

The load in the distribution network under study is assumed to follow the IEEE reliability test system (RTS) load pattern [105]. The load is modeled based on a defined number of states, depending on the desired accuracy, time scale, and speed of simulation. The central centroid sorting process described in [103] is utilized to discretize the hourly RTS load model into seven states $s_l \in \mathcal{S}_L$, where $\mathcal{S}_L$ is the set of load power states, which are listed in Table 3.3. The uncertainty inherent in specific percentages can be used as a means of generating a variety of annual scenarios.

Table 3.2 Wind states

State	From (m/s)	To (m/s)	Output Power
0	0.000	4.000	0
	>25.000		
1	4.000	5.560	For each state, the average speed in the range is used in (2.7) for calculating the output power.
2	5.560	6.280	
3	6.280	7.065	
4	7.065	7.545	
5	7.545	8.200	
6	8.200	8.920	
7	8.920	10.005	
8	10.005	11.330	
9	11.330	12.345	
10	12.345	13.300	
11	13.300	14.140	
12	14.140	16.000	
13	16.000	25.000	P_{WT}^{rated}

Table 3.3 Load states

Load state	State as a percentage of peak load
1	30.0 %
2	43.0 %
3	52.0 %
4	62.4 %
5	70.1 %
6	81.1 %
7	100.0 %

3.3.4 Combined generation-load model

This model describes all system states $s \in \mathcal{S}_{sys}$ and their probabilities $\mathbb{p}_{(t,s)}$ that correspond to different generation and load states. For the generation of this model, the year is divided into 12 months, and each month is modeled for two types of days: weekday and weekend. For each time segment of the 576 (24 h ×2 d × 12 months), the probability of each combined state $s = (s_g, s_w, s_l)$ is then calculated as the convolution of all the probabilities associated with that state, as in (3.2). The probability of the occurrence of each state $s \in \mathcal{S}_{sys}$ during any time segment is also evaluated, as in (3.3). For each time segment (1 h), different random variables representing the load and the generation are assumed to be uncorrelated, an assumption that preserves the spatial correlation between different random variables. Although the NGDG units are considered to be firm generation, the problem formulation is generic: different states can be incorporated for the NGDG. The total number of system states N_s can be given by $N_s = N_{sg} \times N_{sw} \times N_{sl}$, where N_{sg}, N_{sw}, and N_{sl} are the number of states representing the NGDG, the WDG, and the load, respectively.

$$\mathbb{p}_{(t,s)} = \mathbb{p}_{(t,s_g)} \times \mathbb{p}_{(t,s_w)} \times \mathbb{p}_{(t,s_l)} \quad \forall\, s_g \in \mathcal{S}_{NGDG}, s_w \in \mathcal{S}_{WDG}, s_l \in \mathcal{S}_L \tag{3.2}$$

$$\mathbb{p}_{(s)} = \left(\frac{1}{576}\right) \times \sum_{t=1}^{576} \mathbb{p}_{(t,s)} \quad \forall s \in \mathcal{S}_{sys} \tag{3.3}$$

where

$\mathbb{p}_{(t,\cdot)}$ is the probability of state $(\cdot)$ in time segment t;

$\mathbb{P}_{(\cdot)}$ is the probability of the occurrence of state $(\cdot)$;

$\mathcal{S}_{NGDG}$ is the set of states for the NGDG units.

3.4 The DG allocation planning problem

This section is divided into two parts: the first presents a number of approaches for evaluating the three costs considered in this work, and the second introduces the proposed DG planning problem formulation. This work is based on the following assumptions:

- Most of the utilities force the DG units to operate in constant power factor mode, so the DG units are assumed to operate at a unity power factor [18].
- The capacities of the DG units are discretized at a defined step, which is assumed to be 100 kW for this work.

3.4.1 System cost evaluation

3.4.1.1 System upgrades

This subsection describes the methodology proposed for evaluating the cost of system upgrades. A risk factor *RF* is proposed, which represents the expected total duration of the annual overloading and is used in the calculation of the cost of line upgrades.

3.4.1.1.1 Line upgrades

For radial systems with no DG units, the reinforcement cost can be calculated at the extreme power flow condition in the lines, which is simply a single condition at peak load because the power flow is always from the substation to the load points. However, for this study, when DG units are present in the system, load flow analysis is performed for each system state. The procedure for evaluating the cost of system upgrades is illustrated in Figure 3.1 and outlined in the following steps:

1. For each state s, execute steps 2 to 4.
2. For each year y, execute steps 3 to 4.
3. Update loads with the annual rise, and run the load flow analysis for state s and year y.
4. For each line $l \in \mathcal{L}$, record the year $Y_{UP(l)}$ in which the upgrade is required and then calculate the corresponding net present value (NPV) of the cost of the upgrade for each line for each state s.
5. For each line, arrange the combined generation and load states in descending order according to the calculated NPV.

6. For each line $l \in \mathcal{L}$, if the probability of the state corresponding to the maximum cost of the upgrade is greater than the *RF*, proceed to step 7; if not, proceed to the next state that contribute the most to the upgrade of line l. If the sum of the probabilities of this state and the previous state(s) is greater than the *RF*, go to step 7; if not, proceed to the next state and repeat the process specified in the previous statement.
7. Record this upgrade cost and repeat step 6 for the next line.
8. Evaluate the NPV of the reinforcement investments for the required lines NPV_{Lines} during the period under study using the following formula [40]:

$$NPV_{Lines} = \sum_{l \in \mathcal{L}} \frac{C_{UP(l)}}{(1+d')^{Y_{UP(l)}}} \tag{3.4}$$

where

$C_{UP(l)}$ is the cost of the reinforcement l;

d' is the effective discount rate, which is related to the discount rate d and the inflation rate e by $d' = \frac{d-e}{1+e}$, as given in [106].

For evaluating the cost of line upgrades in the case of WDG units, if the *RF* is taken to be zero, the cost is greater than or equal to the cost of the line upgrades without the DG. For example, if the combined load and generation states are assumed to be 224 states, these states have two extremes, defined as zero DG output power at the peak load and as the rated DG output power at the minimum load. Each state contributes to the line *l* upgrade. For zero *RF*, all states are considered, including the first extreme mentioned above: the case without DG, which does not affect the upgrades. Moreover, the second extreme must be included, which may result in higher upgrade costs due to reverse power. Thus, if the *RF* is zero, the cost of each line upgrade is greater than or equal to the case without DG.

Assuming that the state that contributes the most to the cost of the reinforcement l has a probability of occurrence of 0.05 %, which corresponds to almost 4 hours per year. For an *RF* of 6 hours per year, this state is neglected because the probability of its occurrence is less than the *RF*, and other states will be considered. This process may result in the reduction of the cost of the line upgrade to a level lower than the cost with the base case based on predefined risk.

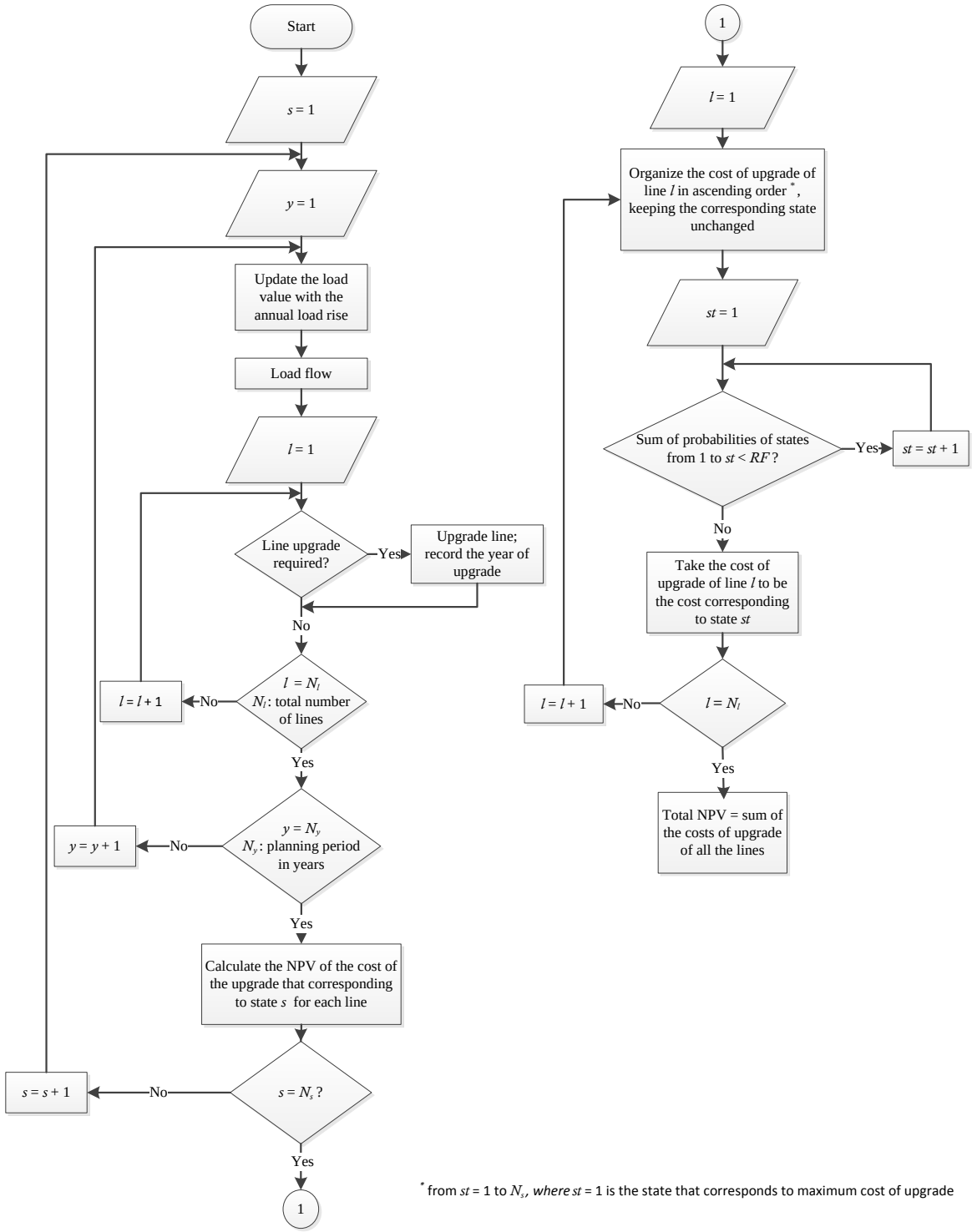

Figure 3.1 Evaluation of the NPV of the cost of the upgrades [102]

3.4.1.1.2 Metering equipment upgrade

At the substation terminals where the metering devices are installed, the direction of the power flow is checked with respect to the state of the minimum load and the rated DG output. The cost of upgrading the metering devices is then calculated accordingly.

3.4.1.1.3 Protection switch gear upgrade

To prevent false tripping and for effective fault clearing, a short circuit analysis of the system must be performed when DG units have been installed in the system. The cost of upgrading the protective equipment is therefore calculated, with the installed DG units being classified as one of the following:

- Synchronous machines (Diesel, natural gas DG units)
- Induction machines (Class A, B, and C wind turbines)
- Inverter-based (Class D WDG and PVDG units)

3.4.1.2 Cost of energy loss

The power loss for each of the combined generation and load states $s \in \mathcal{S}_{sys}$ is calculated for each year in the period under study, incorporating load growth. The NPV of the cost of the energy loss for the period under study is then calculated according to the methodology shown in Figure 3.2, which can be described as follows [102]:

The power loss for each year is represented as a vector $P_{loss(y)}^{Annual}$ of length N_s in which each element represents the power loss corresponding to state $s \in \mathcal{S}_{sys}$, as follows:

$$P_{loss(y)}^{Annual} = [P_{loss(1)}\ P_{loss(2)}\ \cdots\ P_{loss(N_S)}] \tag{3.5}$$

A binary matrix $\Psi_{(g)}$ is also defined for each scenario $g = 1,2,\cdots,N_{MCS}$ generated in the probabilistic chronological model, using an MCS. This binary matrix is of size $8760 \times N_s$, where each row consists of $N_s - 1$ zeroes and one element of value 1; this element corresponds to the actual load state. This matrix is generated only once for a system with specific load and generation profiles, providing an hourly calculation of the cost of the energy losses.

For example, assume a system with only WDG, in which the load states are given by $\mathcal{S}_L = \{0.5,1\}$ and the generation states are given by $\mathcal{S}_{WDG} = \{0,1\}$. There are thus four combined load and generation states, as given by $\mathcal{S}_{sys} = \{(0.5,0),(0.5,1),(1,0),(1,1)\}$. If the period under study is assumed

to be 5 h, the hourly load curve and the hourly DG output for a specific scenario $(\cdot)$ are given by [0.5 0.5 1 0.5 1] and [1 0 1 0 0], respectively. The result is that during the first time segment, the second state (0.5,1) occurs; then the first state (0.5,0) occurs; and so on. The state number represents the locations of the ones in the rows of the binary matrix $\Psi_{(\cdot)}$, which is given by

$$\Psi_{(\cdot)} = \begin{bmatrix} 0 & 1 & 0 & 0 \\ 1 & 0 & 0 & 0 \\ 0 & 0 & 0 & 1 \\ 1 & 0 & 0 & 0 \\ 0 & 0 & 1 & 0 \end{bmatrix} \tag{3.6}$$

The cost of the annual energy losses $C_{loss(y)}^{Annual}$ can then be evaluated as follows:

$$C_{loss(y)}^{Annual} = \frac{1}{N_{MCS}} \sum_{g=1}^{N_{MCS}} \left[\Psi_{(g)_{8760\times N_s}} \times P_{loss(y)}^{Annual}{}_{N_s\times 1} \right]^T \times C_{kWh(y)_{8760\times 1}} \tag{3.7}$$

Vector $C_{kWh(y)}$ represents the hourly energy price in \$/kWh for the 8760 h for year y, which is assumed as input for this study. For simplicity, the hourly market clearing prices of electric energy in 2010 from the IESO website [107] are therefore utilized as vector $C_{kWh(y)}$. The final step is to calculate the NPV of the total cost of energy losses NPV_{Loss} for the period under study, as follows:

$$NPV_{Loss} = \sum_{y} \frac{C_{loss(y)}^{Annual}}{(1+d')^y} \tag{3.8}$$

3.4.1.3 Cost of interruptions

A distribution network usually contains a mix of residential, commercial, and industrial customers. According to [108], the cost of interruptions, which is known as the cost damage function (CDF), is nonlinear and varies according to the duration of the interruption, as indicated in Figure 3.3 [108], which shows estimates of the average cost of an interruption expressed as a function of the duration of the interruption for each customer sector.

Since the CDF is nonlinear, as can be seen in Figure 3.3, the outage cost cannot be determined analytically; an MCS is therefore utilized. The outage cost for load point $i \in \mathcal{I}$ is thus evaluated using

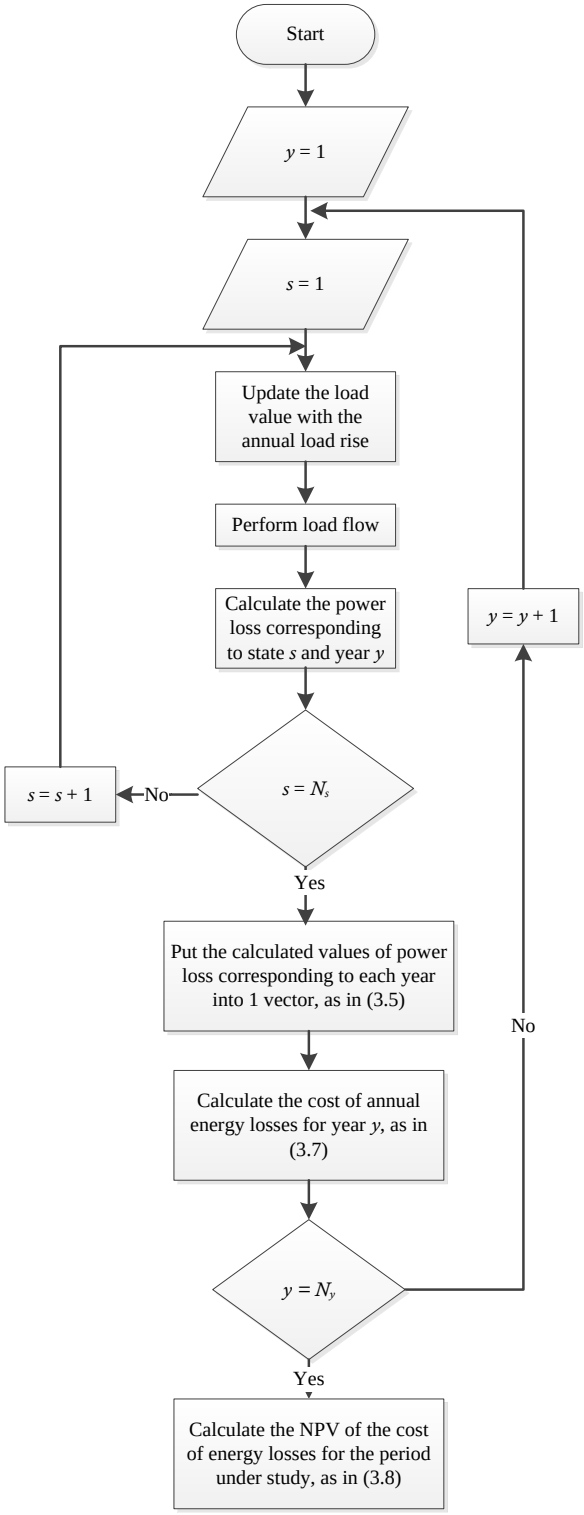

Figure 3.2 Evaluating the NPV of the cost of energy losses

$$C_{OUT(y,i)} = \frac{1}{N_{MCS}} \times P_{Load(i)}^{AVG} \times \sum_{z \in \mathcal{Z}_{(i)}} CDF(t_{OUT(z)}) \tag{3.9}$$

where

$C_{OUT(y,i)}$ is the outage cost of load point i in year y;

$CDF(t_{OUT(z)})$ is the outage cost corresponding to interruption event $z \in \mathcal{Z}_{(i)}$ with an outage duration of $t_{OUT(z)}$;

$\mathcal{Z}_{(i)}$ is the set of interruption events for load i;

$P_{Load(i)}^{AVG}$ is the average demand power for load point i.

In the above method of calculating the contribution of DG to the interruption cost of different types of customers, the CDF is assumed to be constant for specific outage duration. For example, the cost of a 2 h interruption is the same for a specific customer type whenever the 2 h interruption occurs during the day. To accurately express the effect of these DG units on the reduction in the cost of interruptions, the CDF has been modified to reflect an assumed dependency on the time of the interruption event. For example, an interruption event of 4 h at peak load costs more than a similar event at minimum load. The cost of an interruption for a specific load point can therefore be calculated as

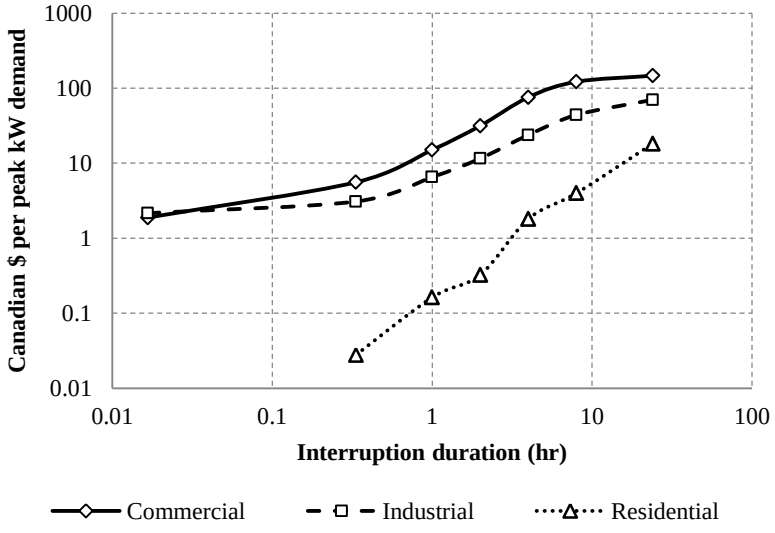

Figure 3.3 CDFs for different types of customers [108]

$$C_{OUT(y,i)} = \frac{1}{N_{MCS}} \times \sum_{z \in Z_{(i)}} \sum_{t=1}^{t_{OUT(z)}} \left(\frac{CDF(t_{OUT(z)})}{t_{OUT(z)}} \times P_{Load(i,t)}^{Actual} \right) \quad (3.10)$$

where $P_{Load(i,t)}^{Actual}$ is the actual load power at time t for load point i.

The procedure for calculating the cost of interruptions is as follows [102]:

1. Divide the system into segments based on the locations of the protective devices, as in [109].
2. For each segment, perform steps 3 to 11.
3. Define two sets: set (1), which includes all elements outside the segment whose failure has caused the power outage to that segment, and set (2), all elements within the segment whose failure has caused the outage to all load points within that segment.
4. Generate a two-state model for each element within the two sets using the failure rate and repair time for each element, and then combine these models to construct a two-state model for each set.
5. Repeat steps 6 to 10 for each year in the period under study.
6. If no dispatchable DG units are installed within the segment, go to step 9.
7. If the percentage of dispatchable DG units within the segment is below the dispatchable share threshold, deactivate all renewable DG units within the segment. This threshold is not yet defined in the standards [96], and for this work, it is assumed to be 60 %.
8. For each outage event in set (1), determine whether the islanding is successful or not. No standard yet exists with respect to the reserve margin required within the island because it is dependent on the variability and magnitude of the load, reliability requirements, and types and availability of DG units [96]. It is therefore assumed that the island is successful if the sum of the output power generated from all DG units within the segment is greater than or equal to a specific percentage of the required load power that represents load requirements, system losses, and the reserve margin. For dispatchable DG units only, this percentage is assumed to be 110 %; when both renewable and dispatchable DG units are connected to the system, the percentage is 115 % because an excess reserve margin is required due to the variability and uncertainty associated with renewable DG units. The outage event in set (1) is therefore modified to up time for successful islanding or left as down time for unsuccessful islanding.
9. Generate the final availability model for the segment under study from the convolution of set (1) and set (2).

10. Calculate the cost of the interruption using (3.10).
11. Calculate the NPV of the cost of interruption NPV_{INT}, as follows:

$$NPV_{INT} = \sum_{y} \frac{\sum_{i \in \mathcal{I}} C_{OUT(y,i)}}{(1+d')^{y}} \tag{3.11}$$

3.4.2 Problem formulation

For a determination of the effects of the installation of DG units with respect to system upgrades, energy losses, and reliability, typical costs in Canadian dollars are used for each individual objective. The next subsection explains how a GA is utilized as a means of finding the optimal sizes and locations of DG units in order to minimize the objective function. For simplicity, the DG units are assumed to have been placed in the first year of the study. The proposed planning problem is thus mixed-integer nonlinear programming that can be described by (3.12). The costs included in (3.12) are defined in (3.4), (3.8), (3.11), and (3.13).

$$\begin{gathered} \min_{\Omega} \left(NPV_{Upgrade} + NPV_{Loss} + NPV_{INT} - NPV_{INC} \right) \\ s.t. \ \text{(3.14) - (3.28)} \end{gathered} \tag{3.12}$$

$$NPV_{Upgrade} = NPV_{Lines} + NPV_{meter} + NPV_{CB} \tag{3.13}$$

where

Ω denotes the vector of decision variables;

NPV_{INC} is the NPV of the monetary incentives;

$NPV_{Upgrade}$ is the corresponding NPV of the total upgrades required;

NPV_{meter} is the NPV of upgrading the metering equipment at the substation;

NPV_{CB} is the NPV of the protection switch gear upgrades.

The incentives included in (3.12) are assumed to be the monetary amounts received by the LDC for each renewable MW connected to the system [102] and are not considered in the case study presented. The problem constraints can be described as follows:

1. Power flow constraints:

$$P_{G(i,s,y)} - P_{L(i,s,y)} = \sum_{j \in \mathcal{J}} V_{(i,s,y)} V_{(j,s,y)} Y_{(i,j,y)} \cos\left(\theta_{(i,j,y)} + \delta_{(j,s,y)} - \delta_{(i,s,y)}\right) \ \forall i, s, y \tag{3.14}$$

$$Q_{G(i,s,y)} - Q_{L(i,s,y)} = -\sum_{j\in J} V_{(i,s,y)} V_{(j,s,y)} Y_{(i,j,y)} \sin\left(\theta_{(i,j,y)} + \delta_{(j,s,y)} - \delta_{(i,s,y)}\right) \ \forall i,s,y \quad (3.15)$$

where

$P_{L(i,s,y)}$ and $Q_{L(i,s,y)}$ are the active and reactive power demands at bus i corresponding to state s and year y;

$P_{G(i,s,y)}$ and $Q_{G(i,s,y)}$ are the active and reactive powers generated at bus i corresponding to state s and year y;

$V_{(i,s,y)}$ and $\delta_{(i,s,y)}$ denote the per unit magnitude and angle of the voltage;

$Y_{(i,j,y)}$ and $\theta_{(i,j,y)}$ are the per unit magnitude and angle of the Y-bus matrix admittance.

2. *Voltage limit constraints:* The voltage limit constraints are defined as follows:

$$V_{min} \leq V_{(i,s,y)} \leq V_{max} \quad \forall i,s,y \quad (3.16)$$

where V_{min} and V_{max} are the minimum and maximum allowable voltage limits in the systems, respectively.

3. *Constraints related to the discrete DG size:* The DG capacities connected at each bus are assumed to be discretized at a fixed step that is dependent on the type of DG:

$$P_{NGDG(i)} = a_{NGDG(i)} \times \mathscr{b}_{NGDG(i)} \times P_{NGDG}^{Step} \quad \forall i \quad (3.17)$$

$$P_{WDG(i)} = a_{WDG(i)} \times \mathscr{b}_{WDG(i)} \times P_{WDG}^{Step} \quad \forall i \quad (3.18)$$

where

$a_{NGDG(i)}$ and $a_{WDG(i)}$ are integer variables indicating the installed DG size as a multiple of a fixed step for the NGDG and WDG, respectively;

$\mathscr{b}_{NGDG(i)}$ and $\mathscr{b}_{WDG(i)}$ are binary variables indicating the decision to install NGDG and WDG units at bus i, respectively;

P_{NGDG}^{Step} and P_{WDG}^{Step} are the discretized steps for NGDG and WDG capacities, respectively.

4. *Load rise constraints:* In this work, the annual load rise is assumed to be an input value and to be constant, which is a typical assumption for this type of study [10]:

$$P_{L(i,s,y)} = P_{L(i,s,1)} \times (1+\alpha)^{y-1} \quad \forall i,s,y > 1 \tag{3.19}$$

$$Q_{L(i,s,y)} = Q_{L(i,s,1)} \times (1+\alpha)^{y-1} \quad \forall i,s,y > 1 \tag{3.20}$$

where α is the annual load rise.

5. *Maximum reverse power flow constraints:* The maximum allowable DG penetration is the penetration that causes the maximum reverse power flow for the minimum loading condition. In this study, the minimum loading condition occurs at y = 1. According to [110], the maximum reverse active power flow is limited to 60 % of the main substation rating:

$$\sum_{i \in \mathcal{I}} \left(P_{NGDG(i)} + P_{WDG(i)} - \min_{s} \left(P_{L(i,s,1)} \right) \right) \leq P_{MAX}^{Rev} \tag{3.21}$$

where P_{MAX}^{Rev} denotes the allowable limit of reverse power flow at the substation.

6. *Limit on the number of DG units:* The number of DG units installed in the system during the planning horizon is assumed to be limited to a maximum value, as follows:

$$\sum_{i \in \mathcal{I}} \mathscr{b}_{NGDG(i)} \leq M_{NGDG}^{Limit} \tag{3.22}$$

$$\sum_{i \in \mathcal{I}} \mathscr{b}_{WDG(i)} \leq M_{WDG}^{Limit} \tag{3.23}$$

where M_{NGDG}^{Limit} and M_{WDG}^{Limit} are the maximum number of DG units installed in the system for NGDG and WGD, respectively.

7. *Candidate bus constraints:* DG units are permitted to be connected only at the candidate buses, depending on the type of DG and the system:

$$a_{NGDG(i)}, \mathscr{b}_{NGDG(i)} = 0 \quad \forall i \in \mathcal{I} - \mathcal{I}_{NGDG} \tag{3.24}$$

$$a_{WDG(i)}, \mathscr{b}_{WDG(i)} = 0 \quad \forall i \in \mathcal{I} - \mathcal{I}_{WDG} \tag{3.25}$$

where $\mathcal{I}_{NGDG} \subset \mathcal{I}$ and $\mathcal{I}_{WDG} \subset \mathcal{I}$ are sets of candidate buses for NGDG and WDG, respectively.

8. *Constraints related to the maximum bus connection:* The maximum capacity of the DG connection to any individual bus is limited based on the voltage level and on the technical constraints associated with the LDC:

$$P_{NGDG(i)} + P_{WDG(i)} \leq P_{DG(i)}^{limit} \qquad \forall i \tag{3.26}$$

where $P_{DG(i)}^{limit}$ is the maximum limit of the connected DG capacity at bus i.

9. *Feeder upgrade constraints*: In this study, substation transformers are assumed to be redundant, which is the common practice in Ontario, Canada. As shown in (3.27), the upgrade costs depend on the upgrade year for each feeder, with the feeder upgrade cost being based on reinforcing that feeder with an additional one. The feeder upgrade constraints can therefore be described as follows:

$$I_{(l,s,y)} \leq I_{MAX(l,y)} \;\; \forall l, s \in \mathcal{S}_{eff(l)}, y \tag{3.27}$$

$$I_{MAX(l,y)} = \begin{cases} I_{(l)}^{CAP} & \forall y < Y_{UP(l)} \\ M_{(l)}^{RNF} \times I_{(l)}^{CAP} & \forall y \geq Y_{UP(l)} \end{cases} \qquad \forall l, y \tag{3.28}$$

where

$I_{(l,s,y)}$ denotes the magnitude of the current for state s and year y flowing in line l;

$I_{MAX(l,y)}$ denotes the maximum allowable current in line l in year y;

$\mathcal{S}_{eff(l)}$ is the set of all considered states that contribute to the upgrade of line l, which can be generated using the algorithm in Figure 3.1;

$I_{(l)}^{CAP}$ denotes the current-carrying capacity of line l;

$M_{(l)}^{RNF}$ is a multiplier that denotes the reinforcement of the line at year $Y_{UP(l)}$ and also indicates that the line require no further upgrading during the remainder of the planning period.

3.4.3 Genetic algorithm implementation

Due to the complexity of the planning problem, a meta-heuristic optimization technique is utilized, as described in this subsection. This family of techniques has been proven to be effective for solving a

number of complicated practical problems, such as DG planning [45], unit commitment [111], and economical dispatch [112]. The planning problem presented in this chapter utilizes a GA, which is a population-based searching algorithm. The population consists of chromosomes, each of which is comprised of a number of genes.

For radial distribution systems, the number of genes corresponding to decision variable vector Ω is selected to be a multiple of the number of candidate buses based on the types of DG units to be installed. For example, when two types of DG units are considered in the allocation problem, such as NGDG and WDG, each chromosome in the population consists of a vector whose length is equal to four times the number of candidate buses, as shown in Figure 3.4. Each candidate bus is represented by four genes, as indicated by the shading in Figure 3.4. Two genes carry binary values that denote the decision about installing each of the two types of DG units at the corresponding bus. The other two genes carry integer values that indicate, for each DG type, the capacity of the corresponding DG units as a multiple of a defined step.

In contrast, for mesh distribution networks, which involve more than one decision for line upgrades, the chromosome should include two additional genes for each line in the system, as shown in Figure 3.4. The first gene carries a binary value that represents the decision about upgrading the corresponding line. The second gene carries an integer value that denotes the year of the upgrade. For each iteration, the fitness of each individual in the population is evaluated. This fitness value represents the total cost of the objective(s) considered in the objective function described in (3.12).

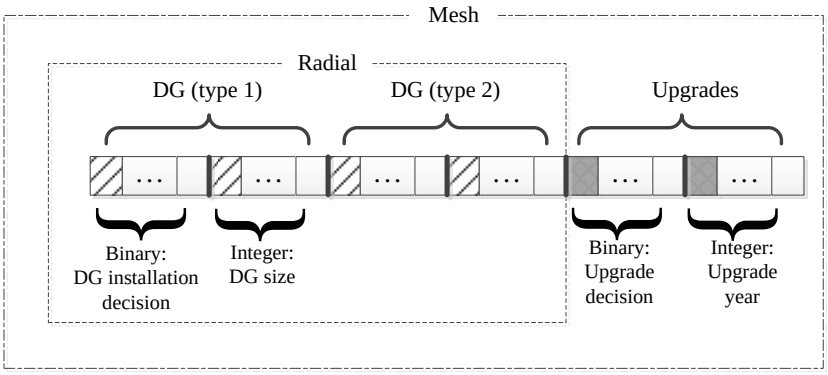

Figure 3.4 Structure of a typical chromosome in the proposed planning problem

3.5 Sample case study

The distribution system considered for the case study is the one described in [113], which contains a mix of residential, commercial, and industrial customers supplied from a common supply point, in a

manner similar to the Canadian distribution, as shown in Figure 3.5. The system data and types of customers are listed in Appendix A. The total system peak load is 4.37 MVA divided into five segments [109]. Candidate DG bus locations are determined based on detailed planning analysis that includes technical, environmental, and economic studies. The results of the analysis are assumed as input but are beyond the scope of the work presented in this thesis. The candidate buses were selected for the case study on a totally arbitrary basis and are located as shown in Figure 3.5. The location of the candidate buses implies that islanding is effective in reducing the cost of interruptions only for segments 3 and 5.

For the purposes of the technical evaluation of the effect of the DG units on reliability, the expected energy not served (EENS) of the system is evaluated as given in [105]. The maximum number of each type of DG unit in the system M_{NGDG}^{Limit} and M_{WDG}^{Limit} is five, as specified in (3.22) and (3.23). Four different cases are included: the base case, NGDG, WDG, and a mix of both types of DG. Each case includes a variety of scenarios. The objective and *RF* for each scenario are listed in Table 3.4. The outcomes of the allocation problem for a 20 year study period are shown in Figure 3.6. For each scenario included in Table 3.4, Table 3.5 provides details based on typical prices in Canadian dollars. The costs of interruption in [108] are used in this study; however, they are updated by a factor of 140.88 % to reflect the inflation rate from 1994 to 2013 according to Bank of Canada statistics [114]. For NPV calculations, the discount and inflation rates are assumed to be 9.15 % [40] and 1.8 %, respectively.

Table 3.4 Scenario descriptions

Case	DG type	Scenario	Objective(s)	*RF*
A	No DG	*A.0*	None	0
B	NGDG	*B.1*	UG	
		B.2	EL	
		B.3	INT	
		B.4	UG+EL+INT	
C	WDG	*C.1.a*	UG	3/8760
		C.1.b		6/8760
		C.2	EL	3/8760
		C.3	UG+EL	
D	NGDG and WDG	*D.1*	UG	
		D.2	EL	
		D.3	INT	
		D.4	UG+EL+INT	

* UG: Cost of upgrades, EL: Cost of energy losses, INT: Cost of interruptions

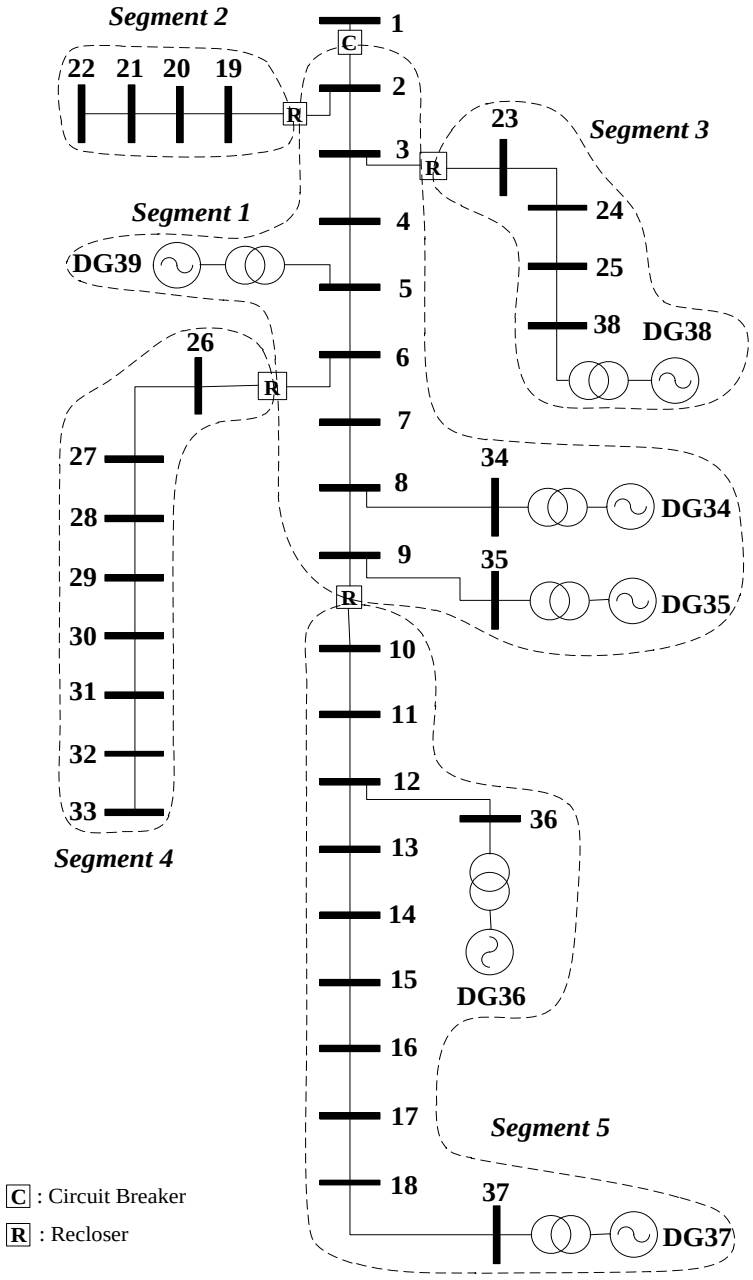

Figure 3.5 System under study

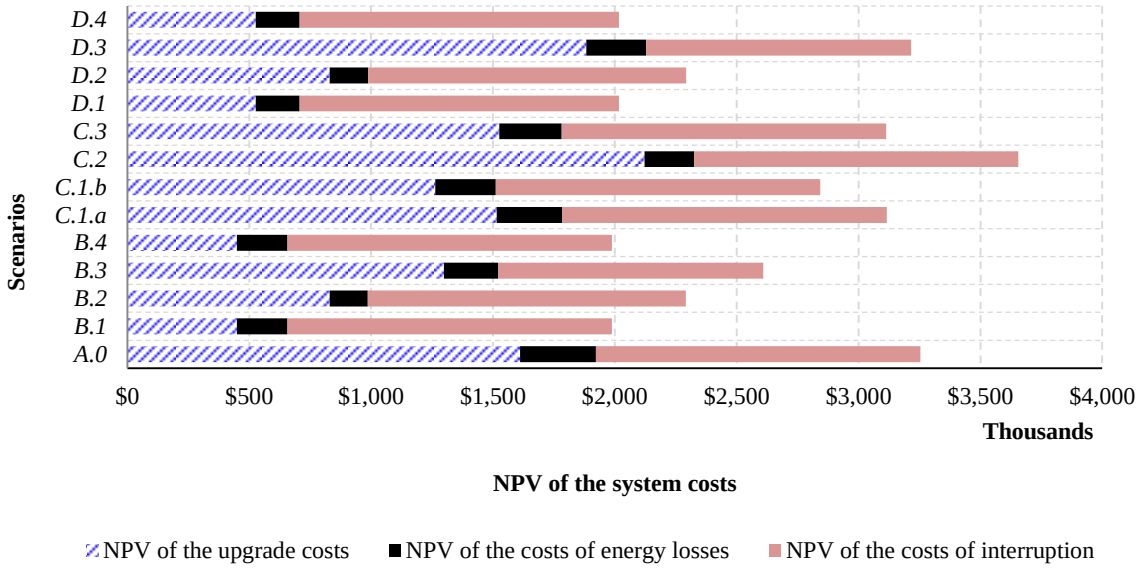

Figure 3.6 Scenario results

3.5.1 Base case results

For the base case defined by scenario (*A*.0), the total cost of system upgrades, energy losses, and interruptions is $3.254 M. The share attributable to system upgrades is 49.53 %, to energy losses is 9.565 %, and to interruptions is 40.90 %. These costs are system dependent, and upgrade costs represent the greatest percentage; however, the impact of each type of cost is dependent on the savings that can be obtained, as described for subsequent cases.

3.5.2 Dispatchable DG results

The next four scenarios illustrate the results obtained when dispatchable DG units are allocated in the system under study, which is denoted case (*B*); the objective of each scenario is shown in Table 3.4. For scenario (*B*.1), the results were found to be at the boundary of upgrading the protection and metering equipment because increasing any DG unit size beyond the values obtained triggers an upgrade to this equipment, which increases the total cost of the required upgrades. The reduction in the cost of upgrades is 72.1 %, which is highly significant. However, for a lower value of discount rate, the effect of deferring the investments becomes less significant, as the NPV of the investments increases. For example, the total cost for scenarios (*A*.0) and (*B*.1) are $3.968 M and $2.578 M respectively, for a discount rate of 6 %, i.e., $d = 0.06$. The total savings are 35.04 % compared to

38.91 % with $d = 0.0915$, which shows that the percentage reduction decreases for a lower discount rate.

The upgrade cost savings are due to the deferral of most of the line upgrades to later years. For example, the line between buses 3 and 23 in the base case needed to be upgraded in the third year; however, in scenario (*B*.1), the upgrade is deferred to the 19th year. The cost of energy losses is reduced by 33.4 %, which represents a positive result, although it is not the objective in this scenario. On the other hand, the cost of interruptions is unaffected because DG units 36, 37, and 38 affect the cost of interruptions only in segments 3 and 5, as indicated in Figure 3.5. The outcomes with scenario (*B*.1) also show small capacities at these locations, which have no effect on interruptions, as shown by the results. The total percentage saved is 38.91 %, which effectively demonstrates that the proposed methodology can significantly reduce system costs.

With scenario (*B*.2), the cost of energy losses is reduced by 49.7 %, and the cost of upgrades is reduced by 48.5 %, while the cost of interruptions is affected only slightly. This slight reduction is due to the higher capacities of the DG units in segments 3 and 5 than with the previous scenario. However, the reduction in the cost of interruptions is still almost negligible, because this factor is not the objective in this scenario. The percentage saved is 29.6 %, which indicates that, with this scenario, the cost of upgrades is more significant because the total savings are greater than with scenario (*B*.1).

For scenario (*B*.3), because of the technical limitations associated with the DG units in segments 3 and 5 and the fact that the DG units in other segments have no effect on the cost of interruptions, there may be infinite solutions that provide the minimum cost of interruptions. Thus, the solution presented represents the minimum penetration solution. The result is that the outcomes of the planning problem show installed DG units only in segments 3 and 5. It is important to note that the cost of interruptions in segments 3 and 5 cannot be reduced to zero because only outages due to the failure of set (1) elements are affected by islanding, while outages due to set (2) element failures are unavoidable, as explained earlier in this chapter. The percentage saved with respect to the cost of interruptions is 18.3 %, which corresponds to an EENS reduction from 13,855 to 11,561 kWh/yr. In contrast, the savings in the costs of upgrades and energy losses are 19.4 % and 28.5 %, respectively. It should be further noted that any increase in the size of the DG units does not affect the cost of interruptions because no additional reductions can be achieved. The total percentage saved is about 19.8 %, which confirms that the cost of interruptions is the least significant cost in the case under study. These results are indeed system dependent.

In scenario (*B*.4), the objective is to minimize the three costs under consideration. The results are the same as for scenario (*B*.1) and indicate that for the case under study, the cost of upgrades is the most dominant type of cost. However, if the discrete size constraints incorporated in (3.17) and (3.18) are relaxed, scenario (*B.4*) produces slightly better results than scenario (*B.1*).

All the mentioned NPVs are the expected costs to occur during the planning period. However, these costs have a pdf that describes their probability distribution. Figure 3.7 shows the cumulative distribution function that describes the probabilities of the total cost NPVs for scenarios (*A*.0) and (*B*.4). As shown in Figure 3.7, the mean and the minimum of the total system cost are reduced in scenario (*B*.4) compared to scenario (*A*.0) as a result of the optimal DG allocation.

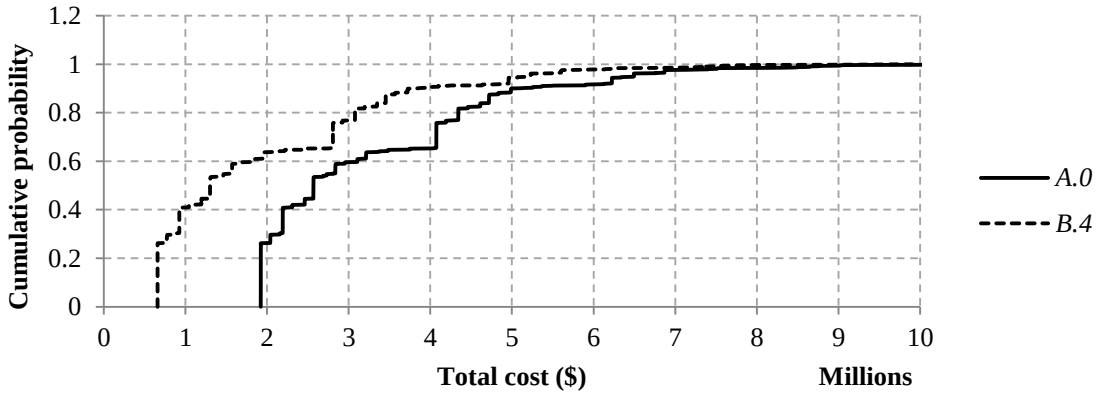

Figure 3.7 Cumulative distribution function of the total system cost

3.5.3 WDG results

In this case, only WDG units are considered, so the cost of interruptions is unaffected because the percentage of dispatchable DG units in the system is lower than the 60 % threshold, as explained earlier.

For the case under study, the outcomes of the allocation problem for the cost of upgrades at a zero *RF* are found to converge to the base case without DG units. A zero *RF* means that all combined wind and load states are considered regardless of the associated probability because the LDC is unwilling to risk overloading their lines. Based on this result, if the *RF* is taken to be zero, the variability and uncertainty associated with WDG result in equal or higher upgrade costs compared to the case without DG, as explained in section 3.4. In the subsequent scenarios, which are characterized by a non-zero *RF*, the *RF* defines the risk of overloading the system. This risk arises from the neglecting of one or more states that contribute most to the reinforcement requirements. For this

study, the *RF* was assigned a number of values (scenarios *C.1.a* and *C.1.b*), as can be seen in Table 3.5 (b).

Table 3.5 Detailed results for each scenario

(a) Results for cases (*A*) and (*B*)

DG type		**No DG**	**Dispatchable**			
Scenario		***A.0***	***B.1***	***B.2***	***B.3***	***B.4***
Objective			**UG**	**EL**	**INT**	**UG + EL + INT**
DG units (MW) installed at candidate buses	DG 34	0.0	0.5	0.3	0	0.5
	DG 35	0.0	0.0	0.0	0	0.0
	DG 36	0.0	0.0	0.2	0.6	0.0
	DG 37	0.0	0.1	0.2	0	0.1
	DG 38	0.0	0.2	0.4	1.1	0.2
	DG 39	0.0	0.1	0.9	0	0.1
Total penetration (MW)		**0.0**	**0.9**	**2.0**	**1.7**	**0.9**
NPV of cost of system upgrades	Line upgrades ($)	1,611,533	449,572	489,515	1,199,013	449,572
	Metering upgrades ($)	0	0	40,000	40,000	0
	Protection upgrades ($)	0	0	300,000	60,000	0
	Total ($)	**1,611,533**	**449,572**	**829,515**	**1,299,013**	**449,572**
	% saved	**0.00 %**	**72.10 %**	**48.53 %**	**19.39 %**	**72.10 %**
NPV of cost of energy losses	**Cost ($)**	311,190	207,187	156,597	222,339	207,187
	% saved	**0.00 %**	**33.42 %**	**49.68 %**	**28.55 %**	**33.42 %**
NPV of cost of interruptions	Segment 1 ($)	211,540	211,540	211,540	211,541	211,541
	Segment 2 ($)	67,227	67,227	67,227	67,227	67,227
	Segment 3 ($)	374,568	374,568	366,029	265,414	374,569
	Segment 4 ($)	431,081	431,081	431,081	431,082	431,082
	Segment 5 ($)	246,413	246,413	229,934	111,903	246,414
	Total ($)	**1,330,829**	**1,330,829**	**1,305,811**	**1,087,167**	**1,330,832**
	% saved	**0.00 %**	**0.00 %**	**1.88 %**	**18.31 %**	**0.00 %**
Average annual EENS (kWh/yr)		13,855	13,855	13,261	11,561	13,855
Total cost ($)		**3,253,552**	**1,987,588**	**2,291,923**	**2,608,519**	**1,987,591**
% of total savings		**0.00 %**	**38.91 %**	**29.56 %**	**19.83 %**	**38.91 %**
UG share of cost savings		**0.00 %**	**35.71 %**	**24.04 %**	**9.61 %**	**35.71 %**
EL share of cost savings		**0.00 %**	**3.20 %**	**4.75 %**	**2.73 %**	**3.20 %**
INT share of cost savings		**0.00 %**	**0.00 %**	**0.77 %**	**7.49 %**	**0.00 %**

(b) Results for case (*C*)

DG type		**WDG**			
Scenario		***C.1.a***	***C.1.b***	***C.2***	***C.3***
Objective		**UG** ***RF* = 3/8760**	**UG** ***RF* = 6/8760**	**EL**	**UG + EL**
DG units (MW) installed at candidate buses	DG 34	0.0	0.3	0.4	0.2
	DG 35	0.0	0.0	0.0	0.0
	DG 36	0.0	0.0	0.3	0.1
	DG 37	0.2	0.2	0.3	0.2
	DG 38	0.5	0.6	0.7	0.2
	DG 39	0.0	0.0	1.3	0.0
Total penetration (MW)		**0.7**	**1.1**	**3.0**	**0.7**
NPV of cost of system upgrades	Line upgrades ($)	1,515,014	1,262,909	1,781,822	1,526,419
	Metering upgrades ($)	0	0	40,000	0
	Protection upgrades ($)	0	0	300,000	0
	Total ($)	**1,515,014**	**1,262,909**	**2,121,822**	**1,526,419**
	% saved	**5.99 %**	**21.63 %**	**-31.66 %**	**5.28 %**
NPV of cost of energy losses	**Cost ($)**	270,204	249,095	203,197	256,249
	% saved	**13.17 %**	**19.95 %**	**34.70 %**	**17.66 %**
NPV of cost of interruptions	Segment 1 ($)	211,540	211,540	211,540	211,540
	Segment 2 ($)	67,227	67,227	67,227	67,227
	Segment 3 ($)	374,568	374,568	374,568	374,568
	Segment 4 ($)	431,081	431,081	431,081	431,081
	Segment 5 ($)	246,413	246,413	246,413	246,413
	Total ($)	**1,330,829**	**1,330,829**	**1,330,829**	**1,330,829**
	% saved	**0.00 %**	**0.00 %**	**0.00 %**	**0.00 %**
Average annual EENS (kWh/yr)		13,855	13,855	13,855	13,855
Total cost ($)		**3,116,050**	**2,842,836**	**3,655,851**	**3,113,500**
% of total savings		**4.23 %**	**12.62 %**	**-12.36 %**	**4.30 %**
UG share of cost savings		**2.97 %**	**10.72 %**	**-15.68 %**	**2.62 %**
EL share of cost savings		**1.26 %**	**1.91 %**	**3.32 %**	**1.69 %**
INT share of cost savings		**0.00 %**	**0.00 %**	**0.00 %**	**0.00 %**

(c) Results for case (*D*)

DG type		**WDG and NGDG**							
Scenario		***D.1***		***D.2***		***D.3***		***D.4***	
Objective		**UG**		**EL**		**INT**		**UG + EL + INT**	
		NGDG	**WDG**	**NGDG**	**WDG**	**NGDG**	**WDG**	**NGDG**	**WDG**
Installed DG units (MW) at candidate buses	DG 34	0.2	0.0	0.2	0.0	0.0	0.0	0.2	0.0
	DG 35	0.1	0.4	0.0	0.2	0.0	0.0	0.1	0.4
	DG 36	0.2	0.0	0.2	0.0	0.4	0.4	0.2	0.0
	DG 37	0.1	0.0	0.2	0.0	0.2	0.2	0.1	0.0
	DG 38	0.3	0.1	0.3	0.2	1.1	0.5	0.3	0.1
	DG 39	0.0	0.1	0.6	0.7	0.0	0.1	0.0	0.1
Total penetration (MW)		**0.9**	**0.6**	**1.5**	**1.1**	**1.7**	**1.2**	**0.9**	**0.6**
NPV of cost of system upgrades	Line upgrades ($)	426,337		489,515		1,663,194		426,337	
	Metering upgrades ($)	40,000		40,000		40,000		40,000	
	Protection upgrades ($)	60,000		300,000		180,000		60,000	
	Total ($)	**526,337**		**829,515**		**1,883,194**		**526,337**	
	% saved	**67.34 %**		**48.53 %**		**-16.86 %**		**67.34 %**	
NPV of cost of energy losses	**Cost ($)**	**179,967**		**157,563**		**245,091**		**179,967**	
	% saved	**42.17 %**		**49.37 %**		**21.24 %**		**42.17 %**	
NPV of cost of interruptions	Segment 1 ($)	211,541		211,541		211,541		211,541	
	Segment 2 ($)	67,227		67,227		67,227		67,227	
	Segment 3 ($)	366,030		366,030		265,414		366,030	
	Segment 4 ($)	431,081		431,081		431,081		431,081	
	Segment 5 ($)	235,011		229,935		111,903		235,011	
	Total ($)	**1,310,890**		**1,305,813**		**1,087,166**		**1,310,890**	
	% saved	**1.50 %**		**1.88 %**		**18.31 %**		**1.50 %**	
Average annual EENS (kWh/yr)		13,382		13,379		12,069		13,382	
Total cost ($)		**2,017,194**		**2,292,891**		**3,215,451**		**2,017,194**	
% of total savings		**38.00%**		**29.53%**		**1.17%**		**38.00%**	
UG share of cost savings		**33.35 %**		**24.04 %**		**-8.35 %**		**33.35 %**	
EL share of cost savings		**4.03 %**		**4.72 %**		**2.03 %**		**4.03 %**	
INT share of cost savings		**0.61 %**		**0.77 %**		**7.49 %**		**0.61 %**	

In scenario (*C.1.a*), the *RF* value is taken to be 3 h per year. The outcomes of the allocation problem show a savings of 6 % with respect to upgrade costs, while the percentage saved in the cost of energy losses is 13.2 %. In scenario (*C.1.b*), the objective is still the minimization of the upgrade costs. The *RF* value is taken to be 6 h per year; the cost of upgrades is further reduced by 21.6 %. It can also be observed that, as the *RF* increases, the cost of upgrading decreases correspondingly. In other words, as the LDC increases the risk of overloading their lines due to the stochastic nature of renewable DG units, the cost of expected upgrades declines, as shown in Figure 3.8, where the results of scenario (*C.1.b*) are reiterated for different values of *RF*. The results also reveal that the reduction in the upgrade costs is not uniform but is dependent on wind pattern, the load curve, and the system under study. On the other hand, if the renewable DG units are represented by constant DG output power, the outcomes of the allocation problem are considered to be misleading because the inherent risk of overloading system lines is not reflected.

Therefore, for the sake of comparison, the capacity credit equivalent for wind DG units is used for the calculation of the upgrade costs, as used traditionally in evaluating the upgrade costs [34]. As shown in Figure 3.8, modeling the wind DG units with a 30 % capacity credit is equivalent to a risk of almost 44 h of overloading per year. These results demonstrate the value of the proposed methodology for providing a superior assessment of system upgrades in the presence of renewable DG connections. The LDC can thus define the *RF* according to its preference, which allows the renewable DG to contribute to a reduction in the system upgrade costs within a predefined level of risk.

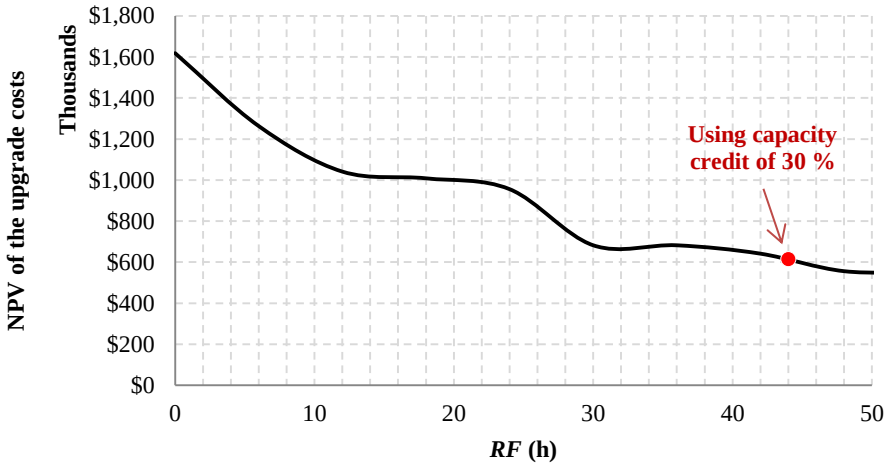

Figure 3.8 Relation of upgrade costs with the *RF*

For scenario (*C.2*), with an *RF* of 3 h per year, the cost of energy losses is reduced by 34.7 %, while the cost of upgrades is higher than the base case by 31.7 %. The increase in the upgrade costs is due to the objective in this scenario, which is to minimize energy losses only. A comparison of scenario (*C.2*) with scenario (*B.2*) makes it clear that the variability and uncertainty associated with WDG result a smaller reduction in energy losses than that associated with dispatchable DG units.

As well, to demonstrate the importance of including consideration of the variable hourly cost of energy in the renewable DG planning problem, the results of scenario (*C.2*) can be compared to the approaches previously proposed in [11, 18, 38, 42, 43], which provide examples of the traditional technique in which the energy losses or the cost of the energy losses is minimized based on a fixed energy price. As shown in Table 3.6, the results obtained using a variable hourly energy cost show an NPV of $0.203 M for energy losses. On the other hand, the NPV of the cost of energy losses for the same DG configuration from scenario (*C.2*) was found to be $0.193 M, based on the average energy cost. This result is 4.9 % lower than the result produced in the case with a variable cost, which proves that assuming an average energy cost in renewable DG planning problems may result in inaccurate outcomes because the effect of renewable DG on system losses is not uniform over time and may be concentrated during periods of low or high energy costs.

Table 3.6 Scenario (*C.2*) results based on variable and fixed hourly energy prices

DG type		**WDG**	
Scenario		***C.2***	
Objective		**Cost of energy losses**	
DG units (MW) installed at candidate buses	DG 34	0.4	
	DG 35	0.0	
	DG 36	0.3	
	DG 37	0.3	
	DG 38	0.7	
	DG 39	1.3	
Energy prices		Variable as in Table 3.5 (b)	Fixed
Total penetration (MW)		**3.0**	**3.0**
NPV of the cost of energy losses ($)		**203,197**	**193,202**
% saved compared to base case		**34.70 %**	**37.9 %**

For scenario (*C.3*), the total percentage saved with respect to the costs of upgrades and energy losses is 4.3 %, which is slightly higher than for scenario (*C.1.a*), in which the percentage saved in the cost of upgrades is 5.29 % and the percentage saved in the cost of energy losses is 17.66 %. A comparison of the outcomes produced with the different case (*C*) scenarios reveals that, for WDG units, the most significant reduction is in the cost of energy losses, despite the risk of overloading system lines. The stochastic nature of renewable DG units limits their ability to reduce the cost of upgrades and energy losses; however, the effect of the reduction in upgrade costs on the total savings is the most due to impact of the *RF*.

3.5.4 Dispatchable and WDG results

In case (*D*), dispatchable and WDG units are considered. Due to the superiority of dispatchable DG relative to WDG with respect to minimizing the costs under consideration, the optimization outcome converges to the results from case (*B*), in which only dispatchable DG units are deployed. Therefore, to ensure that the integration of renewable DG is included in the problem, a minimum of 40 % renewable DG capacity is assumed to be installed. In other words, the capacities of the wind DG units should be at least two-thirds of the capacities of the dispatchable DG units installed in the system. Accordingly, the following green energy constraint is added to the constraints included in (3.29):

$$\sum_{i\in\mathcal{I}} P_{WDG(i)} \geq \frac{2}{3} \times \sum_{i\in\mathcal{I}} P_{NGDG(i)} \tag{3.29}$$

Another way to increase WDG penetration is to add a monetary value incentive in the objective function from (3.12) in order to mimic the actual incentives the LDC receives from the government for each MW of renewable DG capacity installed in their system. With scenario (*D.1*), the percentage saved with respect to the cost of upgrades is 67.34 %, which is lower than with scenario (*B.1*) due to the green energy constraint included in (3.29). The total capacity of the wind DG units is 0.6 MW, which is exactly two-thirds of the total capacity of the dispatchable DG units. This result shows that the system is at the boundary of the limits imposed by the green energy constraint. In fact, if this constraint is relaxed, the outcomes of the planning problem include only dispatchable DG units, as mentioned previously. With scenario (*D.2*), the reduction in the cost of energy losses is 49.4 %, which is close to the savings produced with scenario (*B.2*) but with higher DG capacities connected to the system. This result indicates that a mix of dispatchable and renewable

DG units in the system can have almost the same effect on annual energy losses, but when both types of DG are considered, higher capacities are entailed as a consequence of the capacity factor of the renewable DG units [18].

In scenario (*D.3*), the objective function is the cost of interruptions. Although the total DG capacity connected to the system with scenario (*D.3*) is greater than that with scenario (*B.3*), the maximum savings with respect to interruption costs are lower due to the intermittent effect of WDG units, which limits their contribution to the reduction in interruption costs.

The difference between the use of a time-independent CDF in (3.9) and a time-dependent CDF in (3.10) was also evaluated. As described in subsection 3.2.1 but using (3.9) rather than (3.10), the same DG configuration employed with scenario (*D.3*) is used for the calculation of the NPV of the cost of interruptions based on a time-independent CDF. The NPV of the cost of interruptions is \$1.087 M for scenario (*D.3*) when a time-dependent CDF is used, as shown in Table 3.5 (c). On the other hand, for the same DG configuration, the cost of interruptions was found to be lower by only 1 % when a time-independent CDF is used. This result is attributable to the effect of the incorporation of wind DG on the cost of interruptions, which is concentrated during periods characterized by low load requirements. In the sample case, the difference between the two methods is insignificant for two reasons: 1) the cost of interruptions in the system under study is insignificant, and 2) the DG configuration used in the comparison tends to saturate the cost of interruptions, which is minimized according to the objective of scenario (*D.3*). Although the difference between the two methods is almost negligible, it might be significant for other systems. The recommendation is therefore to use a time-dependent CDF, which is assumed to provide a better assessment of the impact of DG on the cost of interruptions.

For scenario (*D.4*), in which the objective function contains all three of the previously mentioned costs, the outcomes are the same as for scenario (*D.1*), which demonstrates that the savings related to the cost of upgrades are still the most significant.

A comparison of scenario (*D.4*), for which the total savings are 38 %, with scenario (*B.4*), for which the total savings are 38.9 %, reveals that the savings provided by a mix of dispatchable and WDG units are slightly less than those resulting from the incorporation of dispatchable DG units alone. However, scenario (*B.4*) entails no risk of overloading system lines, while scenario (*D.4*) is associated with a risk of 3 h of overloading per year. Moreover, the system is able to accommodate higher DG capacities of 1.5 MW in scenario (*D.4*) compared to 0.9 MW in scenario (*B.4*).

The results presented in this section demonstrate the effectiveness of the proposed methodology for maximizing the benefits of incorporating renewable DG in distribution networks. The developed methodology also provides a more accurate means of evaluating the value of connecting renewable DG.

3.6 Conclusion

This chapter has presented a proposed GA-based, multi-objective optimization approach for the optimal allocation of a variety of types of DG units into a distribution system. The primary objective of the optimization is to maximize savings with respect to the deferral of investments in system upgrades, the cost of annual energy losses, and the cost of interruptions. The benefits of connecting DG to the system are represented in monetary terms as a means of facilitating the comparison and avoiding the use of weighting factors, which are usually questionable and may produce misleading results.

The proposed method is based on the generation of combined generation-load model, which addresses all possible operating conditions. The uncertainty inherent in the output from renewable DG units is taken into account in the model, as are load type and variability. Technical system constraints, protection equipment upgrades, metering equipment upgrades, and the cost of interruptions with respect to a variety of customer types are all considered.

With respect to the evaluation of upgrade requirements when a distribution system incorporates renewable DG, this work has also introduced an innovative approach involving the introduction of a new factor for representing the risk of overloading system lines.

The research has also resulted in the development of a new technique for incorporating the variable hourly cost of energy along a planning horizon, while limiting the computational complexity to the number of combined generation-load model states. This method is expected to provide a more accurate evaluation of the cost of energy losses in long-term planning problems, especially when renewable DG is connected.

Due to variations in the DG contribution to the outage events, a time-dependent CDF is utilized in this work as a means of achieving more accurate results with respect to the interruption cost because the effect of renewable DG units during islanding mode may vary according to the timing of outage events. The proposed planning technique has been applied for a number of scenarios involving a typical distribution system. The results reveal the effectiveness of the proposed long-term multi-objective allocation algorithm with respect to significantly reducing the types of costs

mentioned. However, it was shown that reducing the cost of upgrades is the most significant economic benefit, while the cost of interruption is the least significant.

All possible factors that can affect the costs are considered, which provides benefits for both the LDC and consumers. For the LDC, the use of a GA allows the determination of a satisfactory feasible solution to the planning problem in a timely manner, identifying the best locations in the system for connecting different types of DG units. The proposed method can be easily applied to any radial system, and a variety of incentives could be added to the planning problem based on the priorities of the LDC. The algorithm can also be applied to any type of DG unit. Dispatchable DG units are handled in the same manner as natural gas DG units, and renewable DG units are managed in the same way as WDG units. However, any differences that may arise must be taken into account in the modeling of each DG type.

Chapter 4
PEV Modeling

4.1 Introduction

The work presented in this chapter tackles the PEV modeling in power systems based on the current situation of the grid, where smart signals to charging locations are not yet available. The near future PEV charging mechanism is thus expected to be uncontrolled. For the electricity providers, the best time to charge the vehicles in their territory is typically at night, when normal load demand in minimum and low cost generating units are the marginal producers. The extra load due to vehicles charging is therefore met at low cost and without straining the existing transmission and distribution systems [115]. On the other hand, the preferred time for consumers is as soon as they return home from a trip, when the charging is most convenient, as the driver is already at the vehicle. In addition, the drivers will want their vehicles batteries to be as fully charged as possible whenever needed. This situation of the consumers is denoted as the uncontrolled charging scenario.

As charging process takes hours with level 2_R charger, it is not likely to be performed in charging stations. The PEV charging is thus assumed to occur at home in the work introduced in this chapter, where the chargers are assumed to be of level 0_{cc}, as shown in Table 2.2.

4.2 Modeling PEV charging for power flow analysis

Two models have been reported in the literature to model the PEV charging load for the power flow analysis. The first model represents the PEV charging load as a constant-power load, which is the most popular model in the literature. On the other hand, in the second model, the PEV charging load is modeled as a constant-current load [116-118]. The rationale for this model is that: most of the PEV charging is performed in a constant-current mode.

Therefore, to adopt the correct model, the following brief explanation is introduced. The PEV charging system consists of two converters: the AC/DC grid side converter, and the DC/DC battery side converter [119], as shown in Figure 4.1. The DC/DC converter controls the delivered power to the battery pack, which depends on the battery characteristics. On the other hand, the grid side converter maintains a constant DC link voltage and a constant power factor on the grid side, which is typically unity. Therefore, it is obvious that the delivered power to the battery pack is independent on the grid voltage due to the isolation via the power electronics converters. The PEV charging load is thus modeled as a constant-power load at unity power factor. With this assumption, a probabilistic

model for the charging power of a PEV fleet is explained in details in the next section.

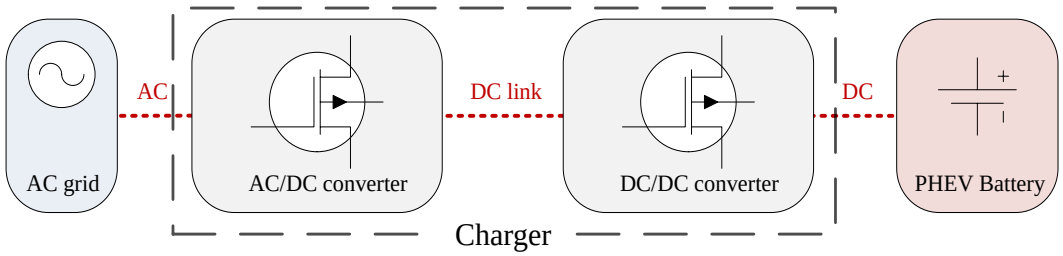

Figure 4.1 PEV battery charger [119]

4.3 Probabilistic model of uncontrolled PEV charging load

In this work, a novel annual model for the energy consumption of a LDF of PEVs is developed. MCS is utilized to generate this model, which includes consideration of:

- Driver habits by incorporating the trip purpose
- Diversity of usage from a vehicle to another
- Different trip mileage
- Different AER vehicles and charger ratings
- Ambient temperature effect

The proposed model mainly consists of two consecutive models: the travel pattern model and the energy consumption model, where the second model utilizes the outcomes of the first model. Figure 4.2 shows the proposed model, where the details are described in the next subsections.

4.3.1 Travel Pattern Model

The output of this model can be described as the covered distances by finished trips for each time segment. To incorporate the driving habits of the vehicles users, the model takes into consideration the purpose of the trip, e.g., commuting, education, holiday trip, etc. MCS is utilized to generate virtual trip distances for each purpose to cover the diversity in usage. The outcomes of the hourly trip model are further utilized in the next subsection for energy consumption model. The model consists of six stages, which are illustrated in Figure 4.2 and outlined as follows:

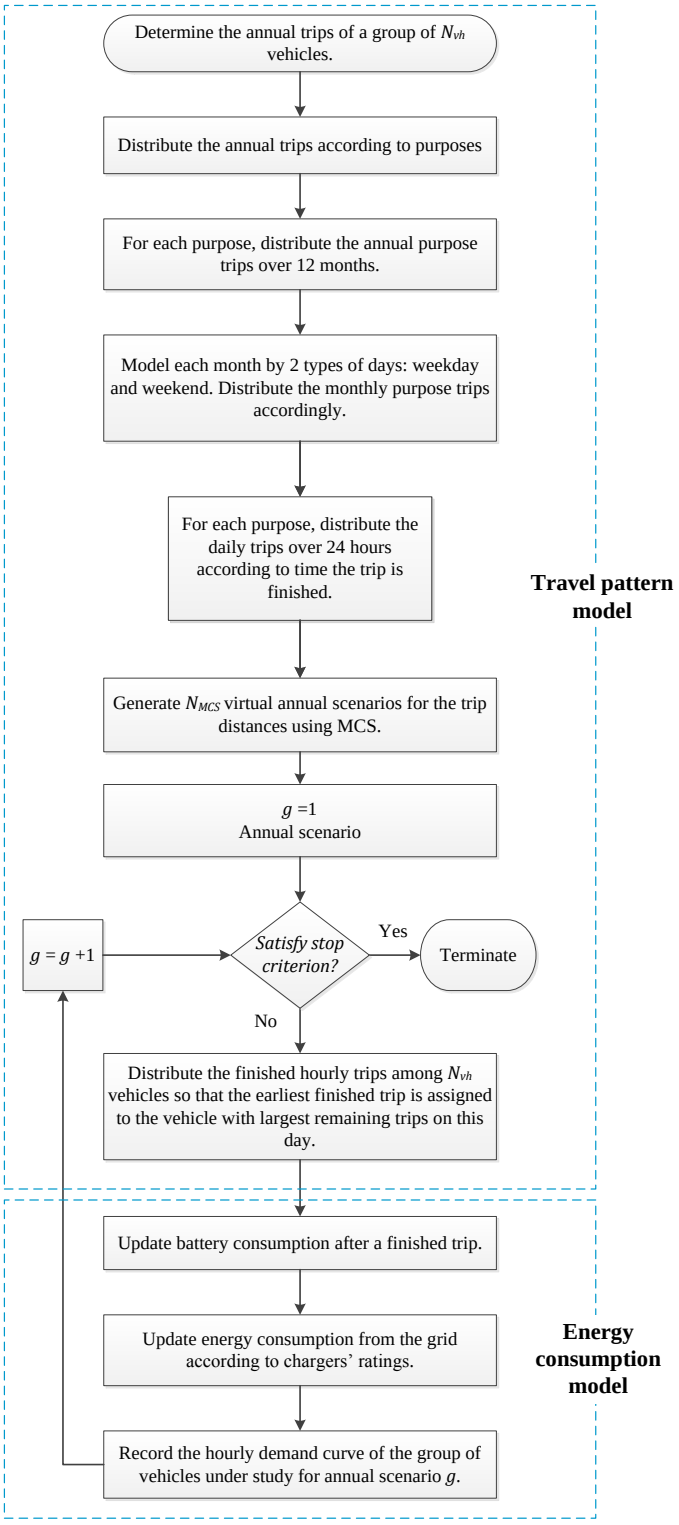

Figure 4.2 Proposed PEV charging model

1. *Purpose annual trips:*

The annual trips are distributed into a predefined number of purposes N_q. This distribution is performed according to the probability of a trip being for any purpose $\mathbb{p}_{trip(q)}^{Annual}$. Since the trip purpose is a random, discrete, multi-valued variable; therefore, it is represented by a categorical distribution [120] defined in (4.1). This pdf is utilized to calculate the annual trips for each purpose $q \in \mathcal{Q}$ as in (4.2).

$$f_1(z_{1(q)}) = \prod_{q=1}^{N_q} \left(\mathbb{p}_{trip(q)}^{Annual}\right)^{[z_{1(q)}=q]_{\text{IB}}} \qquad \forall q \in \mathcal{Q} \tag{4.1}$$

$$M_{trip(q)}^{Annual} = N_{vh} \times M_{trip}^{AVG} \times f_1(z_{1(q)}) \qquad \forall q \in \mathcal{Q} \tag{4.2}$$

where

$[(\cdot)]_{\text{IB}}$ is the Iverson bracket (evaluates to 1 if $(\cdot)$ is true and 0 otherwise);

$\mathcal{Q}$ is the set of the trip purposes;

$z_{1(q)}$ is a vector of length N_q, which consists of zeroes except for the q^{th} element, which is 1;

$M_{trip(q)}^{Annual}$ is the annual number of trips for purpose q;

M_{trip}^{AVG} is the average annual trips per vehicle;

N_{vh} is the total number of vehicles in the considered fleet.

2. *Purpose monthly trips:*

The annual trips of each purpose are distributed monthly. The categorical pdfs $f_{2(q)}(\cdot)$ defined in (4.3) represent the probability of a trip of a certain purpose $q \in \mathcal{Q}$ to be in a certain month. These pdfs are hence utilized to distribute the annual trips of each purpose into 12 months, as in (4.4).

$$f_{2(q)}(z_{2(m)}) = \prod_{m=1}^{12} \left(\mathbb{p}_{trip(q,m)}^{month}\right)^{[z_{2(m)}=m]_{\text{IB}}} \qquad \forall q \in \mathcal{Q}, m \tag{4.3}$$

$$M_{trip(q,m)}^{month} = M_{trip(q)}^{Annual} \times f_{2(q)}(z_{2(m)}) \qquad \forall q \in \mathcal{Q}, m \tag{4.4}$$

where

m is the index of months;

$z_{2(m)}$ is a vector of length 12, which consists of zeroes except for the m^{th} element, which is 1;

$\mathbb{p}^{month}_{trip(q,m)}$ is the probability of a trip of purpose q to be in month m;

$M^{month}_{trip(q,m)}$ is the total number of trips of purpose q in month m.

3. *Daily trips per purpose:*

Each month is modeled by a typical week. The categorical pdfs $f_{3(q)}(\cdot)$ defined in (4.5) represent the probability of a trip of a certain purpose q to be in a specific day. These pdfs are utilized to calculate the number of daily trips for each purpose as in (4.6). In this work, each month is modeled by 2 days: weekday and weekend. In other words, $\mathbb{p}^{day}_{trip(q,d)}$ is the same for d = 1, 2, 3, 4 and 5 (weekdays), and it has another value for both d = 6 and 7 (weekend).

$$f_{3(q)}\left(z_{3(d)}\right) = \prod_{d=1}^{7}\left(\mathbb{p}^{day}_{trip(q,d)}\right)^{[z_{3(d)}=d]_{\mathrm{IB}}} \qquad \forall q \in Q, d \tag{4.5}$$

$$M^{day}_{trip(q,m,d)} = M^{month}_{trip(q,m)} \times \frac{7}{N_{day(m)}} \times f_{3(q)}\left(z_{3(d)}\right) \qquad \forall q \in Q, m, d \tag{4.6}$$

where

d is the index of days;

$z_{3(d)}$ is a vector of length 7, which consists of zeroes except for the d^{th} element, which is 1;

$\mathbb{p}^{day}_{trip(q,d)}$ is the probability of a trip of purpose q to be in day d;

$M^{day}_{trip(q,m,d)}$ is the total number of trips of purpose q in month m and day d;

$N_{day(m)}$ is the number of days in month m.

4. *Hourly trips per purpose:*

In this stage, the daily trips of each purpose are distributed hourly. The categorical pdfs $f_{4(q)}(\cdot)$ defined in (4.7) represent the probability of a trip of a specific purpose q to be finished in a specific hour. Hence, these pdfs are utilized to distribute the daily trips of each purpose into 24 hours, as in (4.8).

$$f_{4(q)}(z_{4(h)}) = \prod_{h=1}^{24} \left(\mathbb{p}_{trip(q,h)}^{hour}\right)^{[z_{4(h)}=h]_{\text{IB}}} \qquad \forall q \in Q, h \tag{4.7}$$

$$M_{trip(q,m,d,h)}^{hour} = M_{trip(q,m,d)}^{day} \times f_{4(q)}(z_{4(h)}) \qquad \forall q \in Q, m, d, h \tag{4.8}$$

where

h is the index of hours;

$z_{4(h)}$ is a vector of length 24, which consists of zeroes except for the h^{th} element, which is 1;

$\mathbb{p}_{trip(q,h)}^{hour}$ is the probability of a trip of purpose q to be in hour h;

$M_{trip(q,m,d,h)}^{hour}$ is the total number of trips of purpose q in month m, day d, and hour h.

5. *Trips per vehicle:*

The daily trips generated from the third stage are utilized in this stage. The total number of daily trips is distributed among the group of vehicles according to a discrete lognormal pdf $f_{5(m,d)}(\cdot)$, which has a mean defined by the average daily trips per vehicles and a standard deviation of one trip, as in (4.9)-(4.11). The outcomes for a typical day show that almost 49% of the daily vehicle's trips are single trip per day, and almost 32% are two trips per day, as shown in Figure 4.3. The remained vehicles have either more than two trips per day, or no trips at all.

$$N_{(m,d)}^{trip/vh}(tr) = \mathbb{p}_{(m,d)}^{trip/vh}(tr) \times N_{vh} \qquad \forall m, d, tr = 0,1,2,\cdots \tag{4.9}$$

$$f_{5(m,d)}(x_0) = \begin{cases} \dfrac{1}{x_0\ \sigma_{trip/vh}\sqrt{2\pi}} exp \dfrac{-\left(\ln x_0 - \sum_{q=1}^{N_q} M_{trip/day(q,m,d)}^{AVG}\right)^2}{2\left(\sigma_{trip/vh}\right)^2} & \forall x_0 \geq 0 \quad \forall m, d \\ 0 & \forall x_0 \geq 0 \end{cases} \tag{4.10}$$

$$\mathbb{P}_{(m,d)}^{trip/vh}(tr) = \begin{cases} \int_{x_0=0}^{0.5} f_{5(m,d)}(x_0) & \forall tr = 0 \\ & \forall m, d, tr = 0,1,2,\cdots \\ \int_{x_0=tr-0.5}^{tr+0.5} f_{5(m,d)}(x_0) & \forall tr = 1,2,\cdots \end{cases} \quad (4.11)$$

where

tr is a positive integer number indicating the number of daily trips per vehicle, which is assumed to be the nearest integer to variable x_0;

$N_{(m,d)}^{trip/vh}(tr)$ is the total number of vehicles with daily trips tr in month m and day d;

$M_{trip/day(q,m,d)}^{AVG}$ is the mean daily trip per vehicle, which is defined as $M_{trip(q,m,d)}^{day}/N_{vh}$;

$\sigma_{trip/vh}$ is the standard deviation, which is assumed to be one trip;

$\mathbb{P}_{(m,d)}^{trip/vh}(tr)$ is the probability of having daily trips tr per vehicle in month m and day d.

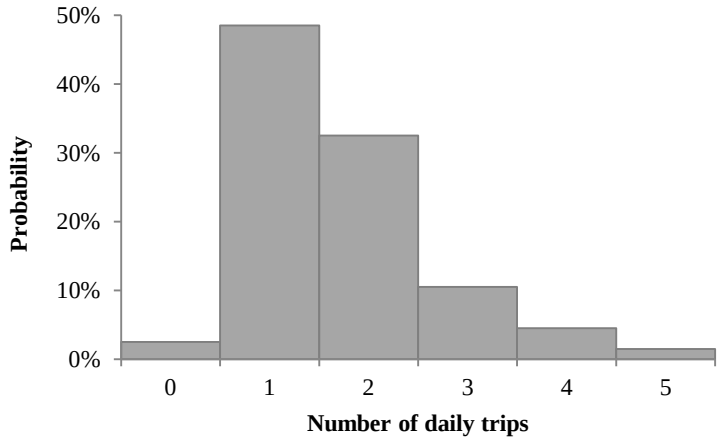

Figure 4.3 Probability of daily trips per vehicle

6. Distance per trip:

In the last stage, the outcomes of the fifth and fourth stages are utilized to generate the final trip model. Therefore, to generate N_{MCS} equiprobable virtual scenarios with a probability of occurrence of $1/N_{MCS}$, MCS is utilized to generate virtual trip distances of $M_{trip(q,m,d,h)}^{hour} \times N_{MCS}$ for every purpose

trips finished in a specific hour. This should cover the diverse of usage among the vehicles in the same scenario and in different scenarios. Further, for each scenario, the daily trips are assigned to the vehicles according to the following assumption: the trips with the earliest finish time are assigned to the vehicles with the largest number of remaining trips per day. $D^{mile}_{(q,m,d,h,g)}$, which represents the finished trip distance in mi for purpose q in month m, day d, hour h, and scenario g, can thus be given by

$$D^{mile}_{(m,d,h,g)} = CDF^{-1}_{6(q)}(rn) \quad \forall m, d, h, g, rn \in \mathcal{RN}_{(q,m,d,h,g)} \tag{4.12}$$

where

$\mathcal{RN}_{(q,m,d,h,g)}$ is a vector of length $M^{hour}_{trip(q,m,d,h)}$ of uniformly distributed random variable between 0 and 1 corresponding to the g^{th} scenario;

$CDF^{-1}_{6(q)}$ is the inverse of the cumulative density function, which describes the probability of a trip of purpose q to be less than specific distance.

4.3.2 Energy Consumption Model

In this model, the travel pattern model is utilized to generate hourly energy consumption model as shown in Figure 4.2. In this mode, the following assumptions are considered:

- The time step is one hour, i.e., any change within the hour is neglected.
- The vehicle batteries are fully charged at the beginning of the first hour of the annual model.
- Four classes of vehicles are assumed to represent the light duty fleet, which are cars, vans, sports utility vehicle (SUVs) and pick-up trucks [50].
- Two temperature thresholds are assumed, beyond or below these thresholds [57], the vehicle engine starts to provide energy for heating or cooling. This is independent of the battery available charge.
- A transient period of 10 minutes is taken by air conditioner (A/C) and Heater (HT) at start before settling to their continuous normal loading [94]. In the presented model, the starting period is averaged over the hour.

The energy consumption model for each scenario g consists of two main vectors. The first vector $EC_{(g)}$ represents the consumed power by the considered vehicle fleet during each hour. This

vector has a length of 8760 and is initially set to zeroes. The other vector $BT_{(t,g)}^{SOC}$ with length N_{vh} represents the SOC of the fleet batteries at the end of each hour, as in (4.13). The initial value of the battery SOC, which represents the useful battery charge, is defined as in (4.14). It is assumed that this vector is shared between the four classes of the considered fleet according to the percentage sharing of each class, as shown in Table 4.1.

$$BT_{(t,g)}^{SOC} = [bt_{(1,t,g)}\ bt_{(2,t,g)} \cdots bt_{(N_{vh},t,g)}] \quad \forall m, d, h, g \tag{4.13}$$

$$bt_{(vh,0,g)} = \frac{\tau_{(vh)} \times AER_{(vh)}}{\eta_{BT} \times \eta_{PE} \times \eta_M \times \eta_A} \quad \forall m, d, h, g \tag{4.14}$$

where

$bt_{(vh,t,g)}$ represents the battery available charge in kWh for vehicle vh in scenario g at the end of hour t;

$AER_{(vh)}$ is AER in miles for vehicle vh in scenario g;

$\tau_{(vh)}$ is the average tractive effort required in kWh/mi, which depends on the class of the vehicle;

η_{BT}, η_{PE}, η_M, and η_A are the efficiency of battery, onboard power electronics, motor and accessory load, respectively.

To generate the hourly energy consumption model, vectors $BT_{(t,g)}^{SOC}$ and $EC_{(g)}$ are required to be updated each hour. This is performed through the following procedure, which can be described in two major stages: battery discharging model and battery charging model.

Table 4.1 Vehicle class percentage sharing [50]

	CAR	VAN	SUV	PICK-UP
Percentage share	53.0%	8.9%	19.4%	18.7%

1. *Battery Discharging Model*

In this stage the battery SOCs are updated hourly by the consumed energy for each finished trip by vehicle $E_{total(vh,t,g)}^{Cons}$, as in (4.15) and (4.16). The consumed energy by each finished trip is calculated

as a sum of two values: the total tractive energy required to overcome vehicle inertia, road resistance, and aerodynamics drag as defined in (4.17), and the energy required to maintain a comfortable cabin temperature for the vehicle driver and the passengers as in (4.18)–(4.21).

$$E^{Cons}_{total(vh,t,g)} = E^{Cons}_{1(vh,t,g)} + E^{Cons}_{2(vh,t,g)} \quad \forall vh, t, g \tag{4.15}$$

$$bt_{(vh,t,g)} = \begin{cases} bt_{(vh,t,g)} - E^{Cons}_{total(v,t,g)} & \forall E^{Cons}_{total(vh,t,g)} < bt_{(vh,t,g)} \\ 0 & \forall E^{Cons}_{total(vh,t,g)} \geq bt_{(vh,t,g)} \end{cases} \quad \forall vh, t, g \tag{4.16}$$

$$E^{Cons}_{1(vh,t,g)} = \begin{cases} \dfrac{\tau_{(vh)} \times D^{mile}_{VH(m,d,h,vh,g)}}{\eta_{BT} \times \eta_{PE} \times \eta_M \times \eta_A} & \forall \Theta_{min} \leq \Theta_{(t)} \leq \Theta_{max} \quad \forall vh, t, g \\ 0 & elsewhere \end{cases} \tag{4.17}$$

$$E^{Cons}_{2(vh,t,g)} = \begin{cases} E_{AC(vh,t,g)} & \forall \Theta_{AC} \leq \Theta_{(t)} \leq \Theta_{max} \\ E_{HT(vh,t,g)} & \forall \Theta_{min} \leq \Theta_{(t)} \leq \Theta_{HT} \quad \forall vh, t, g \\ 0 & elsewhere \end{cases} \tag{4.18}$$

$$\mathrm{t}_{trip(vh,t,g)} = \frac{60 \times D^{mile}_{VH(m,d,h,vh,g)}}{v^{AVG}_{mile/h(q)}} \tag{4.19}$$

$$E_{AC(vh,t,g)} = \begin{cases} P^{AC}_{ST} \times \dfrac{\mathrm{t}_{trip(vh,t,g)}}{60} & \forall \mathrm{t}_{trip(vh,t,g)} \leq 10 \\ (10/60) \times P^{AC}_{ST} + P^{AC}_{CONT} \times \dfrac{(\mathrm{t}_{trip(vh,t,g)} - 10)}{60} & \forall \mathrm{t}_{trip(vh,t,g)} > 10 \end{cases} \quad \forall vh, t, g \tag{4.20}$$

$$E_{HT(vh,t,g)} = \begin{cases} P^{HT}_{ST} \times \dfrac{\mathrm{t}_{trip(vh,t,g)}}{60} & \forall \mathrm{t}_{trip(vh,t,g)} \leq 10 \\ (10/60) \times P^{HT}_{ST} + P^{HT}_{CONT} \times \dfrac{(\mathrm{t}_{trip(vh,t,g)} - 10)}{60} & \forall \mathrm{t}_{trip(vh,t,g)} > 10 \end{cases} \quad \forall vh, t, g \tag{4.21}$$

where

$E_{1(v,t,g)}^{Cons}$ denotes the total tractive energy required in kWh to overcome vehicle inertia, road resistance, and aerodynamics drag for the trip finished by vehicle vh in scenario g at the end of hour t;

$E_{2(v,t,g)}^{Cons}$ denotes the energy in kWh required to maintain a comfortable cabin temperature for the vehicle driver and the passengers during the trip finished by vehicle vh in scenario g at the end of hour t;

$D_{VH(m,d,h,vh,g)}^{mile}$ is the distance in mi of the finished trip for purpose q in month m, day d, hour h, vehicle vh, and scenario g;

Θ_{max}, Θ_{min} denote the maximum and minimum temperature limits for battery usage in BCD mode, respectively;

Θ_{AC}, Θ_{HT} are the thresholds for A/C and HT operation, respectively;

$E_{AC(vh,t,g)}$, $E_{HT(vh,t,g)}$ denote the energies in kWh consumed by A/C and HT respectively, during the trip finished by vehicle vh in scenario g at the end of hour t;

$t_{trip(vh,t,g)}$ denotes the duration in minutes of the trip finished by vehicle vh in scenario g at the end of hour t;

$v_{mile/h(q)}^{AVG}$ denote the average vehicle speed in mi/h for purpose q;

P_{ST}^{AC}, P_{CONT}^{AC} denote the powers in kW consumed by A/C during starting and continuous operation, respectively;

P_{ST}^{HT}, P_{CONT}^{HT} denote the powers in kW consumed by HT during starting and continuous operation, respectively.

2. Battery Charging Model:

When a vehicle finishes a trip, it may or may not be plugged in the charger. When plugged, the time and amount of energy supplied by the charger depend on the battery available charge, the allowable charging rate, and the charger ratings. It is assumed that the set of charging vehicles at each hour contains all the plugged vehicles, under the uncontrolled charging scenario. The consumed energy vector $EC_{(g)}$ is initially zero, and is updated each hour for each charging vehicle using (4.22). The hourly demand of the batteries is approximated as in [66] and [121, 122], where the charging process is approximated to two charging levels. In this work, chargers operate with full capacity except for the final charging hour. This is modeled in (4.23) by setting the charging time to 1 hour if

it is a fraction of an hour. Finally, the batteries available charges of the plugged vehicles are updated using (4.24):

$$ec_{(t,g)} = ec_{(t-1,g)} + \sum_{vh \in \mathcal{CV}_{(t)}} \frac{bt_{(vh,0,g)} - bt_{(vh,t,g)}}{\eta_{CH} \times t_{CH(vh,t,g)}} \forall vh, t, g \tag{4.22}$$

$$t_{CH(vh,t,g)} = \begin{cases} \dfrac{bt_{(vh,0,g)} - bt_{(vh,t,g)}}{P^{Charger}_{rating(vh)}} & \forall \ \dfrac{bt_{(vh,0,g)} - bt_{(vh,t,g)}}{P^{Charger}_{rating(vh)}} > 1 \\ 1 & \forall \ \dfrac{bt_{(vh,0,g)} - bt_{(vh,t,g)}}{P^{Charger}_{rating(vh)}} \leq 1 \end{cases} \quad \forall vh, t, g \tag{4.23}$$

$$bt_{(vh,t+1,g)} = bt_{(vh,t,g)} + \frac{bt_{(vh,0,g)} - bt_{(vh,t,g)}}{t_{CH(vh,t,g)}} \quad \forall vh, t, g \tag{4.24}$$

where

$ec_{(t,g)}$ denotes the t^{th} element in vector $EC_{(g)}$, and represents the average consumed power in kW during hour t in scenario g;

η_{CH} denotes the charger efficiency;

$t_{CH(vh,t,g)}$ denotes the required charging time in hours to fully charge the battery of vehicle vh at time t in scenario g;

$P^{Charger}_{rating(vh)}$ denotes the charger continuous rating in kW for vehicle vh;

$\mathcal{CV}_{(t)}$ denotes the set of vehicles required to be charged at hour t.

4.4 Sample case study

The outcomes of the energy consumption model for an LDF of PEV under the uncontrolled charging scenario are presented in this case study. Then, the impacts of different penetration levels of PEV uncontrolled charging are investigated on a test distribution system.

The considered purposes in this work are shown in Table 4.2. The data for the pdfs utilized in the travel pattern model are provided by Department of Transportation, Great Britain. For the sixth stage in the travel pattern model, four pdfs are utilized to fit the actual data of each purpose: Exponential, Lognormal, Gamma and Weibull. The maximum likelihood method was used to

estimate the parameters of the closest pdf for each purpose actual data. Then, the highest likelihood pdf is chosen to represent each purpose. Table 4.3 shows the parameters of the fitted pdfs, which are used for $CDF_{6(q)}^{-1}$ in (4.12). It was observed that the purposes with low average distance per trip are more likely fitted by Lognormal pdf, due to its steep curvature specially for low mean values. On the other hand, the purposes with high average distance per trip are more likely fitted with Weibull pdf, due to its flexibility in fitting such types of pdf.

Three levels of chargers are available in the market, as mentioned in chapter 2 and shown in Table 2.1. In this study, level 2_R chargers are only considered in this work, which are recommended by vehicle manufacturers [57], and are expected to be the most commonly used home charger. However, the charger ratings for this level depend on available capacity in the household. The flexibility of the model enables utilizing a mix of different chargers ratings as in [50]. Accordingly, half of the chargers are considered of 16 A current rating , and the other half of 30 A. Regarding the temperature model, the daily temperatures in a specific month are assumed to be normally distributed between maximum and minimum temperatures in the last five years for this month.

As mentioned before, the work presented in this study considers only the uncontrolled at home charging scenario. Hence, the set of the vehicles that are required to be charged $\mathcal{CV}_{(t)}$ includes all the vehicles in the fleet under study. Moreover, the PEV AERs assumed in this study are samples of the commercially available ranges. However, there are other available ranges (released or under development) that have different impacts on the system. Higher AER vehicles consume more energy and have less diversity in charging. They are thus accompanied with more stress on the system compared to lower AERs, which will be proven in the case study.

Table 4.2 Considered purposes in the PEV model

q	Purpose	q	Purpose
1	Commuting	**6**	Other escort and personal business
2	Business	**7**	Visit friends
3	Education	**8**	Holiday trip
4	Escort education	**9**	Day trip
5	Shopping	**10**	Other like: entertainment, public activity, etc.

Table 4.3 Fitted pdfs parameters for different purposes

q	Fitted pdf	Parameters		*q*	Fitted pdf	Parameters	
1	Lognormal	μ = 3.27	σ = 1.02	6	Lognormal	μ = 3.02	σ = 1.32
2	Weibull	c = 111.75	k = 1.27	7	Weibull	c = 83.81	k = 0.93
3	Lognormal	μ = 2.48	σ = 1.16	8	Weibull	c = 176.47	k = 2.67
4	Lognormal	μ = 2.16	σ = 1.38	9	Weibull	c = 79.63	k = 1.19
5	Lognormal	μ = 2.76	σ = 1.18	10	Lognormal	μ = 3.42	σ = 1.29

where

μ and σ are mean and standard deviation of the Lognormal pdf respectively;

k and c are the shape and scale parameters of the Weibull pdf respectively.

4.4.1 Energy consumption model results

The results presented in this case study are based on the values shown in Table 4.4, where the temperature thresholds are assumed to be the average thresholds of the collected data from the vehicles manufacturers and the PEVs users. Unfortunately, this data is not available; therefore, the presented temperature thresholds are reasonably assumed.

Figure 4.4 (a) and (b) show 10 scenarios for the uncoordinated charging of 100 vehicles in a typical weekday and weekend in March, respectively. As shown in the figures, consumption is higher during the weekend compared weekdays, and the consumption peaks occur at later times during the weekends: between 5:00 pm and 6:00 pm rather than 4:00 pm to 5:00 pm on weekdays. It can also be observed that relatively higher consumption occurs during the period between 7:00 pm and 10:00 pm, which is due to the higher probability of longer daily trips during weekends.

On the other hand, Figure 4.4 (c) shows 10 scenarios for the uncoordinated charging of 100 vehicles during a typical July weekday. The effects of considering the trip purpose and ambient temperature are striking with respect to the energy consumed. In July, the peaks are higher because of the longer day trips and increased air conditioner usage. In addition, the peaks of the consumption in March occur between 4:00 pm to 5:00 pm; however, the peaks in July are shifted to the period

between 6:00 pm and 7:00 pm because of longer daylight hours and fewer education-related trips during July, when drivers tend to return home at a later time compared to March. Education-related trips also result in relatively lower peaks occurring in March between 1:00 pm and 2:00 pm.

4.4.2 PEV uncontrolled charging penetration limits

To investigate the impacts of a high penetration of PEV uncontrolled charging on distribution systems, three scenarios are studied: 30-mile AER, 50-mile AER and a mix. The mix scenario has 50 % of the PEVs with 30-mile AER and 50 % with 50-mile AER. It is assumed in this study that the PEV charging occurs only at home (residential customer busses), there are 1.86 vehicles per household [123], and the average peak demand is 5 kW [124] for a typical residential home. Due to lack of customers' hourly load data, the customer load curve is represented by the reliability test system load model [125].

Two systems are studied for each scenario, where each system is characterized by different residential customer sharing percentage. The system in Figure 4.5 is used in this study. The customer types are given in Table 4.5 [5], while the system line and load data are given in Appendix A.

Table 4.4 Simulation parameters

Parameter	Value	Parameter	Value
M_{trip}^{AVG}	395 trip/year [126]	η_M	92 % [50]
Θ_{min}	-10 ^{o}C	η_A	88 % [50]
Θ_{HT}	5 ^{o}C	η_{CH}	95 % [50]
Θ_{AC}	27 ^{o}C	P_{ST}^{AC}	2.99 kW [94]
Θ_{max}	40 ^{o}C	P_{CONT}^{AC}	2.1 kW [94]
η_{BT}	92 % [50]	P_{ST}^{HT}	4 kW [94]
η_{PE}	95 % [50]	P_{CONT}^{HT}	2 kW [94]

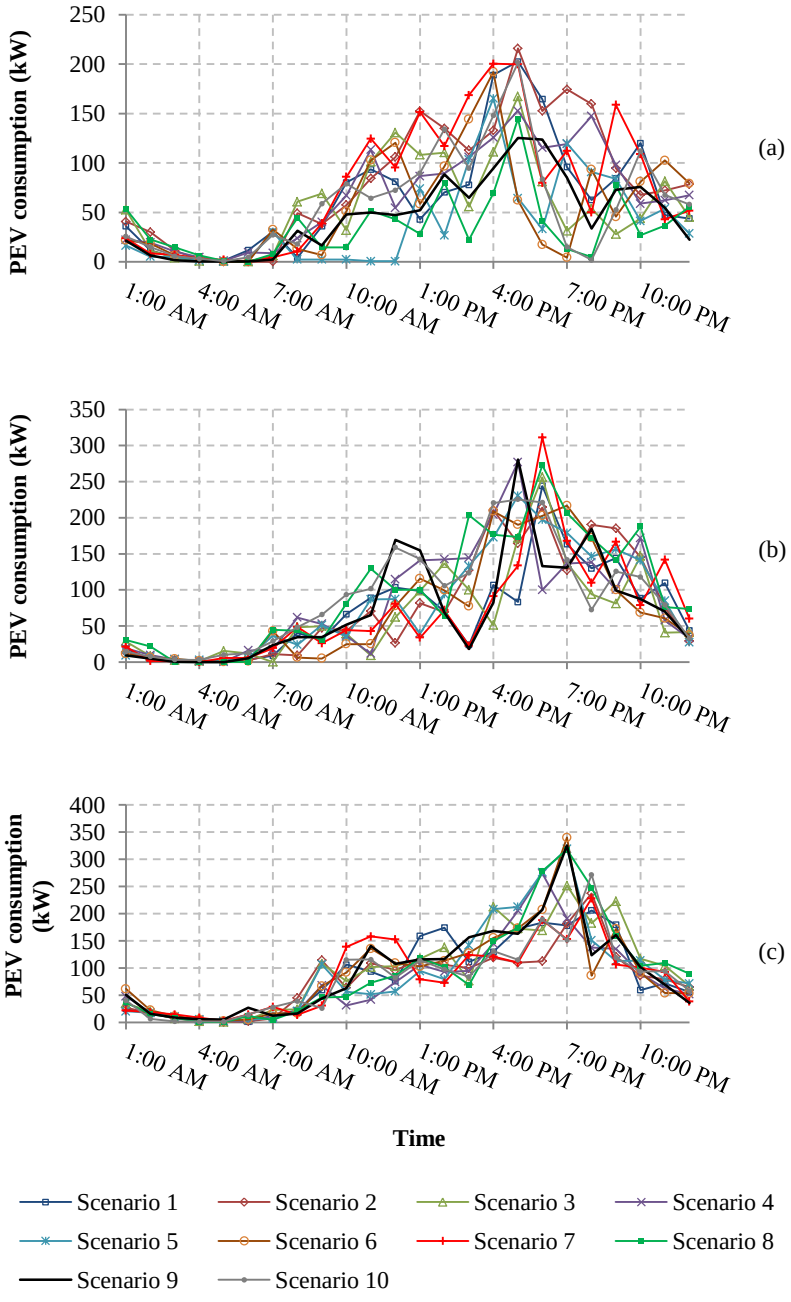

Figure 4.4 PEV consumption of 10 scenarios during a typical: (a) March weekday, (b) March weekend, and (c) July weekday

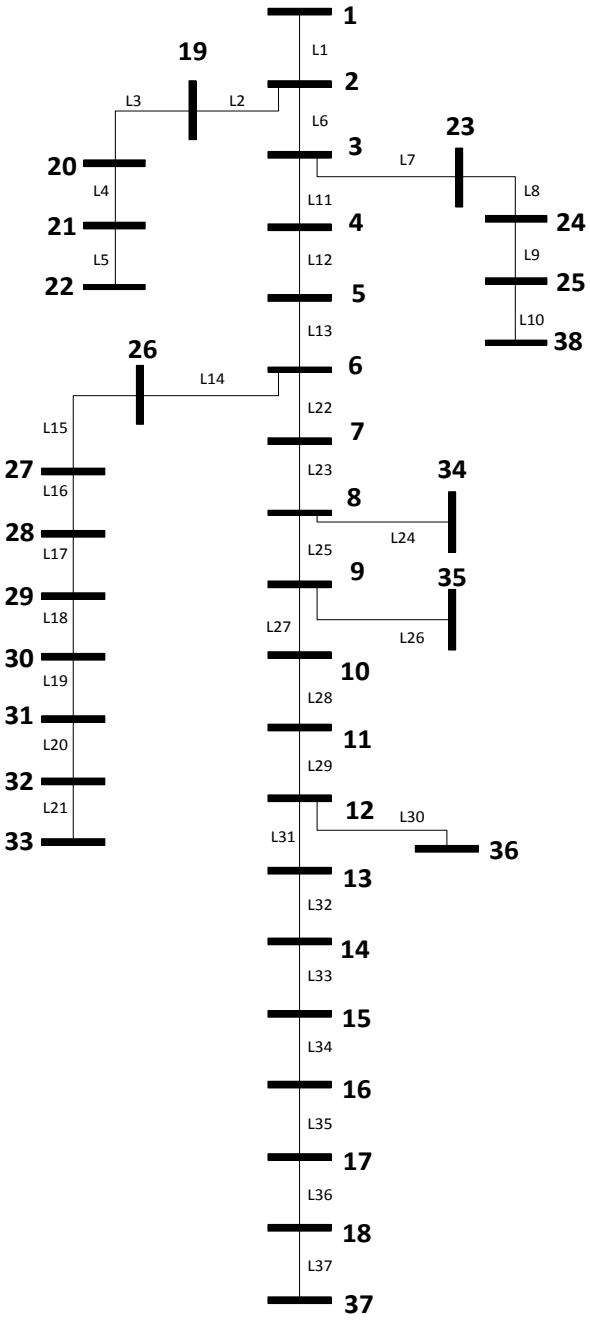

Figure 4.5 System under study

Table 4.5 System data

Bus	System A	System B	Bus	System A	System B	Bus	System A	System B	Bus	System A	System B
2	R	R	10	C	C	18	I	R	26	C	C
3	I	I	11	C	C	19	R	R	27	I	I
4	C	C	12	R	R	20	C	C	28	C	C
5	R	R	13	C	R	21	I	I	29	C	C
6	I	I	14	R	R	22	R	R	30	C	C
7	C	C	15	C	C	23	C	C	31	R	R
8	C	C	16	I	I	24	C	C	32	R	R
9	I	I	17	C	R	25	C	R	33	C	R

* R: residential customer, I: industrial customer, and C: commercial customer.

4.4.2.1 System A

This case represents a 24 % residential customers sharing, in terms of active power demand. The loading levels of the system lines are examined under different penetration levels of PEVs. Three scenarios are studied. These scenarios are defined as 30-mile, mix and 50-mile AER.

Two lines mainly experience significant overloading. One of these lines is line 5 between buses 21 and 22; the other line is line 19 between buses 31 and 33. These are the lines that are significantly affected by the PEV charging. This is because line 19 supplies the required energy for two residential customer buses, which are buses 31 and 32, and line 5 supply residential loads on bus 22. The penetration up to 30 % does not cause severe overloading in the system lines, which are assumed to have a maximum limit of 120 % of the kVA flow at the peak load condition. However, to limit the loading level of each line to its normal level, which is 100 %, the penetration limits of the three scenarios are found to be 23 %, 17.5 %, and 15 % for the 30-mile, mix and 50-mile scenarios respectively, as shown in Figure 4.6. These penetration levels represent the maximum capability of the system to accommodate PEV chargers.

The penetration limits based on worst case condition are shown in Figure 4.6, where all the system chargers are assumed to operate at the same time. As shown in Figure 4.6, the penetration is limited to 2.5 % and it is not affected by the AER. Comparing the penetration limits of the proposed model with the worst case condition, it is assumed that the proposed model takes into consideration the diversity in usage, which is an important factor that has to be considered in planning.

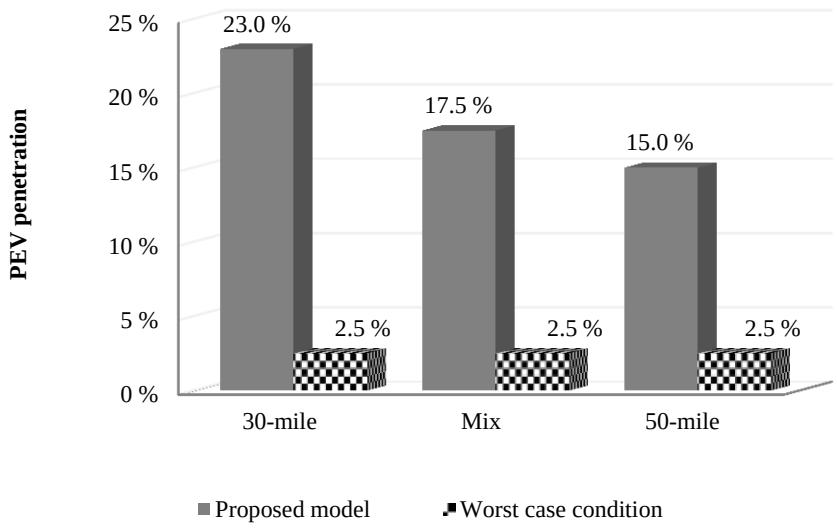

Figure 4.6 Penetration limits for the system A

4.4.2.2 System B

This case represents a distribution network with dominant residential load of 45 % share, which exists in reality in many areas. The same three scenarios mentioned before are applied to this system. It was noticed that lines 4, 5, 9 and 19 experience significant overloading. Line 9 supplies a considerable residential load on bus 25. Lines 4 and 5 supply residential loads on buses 21 and 22. The excess loading on system lines due to the PEV charging limits the penetration of PEVs to 7 %, 6 %, and 4.5 % for the 30-mile, mix and 50-mile scenarios respectively, as shown in Figure 4.7. These are relatively low percentages as the PEV penetration, which is predicted to exceed 20 % in the next decade. The presented results show that PEV charging can have significant effect on systems with dominant residential loads.

The penetration limits based on worst case condition are shown in Figure 4.7, which are limited to 1.8 % and unaffected by the AER. Comparing Figure 4.6 and Figure 4.7, it is shown that as the density of the residential customers increases, the diversity in usage gets closer to the worst case condition.

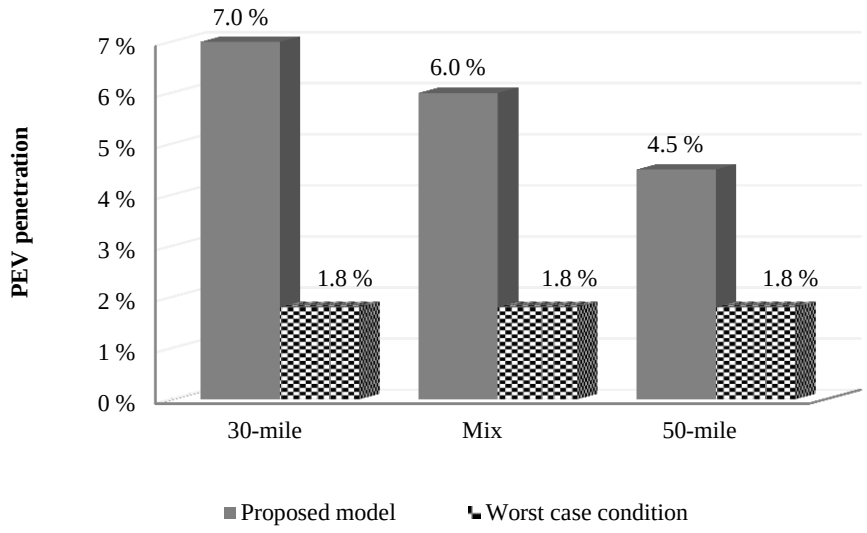

Figure 4.7 Penetration limits for system B

4.5 Conclusions

In this chapter, a novel probabilistic based model for PEVs has been proposed and developed. The model utilizes MCS to generate virtual trip distances for each purpose trips, and takes into consideration different factors, such as the variations in driving habits, different electric range vehicles, multiple charging events per day, and recharging time variation. These aspects are assumed to present more accurate model for the consumed energy by PEVs, compared to the mentioned literature.

Furthermore, the proposed model integrates the effect of ambient temperature on vehicles energy consumption as an important factor that affects the model accuracy. The effect of ambient temperature can be very significant, especially in regions with severe weather conditions like Canada, north USA, and north Europe.

In addition, the model represented the PEVs consumption as an annual model which coincides with the normal load model, resulting in more accurate evaluation of the impacts of the extra load imposed by vehicles charging on the distribution networks. Aggregating this model in a daily model, as in most of the mentioned literature, may result in misleading outcomes that cannot be relied upon. This is because a significant consumption peaks may occur in certain days in the annual model which are averaged out in the daily model.

The proposed model has been applied to different scenarios for two configurations of a typical distribution system. The results reveal that the effects of high penetration of PEVs are not significant on systems with commercial and industrial dominant loads. On the other hand, they show a significant effect on lines loading levels for systems with dominant residential loads. The proposed model can be utilized by local distribution companies to quantify the penetration limits, expected impacts, and the required upgrades in the distribution networks as a result of PEVs uncontrolled charging. Moreover, the proposed model can be used by grid operators and national energy agencies to quantify the expected impacts of the target PEV penetration levels on the generation level and the distribution level.

Chapter 5
Accommodating High Penetrations of PEVs and Renewable DG in Distribution Systems

5.1 Introduction and motivations

Accommodating a high penetration of PEV charging has been dealt with in the literature using coordinated charging, as in [71, 75, 127, 128]. Obvious gaps exist between the solutions proposed in the literature and the current status of the grid, which can be summarized as follows:

- With only few exceptions, smart signals between the LDCs and the PEV charger load points are currently not available, and their implementation may require decades, especially in developing countries.
- For a charging coordination scheme to be effective, historical data of PEV are required, such as arrival and departure SOC levels, seasonal variations of consumption, and market shares of different battery technologies. This will be available in future, when the PEV penetration becomes significant. For the coordination of PEV charging to be robust and adequate, a transition period of uncoordinated PEV charging is therefore required.
- If the accommodation of the PEV charging load is not to be counterproductive, renewable resources of energy must be taken into account to supply the PEV needs. This aspect is critical because meeting PEV load requirements through conventional generating units transfers the emissions from the transportation sector to the electric sector.

The work proposed in this chapter here was thus undertaken with the goal of filling these gaps through the proposal of a multi-year multi-objective planning algorithm, where the current rising integration of renewable DG is utilized as a means of accommodating the expected growing penetration of uncoordinated PEV charging. The results of this work are therefore assumed to provide an alternative to coordinated charging during a transition period between the current status of the grid and a significant penetration of PEV, where the deployment of smart signaling might be essential.

5.2 Problem description

In this section, the proposed multi-objective long-term planning algorithm is described, including the system emissions and considered costs. The input to the proposed algorithm is comprised of the DG unit models, the load models, and the PEV uncoordinated charging model, all of which are explained

in the next section. The output of the proposed algorithm consists of the location, size, and year of installation of each DG unit, as well as the optimum target PEV penetration.

Normally, no unique solution can simultaneously optimize all of the objectives of a multi-objective problem [129], so different methods are thus employed to address such problems. Some rely on weights as a means of combining all of the objectives into one single objective; however, a drawback of this method is the difficulty sometimes associated with the prior setting of the criteria for selecting the weights [129]. Other methods address the multi-objective problem using a posteriori[2] technique, which results in an optimum set of solutions called a Pareto frontier [131]. The decision-maker (DM) can therefore choose the best solution among the Pareto frontier.

The work presented in this chapter is based on the second type of method, which deals directly with the objectives. The objectives that are minimized by the proposed planning algorithm are as follows.

5.2.1 System Costs

The accommodation of the expected growth in PEV penetration over the next few years requires system reinforcements and recognition that might lead to system losses increase. Further, the cost of interruption proved to be of least importance in Chapter 3 compared to other benefits of installing DG units. The following costs were therefore considered in this work:

- Cost of upgrades: DG units can relieve congestion in network feeders and defer previously required system upgrades, thus reducing the NPV of the required upgrades, as explained in Chapter 3. However, the costs of upgrading the protective equipment are not considered in this work for simplicity.
- Cost of energy losses: The growing extra load imposed by PEVs will increase system losses; however, installing DG units can alleviate this problem because of their proven effectiveness in reducing system losses. In the work presented in this chapter, an average price of energy is used to evaluate the cost of energy losses. This average price is used to avoid using MCS, which require huge computational effort in this problem.

5.2.2 System Emissions

In this work, system emissions are assumed to include three elements, represented by three terms, which are described as follows:

[2] Posteriori techniques or generate-first-choose-later approaches do not require prior preference information from the decision-maker [130].

- The first term represents the carbon footprint of the electricity purchased from the grid, which is dependent on the region or province where the system is located.
- The second term represents the emissions from the DG units connected to the system, which are contingent on the type of DG unit and the amount of energy supplied.
- The last term represents the reduction in transport sector emissions due to the replacement of conventional vehicles with PEVs, which is assumed to be a credit for the grid operator.

5.3 Generation and Load Modeling

In this section, the generation and load models are described. After the models are developed, they are combined into one multi-state gen-load model that represents all possible system states, based on the following assumptions:

- The time step is one hour, i.e., any changes within the hour are excluded.
- The DG units operate at a fixed power factor, which is assumed to be unity for the purposes of this work.
- The DG output power, the normal load, and the PEV load are discretized into a definite number of states, which represents a trade-off between accuracy and the complexity of the planning problem.

5.3.1 DG Modeling

Three types of DG units are considered in this work:

5.3.1.1 NGDG

The NGDG is an example of a dispatchable DG unit, and any other type of dispatchable DG unit can be treated in the same manner. For the long-term study presented in this work, these DG units are considered firm generation units, which is a typical practice for this type of analysis [10]. In other words, these units have no associated uncertainties and operate at rated capacities.

5.3.1.2 WDG

A typical analytical probabilistic model of wind speeds is described in subsection 2.2.2. In the work presented here, six years of historical wind speed data are used to generate the model. First, the entire year is divided into clusters (months), following which, historical data for each cluster is used in order to generate a typical daily frequency distribution of the wind speed measurements. The day that

represents each cluster is further subdivided into hourly time segments. From this data, the mean and standard deviation for each segment are calculated and then become the basis for the generation of the Weibull pdf for each hour. The entire range of wind speeds is next discretized into a definite number of states: in this work, six states are chosen to represent the entire wind speed range for each hour. The values of these states are chosen based on the central centroid sorting process [103]. Finally, the wind speed states are converted into output power based on the wind turbine characteristics described in subsection 2.2.2. The final output of the model is comprised of the probabilities of the six states for the 288 time segments (12 months × 24 h) that represent the year.

5.3.1.3 PVDG

The same technique used to model wind speed is also used to model solar irradiance. However, for a specific time segment, the solar irradiance data usually have a bimodal distribution function [18]. Therefore, the data for each time segment are divided into two groups, each with a unimodal distribution function described by a beta pdf [132]. Six states are chosen to represent the solar irradiance level for each of the 288 states representing a year. Solar irradiance is further converted to output power from the PVDG based on the characteristics of the photo-voltaic panel, as explained in [106].

5.3.2 Normal Load Modeling

Three types of system loads are assumed: residential, commercial, and industrial. The data for each load type are represented by a multi-state model. The year is divided into 12 months, each of which is modeled based on two types of days: weekday and weekend. The probability of each state for the 576 time segments representing the year is calculated based on the historical data. For this work, four states were chosen to represent each type of load; the values of the states are calculated based on the central centroid sorting process [103].

5.3.3 Uncoordinated PEV Charging Model

The probabilistic annual model described in Chapter 4 is utilized in this work, where MCS is used to generate virtual scenarios of PEV energy consumption. The output of this model is N_{MCS} equiprobable virtual scenarios with a probability of occurrence of $1/N_{MCS}$. These scenarios describe the annual 8760 h consumption of a group of PEVs. Further, the powers absorbed by all vehicles at each hour t in scenario g are normalized to their peak value. Then, the central centroid method [103] is used to discretize this model into definite number of states to be able to combine it to other

analytical probabilistic models. In this work, six states are chosen to represent the PEV uncontrolled charging load. Finally, the probability of occurrence of each state in each hour during the weekdays and weekends for each month in the year is evaluated.

5.3.4 Combined Gen-Load Model

This model describes the system state for each load type and for each generation. The details of this model are introduced in 3.3.4. However, the PEV load and the PVDG are considered in the work. Moreover, the normal load is categorized into three types, namely residential, commercial, and industrial. Each customer has different behavior. Thus, the formulas in (3.2) and (3.3) are modified to

$$\mathbb{P}_{(t,s)} = \mathbb{P}_{(t,s_g)} \times \mathbb{P}_{(t,s_w)} \times \mathbb{P}_{(t,s_{pv})} \times \mathbb{P}_{(t,s_{ev})} \times \mathbb{P}_{(t,s_r)} \times \mathbb{P}_{(t,s_c)} \times \mathbb{P}_{(t,s_i)} \quad \forall\, s_g \in \mathcal{S}_{NGDG}, s_w \in \mathcal{S}_{WDG}, s_{pv} \in \mathcal{S}_{PVDG}, s_{ev} \in \mathcal{S}_{EV}, s_r \in \mathcal{S}_{RL}, s_c \in \mathcal{S}_{CL}, s_i \in \mathcal{S}_{IL} \tag{5.1}$$

$$\mathbb{P}_{(s)} = \left(\frac{1}{576}\right) \times \sum_{t=1}^{576} \mathbb{P}_{(t,s)} \qquad \forall s \in \mathcal{S}_{sys} \tag{5.2}$$

where,

$\mathcal{S}_{PVDG}$ is the set of states for the NGDG units;

$\mathcal{S}_{EV}$ is the set of PEV consumption power states;

$\mathcal{S}_{RL}$, $\mathcal{S}_{CL}$, and $\mathcal{S}_{IL}$ are the set of load power states for residential, commercial, and industrial customers, respectively.

5.4 Planning Problem Formulation

In this section, the proposed multi-objective multi-year planning problem formulation and the non-dominated sorting GA (NDSGA) implementation used to solve the problem are presented. The problem is classified as mixed-integer nonlinear programming and is defined by the objective function and constraints explained in the following subsections.

5.4.1 Objective (Fitness) Function

In Ontario, Canada, LDCs are not permitted to connect their own DG units. However, private sector proposals for DG connections in the Feed-in Tariff program are accepted after they pass technical and economical evaluations. Therefore, in this work, the capital, operational and maintenance, and output

energy costs of DG units are not considered in (5.4) because the goal of this study was to encourage the LDCs to accept proposals that maximize their benefits. On the other hand, if the LDC is installing its own DG units, these costs must be considered in (5.4), which completely changes the planning outcomes. This adjustment can be achieved through the addition of a third term in (5.4) to represent DG costs, which are the sum of the capital, installation, and operational costs minus the costs of the energy delivered to the system.

The objectives and problem formulation presented in this work are oriented more toward publicly owned LDCs, where the effect of emissions can be taken into consideration as a decision factor. On the other hand, privately owned LDCs can use the proposed method in order to quantify their carbon footprint and then choose the optimal operating point from the Pareto frontier based on their preferences, which could be the minimum cost operating point.

The proposed dynamic long-term planning problem can be defined by

$$\min_{\Omega}\left([OF_{(1)}(\Omega) \quad OF_{(2)}(\Omega)]\right) \qquad s.t.\ \text{(5.13)-(5.41)} \tag{5.3}$$

$$OF_{(1)}(\Omega) = NPV_{Upgrade} + NPV_{Loss} \tag{5.4}$$

$$OF_{(2)}(\Omega) = E_{CO2}^{Grid} + E_{CO2}^{DG} - E_{CO2}^{PEV} \tag{5.5}$$

$$NPV_{Upgrade} = NPV_{Lines} = \sum_{l\in\mathcal{L}} \frac{C_{UP(l)}}{(1+d')^{Y_{UP(l)}}} \tag{5.6}$$

$$NPV_{Loss} = \sum_{y} \frac{C_{loss(y)}^{Annual}}{(1+d')^{y}} \tag{5.7}$$

$$C_{loss(y)}^{Annual} = \sum_{s\in\mathcal{S}_{sys}} 8760 \times P_{loss(s,y)} \times \mathbb{P}_{(s)} \times C_{kWh}^{AVG} \qquad \forall y \tag{5.8}$$

$$E_{CO2}^{Grid} = \sum_{y} \sum_{s\in\mathcal{S}_{sys}} 8760 \times P_{G(i=1,s,y)} \times \mathbb{P}_{(s)} \times \mathrm{K}_{CO2}^{Grid} \tag{5.9}$$

$$E_{CO2}^{DG} = \sum_{y} \sum_{i \in \mathcal{I}} \sum_{s \in \mathcal{S}_{sys}} 8760 \times P_{NGDG(i,y)} \times P_{NGDG(s)}^{NORM} \times \mathbb{P}_{(s)} \times \mathrm{K}_{CO2}^{NGDG} \quad (5.10)$$

$$E_{CO2}^{PEV} = \sum_{y} \beta_{PEV(y)}^{PEN} \times E_{kWh(y)}^{PEV} \times D_{mi/kWh}^{AVG} \times \mathrm{K}_{CO2/mi} \quad (5.11)$$

$$E_{kWh(y)}^{PEV} = \sum_{s \in \mathcal{S}_{sys}} \left(8760 \times \mathbb{P}_{(s)} \times P_{PEV(s)}^{NORM} \times \left(\sum_{i \in \mathcal{I}} P_{PEV(i,y)}^{Peak} \right) \right) \quad (5.12)$$

where

$OF_{(\sigma)}(\cdot)$ denotes the objective $\sigma \in \mathcal{O}$ required to be minimized;

Ω denotes the vector of decision variables;

E_{CO2}^{Grid}, E_{CO2}^{DG}, and E_{CO2}^{PEV} denote the emissions due to energy purchased from the grid, DG unit emissions, and PEV emission reduction, respectively, in equivalent kg CO2.

$C_{loss(y)}^{Annual}$ denotes the cost of energy losses for year y;

$P_{loss(s,y)}$ denotes the power loss corresponding to state s and year y;

C_{kWh}^{AVG} denotes the average cost of energy;

K_{CO2}^{Grid} denotes the equivalent CO2 emissions for the energy purchased from the grid, in kg/kWh;

K_{CO2}^{NGDG} denotes the equivalent CO2 emissions from NGDG, in kg/kWh;

$P_{NGDG(i,y)}$ denotes the connected capacity of the NGDG on bus i in year y;

$P_{NGDG(s)}^{NORM}$ denotes the generated power corresponding to state s as a fraction of the NGDG capacity;

$\beta_{PEV(y)}^{PEN}$ denotes the optimal penetration of PEV in year y;

$E_{kWh(y)}^{PEV}$ denotes the annual energy consumption for 100 % PEV penetration in the system, in kWh;

$D_{mi/kWh}^{AVG}$ denotes the average distance travelled per kWh;

$\mathrm{K}_{CO2/mi}$ denotes the equivalent CO2 emissions per mile from conventional vehicles in kg /mi;

$P_{PEV(i,y)}^{Peak}$ denotes the peak active power demand for PEVs at 100 % penetration;

$P_{PEV(s)}^{NORM}$ denotes the fraction of the peak PEV demand corresponding to state s.

5.4.2 Constraints

The following are the salient constraints considered in the proposed problem formulation:

1. *Power flow constraints:* The power generated at each bus is dependent on the type of DG and the connected capacity at that bus. On the other hand, the power consumed at each bus is the sum of the normal load power, which is dependent on the type of sector, plus the load power required for PEV charging. It is assumed that the PEV chargers operate at a unity power factor. Thus, the PEV load does not contribute to the load reactive power in the system.

$$P_{G(i,s,y)} - P_{L(i,s,y)} = \sum_{j \in \mathcal{J}} V_{(i,s,y)} V_{(j,s,y)} Y_{(i,j,y)} \cos\left(\theta_{(i,j,y)} + \delta_{(j,s,y)} - \delta_{(i,s,y)}\right) \ \forall i, s, y \tag{5.13}$$

$$Q_{G(i,s,y)} - Q_{L(i,s,y)} = -\sum_{j \in \mathcal{J}} V_{(i,s,y)} V_{(j,s,y)} Y_{(i,j,y)} \sin\left(\theta_{(i,j,y)} + \delta_{(j,s,y)} - \delta_{(i,s,y)}\right) \ \forall i, s, y \tag{5.14}$$

$$P_{G(i,s,y)} = P_{NGDG(i,y)} \times P_{NGDG(s)}^{NORM} + P_{WDG(i,y)} \times P_{WG(s)}^{NORM} + P_{PVDG(i,y)} \times P_{PVDG(s)}^{NORM} \quad \forall i, s, y \tag{5.15}$$

$$Q_{G(i,s,y)} = P_{NGDG(i,y)} \times P_{NGDG(s)}^{NORM} \times \tan(\cos^{-1}(pf_{NGDG})) + P_{WDG(i,y)} \times P_{WG(s)}^{NORM} \times \tan(\cos^{-1}(pf_{WDG})) + P_{PVDG(i,y)} \times P_{PVDG(s)}^{NORM} \times \tan(\cos^{-1}(pf_{PVDG})) \quad \forall i, s, y \tag{5.16}$$

$$P_{L(i,s,y)} = P_{NL(i,s,y)} + P_{L(i,s,y)}^{PEV} \ \forall i, s, y \tag{5.17}$$

$$P_{NL(i,s,y)} = \begin{cases} P_{NL(i,y)}^{Peak} \times P_{RL(s)}^{NORM} & \forall i \in \mathcal{I}_{RL} \\ P_{NL(i,y)}^{Peak} \times P_{CL(s)}^{NORM} & \forall i \in \mathcal{I}_{CL} \quad \forall s, y \\ P_{NL(i,y)}^{Peak} \times P_{IL(s)}^{NORM} & \forall i \in \mathcal{I}_{IL} \end{cases} \tag{5.18}$$

$$P_{L(i,s,y)}^{PEV} = P_{PEV(i,y)}^{Peak} \times P_{PEV(s)}^{NORM} \times \beta_{PEV(y)}^{PEN} \quad \forall i \in \mathcal{I}_{PEV}, s, y \tag{5.19}$$

$$Q_{L(i,s,y)} = P_{NL(i,s,y)} \times \tan\left(\cos^{-1}\left(pf_{L(i)}\right)\right) \quad \forall i, s, y \tag{5.20}$$

where

$P_{PVDG(i,y)}$ and $P_{WDG(i,y)}$ denote the capacities in pu of the connected PVDG, and WDG respectively on bus i in year y;

$P_{PVDG(s)}^{NORM}$ and $P_{WG(s)}^{NORM}$ denote the generated powers corresponding to state s as a fraction of the PVDG and the WDG capacities, respectively;

pf_{NGDG}, pf_{PVDG}, and pf_{WDG} denote the power factor of the NGDG, PVDG, and WDG, respectively;

$P_{NL(i,s,y)}$ and $P_{L(i,s,y)}^{PEV}$ denote the normal load and PEV load respectively at bus i in year y corresponding to state s;

$P_{NL(i,y)}^{Peak}$ denote the peak active power demand for normal loads on bus i in year y;

$P_{RL(s)}^{NORM}$, $P_{CL(s)}^{NORM}$, and $P_{IL(s)}^{NORM}$ denote the fraction of the peak demand corresponding to state s for residential, commercial, and industrial loads, respectively;

$\mathcal{J}_{RL}$, $\mathcal{J}_{CL}$, $\mathcal{J}_{IL}$, and $\mathcal{J}_{PEV}$ denote the sets of residential, commercial, industrial, and PEV load buses respectively, where $\mathcal{J}_{RL}, \mathcal{J}_{CL}, \mathcal{J}_{IL}, \mathcal{J}_{PEV} \subset \mathcal{J}$;

$pf_{L(i)}$ denote the power factor of the normal load on bus $i \in \mathcal{J}$.

2. *Load rise constraints:* In this work, the annual load rise is assumed to be an input value and to be constant, which is a typical assumption for this kind of studies [14]. Thus, the active power demand rise can be defined as in (5.21) and the reactive power demand is assumed to rise with same rate as in (5.20). The annual increase in the normal load demand is assumed to be accompanied by an increase in the number of vehicles. Thus, the value of $P_{PEV(i,y)}^{Peak}$ is assumed to rise at same rate as the normal load. However, the actual penetration $\beta_{PEV(y)}^{PEN}$ for each year in the planning horizon is considered a decision variable, which can vary between the minimum and the maximum limits for each year. For example, assume the value of $P_{PEV(i,y)}^{Peak}$ is equivalent to a load of ρ vehicles in the first year for a certain load point. Therefore, for 1% load rise, the value of $P_{PEV(i,y)}^{Peak}$ in the second year is equivalent to a load of $1.01 \times \rho$ vehicles.

$$P_{NL(i,y)}^{Peak} = P_{NL0(i)}^{Peak} \times (1+\alpha)^{y-1} \quad \forall i, y \tag{5.21}$$

$$P_{PEV(i,y)}^{Peak} = P_{PEV0(i)}^{Peak} \times (1+\alpha)^{y-1} \quad \forall i \in \mathcal{I}_{PEV}, y \tag{5.22}$$

where $P_{NL0(i)}^{Peak}$ and $P_{PEV0(i)}^{Peak}$ denote the peak demand on bus i at the beginning of the planning period for the normal loads and the 100% penetration PEV charging load, respectively.

3. *Years of DG placement constraints:* The DG output power at each bus is set to zero before the DG placement and then updated to the installed capacity at and after the year of placement, as given in (5.23) to (5.25).

$$P_{NGDG(i,y)} = \begin{cases} 0 & \forall y < Y_{(i)}^{NGDG} \\ P_{0(i)}^{NGDG} & \forall y \geq Y_{(i)}^{NGDG} \end{cases} \tag{5.23}$$

$$P_{WDG(i,y)} = \begin{cases} 0 & \forall y < Y_{(i)}^{WDG} \\ P_{0(i)}^{WDG} & \forall y \geq Y_{(i)}^{WDG} \end{cases} \tag{5.24}$$

$$P_{PVDG(i,y)} = \begin{cases} 0 & \forall y < Y_{(i)}^{PVDG} \\ P_{0(i)}^{PVDG} & \forall y \geq Y_{(i)}^{PVDG} \end{cases} \tag{5.25}$$

where

$P_{0(i)}^{NGDG}$, $P_{0(i)}^{PVDG}$, and $P_{0(i)}^{WDG}$ denote the capacities of the installed NGDG, PVDG, and WDG units on bus i, respectively;

$Y_{(i)}^{NGDG}$, $Y_{(i)}^{PVDG}$, and $Y_{(i)}^{WDG}$ denote the years of placing NGDG, PVDG, and WDG units on bus i, respectively.

4. *Voltage limit constraints:* The voltage limits constraints are defined as follows:

$$V_{min} \leq V_{(i,s,y)} \leq V_{max} \quad \forall i, s, y \tag{5.26}$$

5. *Maximum reverse power flow constraints:* These constraints limit the DG penetration in the system for every year, with the maximum allowable DG penetration being that which causes the maximum reverse power flow at the minimum load condition as in (5.27).

$$\sum_{i\in\mathcal{I}}\left(P_{NGDG(i,y)}+P_{WDG(i,y)}+P_{PVDG(i,y)}-\min_{s}\left(P_{L(i,s,y)}\right)\right)\leq P_{MAX}^{Rev} \tag{5.27}$$

6. *Discrete size of DG constraints:* The connected DG capacities at each bus i are assumed to be discretized at a fixed step that is dependent on the type of DG.

$$P_{0(i)}^{NGDG}=\ a_{NGDG(i)}\times \mathcal{b}_{NGDG(i)}\times P_{NGDG}^{Step}\quad \forall i \tag{5.28}$$

$$P_{0(i)}^{WDG}=\ a_{WDG(i)}\times \mathcal{b}_{WDG(i)}\times P_{WDG}^{Step}\quad \forall i \tag{5.29}$$

$$P_{0(i)}^{PVDG}=\ a_{PVDG(i)}\times \mathcal{b}_{PVDG(i)}\times P_{PVDG}^{Step}\quad \forall i \tag{5.30}$$

where

$a_{PVDG(i)}$ denotes an integer variables indicating the installed PVDG size as multiple of fixed step;

$\mathcal{b}_{PVDG(i)}$ denotes a binary variables indicating the decision of installing PVDG on bus i;

P_{PVDG}^{Step} denotes the discretized step of PVDG capacity.

7. *Limit on the number of DG units:* The number of DG units installed in the system during the planning horizon is assumed to be limited based on the preferences of the LDC. It is worth noting that, if these constraints are ignored, the outcomes of the planning problem would result in numerous small-capacity DG units spread throughout the system, which is not practical.

$$\sum_{i\in\mathcal{I}}\mathcal{b}_{NGDG(i)}\leq M_{NGDG}^{Limit} \tag{5.31}$$

$$\sum_{i\in\mathcal{I}} \mathcal{b}_{WDG(i)} \leq M_{WDG}^{Limit} \tag{5.32}$$

$$\sum_{i\in\mathcal{I}} \mathcal{b}_{PVG(i)} \leq M_{PVG}^{Limit} \tag{5.33}$$

where M_{PVDG}^{Limit} denotes the maximum number of PVDG units installed in the system.

8. *Candidate bus constraints:* DG units are not permitted to be connected to any bus in the system other than the candidate buses sets, as in (5.34) to (5.36).

$$a_{NGDG(i)}\,,\mathcal{b}_{NGDG(i)} = 0 \quad \forall i \in \mathcal{I} - \mathcal{I}_{NGDG} \tag{5.34}$$

$$a_{WDG(i)}\,,\mathcal{b}_{WDG(i)} = 0 \quad \forall i \in \mathcal{I} - \mathcal{I}_{WDG} \tag{5.35}$$

$$a_{PVG(i)}\,,\mathcal{b}_{PVDG(i)} = 0 \quad \forall i \in \mathcal{I} - \mathcal{I}_{PVDG} \tag{5.36}$$

where $\mathcal{I}_{PVDG} \subset \mathcal{I}$ denote the set of candidate buses for PVDG units.

9. *PEV penetration constraints:* The constraints in (5.37) limit the PEV penetration to a maximum and a minimum value. Moreover, the constraints in (5.38) are required to ensure that the penetration for each year is higher than or equal to that of the previous year.

$$\beta_{PEV(y)}^{MAX} \geq \beta_{PEV(y)}^{PEN} \geq \beta_{PEV(y)}^{MIN} \quad \forall y \tag{5.37}$$

$$\beta_{PEV(y)}^{PEN} \geq \beta_{PEV(y-1)}^{PEN} \quad \forall y > 1 \tag{5.38}$$

where $\beta_{PEV(y)}^{MIN}$ denotes the allowable minimum PEV penetration in year y.

10. *Maximum bus connection constraint:* The maximum capacity of the DG connection to any individual bus is limited to $P_{DG(i)}^{limit}$, which depends on the voltage level at the bus and on the technical constraints of the LDC.

$$P_{NGDG(i)} + P_{WDG(i)} + P_{PVDG(i)} \leq P_{DG(i)}^{limit} \qquad \forall i \tag{5.39}$$

11. *Feeders upgrade constraints*: The NPV of the feeders' upgrade costs depend on the upgrade year of each feeder, where the feeder upgrade is assumed to be based on reinforcing the feeder by another one. The feeder upgrade constraints can therefore be described as in (5.40) and (5.41).

$$I_{(l,s,y)} \leq I_{MAX(l,y)} \;\; \forall l, s, y \tag{5.40}$$

$$I_{MAX(l,y)} = \begin{cases} I_{(l)}^{CAP} & \forall y < Y_{UP(l)} \\ M_{(l)}^{RNF} \times I_{(l)}^{CAP} & \forall y \geq Y_{UP(l)} \end{cases} \qquad \forall l, y \tag{5.41}$$

5.4.3 NDSGA Implementation

Evolutionary algorithms are well known to be suitable for solving multi-objective problems because they are less sensitive to the shape and continuity of the Pareto frontier [133]. In this work, a NDSGA was utilized for solving the proposed problem. As explained in detail in [134], this method is widely used in multi-objective problems because of its reduced computational effort and faster convergence compared to other methods. However, the obtained solution is no guaranteed to be the true Pareto-optimal front. Still, it is a satisfactory solution and close to the true Pareto-optima front [134].

It is a population-based, algorithm in which each individual Ω in the population consists of four parts. The first part includes the DG capacity integer variables $\mathscr{b}_{NGDG}$, $\mathscr{b}_{PVDG}$, and $\mathscr{b}_{WDG}$, and the second incorporates the binary decision variables a_{NGDG}, a_{PVDG}, and a_{WDG}. The lengths of these two parts are equal and depend on the type of DG units as well as the number of candidate buses for each type. The third part involves the year of installation and the feeders upgrade decisions, which are based on the number of DG units that are permitted to be connected to the system (M_{NGDG}^{Limit}, M_{PVDG}^{Limit}, and M_{WDG}^{Limit}) and the number of feeders, respectively. The final part indicates the optimal PEV penetration $\beta_{PEV(y)}^{PEN}$ and its length equals the years under study.

5.5 Sample Case Study

This section presents a simulated case study, the results of which are discussed in next section. The 38-bus 12.66 kV system [113] shown in Figure 5.1 and described in Appendix A is used as the study

case. The system contains a mix of residential, commercial, and industrial customers who share 23%, 67% and 10% of the total system load respectively. The total peak load of the system is 4.37 MVA.

The PEV uncontrolled charging model developed in Chapter 4 is used in this case study. The minimum and maximum PEV penetration for the 20-year study period are assumed to start at 1 % and to increase linearly until they reach 20 % and 60 % respectively at the end of the study period . The remaining data used in the case study are shown in Table 5.1. In this study, PEV charging is assumed to occur at home so that the PEV extra load on the system is located only at residential buses; i.e., the set of PEV buses $\mathcal{J}_{PEV}$ is the same as the set of residential load buses $\mathcal{J}_{RL}$.

Table 5.1 Simulation parameters

WDG PARAMETERS			
Cut-in, rated, and cut-out speeds (m/s)		4, 16, and 25, respectively	
P_{WDG}^{Step} **(kW)**		100	
PVDG PARAMETERS [18]			
Peak power or P_{PVDG}^{Step} (W)		75	
Open circuit voltage (V)		21.98	
Short circuit current (A)		5.32	
Voltage at maximum power (V)		17.32	
Current at maximum power (A)		4.76	
Voltage temperature coefficient (mV/^{o}C)		14.40	
Current temperature coefficient (mA/^{o}C)		1.22	
Nominal cell operating temperature (^{o}C)		43.00	
PEV MODEL PARAMETERS			
AER **(mi)**	70	**Level 2 charger [5]**	240 V, 16-30 A
COST-RELATED PARAMETERS			
C_{kWh}^{AVG} **($/kWh)**	0.0665 [135]	d **(%)**	9.15
e **(%)**	1.8	$D_{mi/kWh}^{AVG}$ **(mi/kWh)**	3.54 [50]
EMISSIONS PARAMETERS			
K_{CO2}^{Grid} **(kg/kWh)**		143 CO_2 and 0.18 NO_2 [135]	
K_{CO2}^{NGDG} **(kg/kWh)**		307 CO_2 and 0.236 NO_2 [136]	
$K_{CO2/mi}$ **(kg/mi)**		0.21 CO_2 [137]	

Table 5.2 WDG and PVDG states

States as a percentage of DG capacity						
WDG	0.00 %	12.47 %	28.18 %	42.58 %	59.59 %	100.00 %
PVDG	0.00 %	10.15 %	23.56 %	40.13 %	58.84 %	80.20 %

Candidate DG bus locations are determined based on detailed techno-economic planning analysis, which is outside the scope of the work presented here. The locations were assumed as input to the model. All system buses were therefore assumed to be candidates for dispatchable and PVDG connections. However, as a reflection of the limitations on installing wind turbines in populated areas, for WDG, only buses 34, 35, 36, 37, and 38 were assumed as candidate buses.

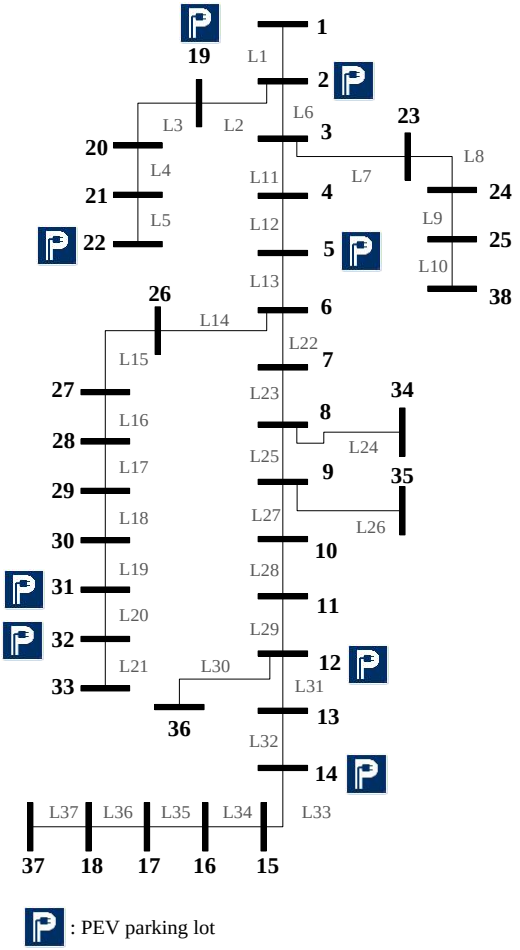

Figure 5.1 System under study

As mentioned in subsection 5.3.1, the WDG and PVDG output powers are discretized into six states based on the central centroid sorting process presented in [103], as shown in Table 5.2. The number of states is a tradeoff between accuracy and the computational time required for the solution of the proposed problem.

5.6 Results and Discussion

This section includes optimization results for the case study described earlier. The values presented are entirely system dependent and are contingent on a number of factors, such as the system structure, candidate buses, allowable DG connections, load types, load demand, load growth, and the region where the system is located.

5.6.1 Base Case Results

The base case, which represents the system with no DG units and with minimum PEV penetration, is shown as scenario *A* in Figure 5.2, with the details appearing in Table 5.3 and Figure 5.3. As shown in Table 5.3, the total system costs are $2.219 M, and the total system emissions are 6.5818×10^7 kg CO_2 over the 20 years under study. The shares of the system costs represented by upgrades and losses are 80.7 % and 19.3 %, respectively, which shows that, in the system under study, reducing upgrade costs is more effective than reducing the costs associated with losses. On the other hand, the reduction in emissions associated with PEV charging decreased the total emissions by 21.4 % for the minimum PEV penetration permitted. This percentage can be increased if the target PEV penetration in the system is expanded, as can be observed in the next scenarios. For the system under study, the total system costs and emission values are assumed to be significant with a peak load of 4.37 MVA.

5.6.2 Pareto Frontier Results

In this case, the NDSGA technique is used to generate the Pareto frontier, which represents the optimal system scenarios. Two points represent the boundary scenarios: scenario *B* represents minimum system costs, and scenario *C* represents minimum system emissions. For these two boundary scenarios, the details of the system costs and emissions, and of the DG units in the system, are shown in Table 5.4. The target penetration levels for both scenarios are shown in Figure 5.3. As shown in Table 5.4, the system costs for scenario *B* are lower than the base case by 69.35 %, which is very significant. However, the system emissions are 61.41 % higher than the emissions in the base case, and the target PEV penetration is set to the minimum. The outcome of the problem shows 1.6 MW of dispatchable DG units and 0.22 MW of PVDG connected to the system, which represent the

optimal mix of DG units for minimizing the system costs. The connected DG units have a significant effect on reducing system costs, but also dramatically increase emissions. The mix of NGDG and PVDG is able to reduce the cost of upgrades and the cost of system losses by 73.45 % and 52.21 %, respectively. This scenario shows the effect of the stochastic nature of renewable DG units, which limits their ability to reduce system costs. It has previously been proven [18, 44] that renewable DG units can effectively reduce system losses. However, as explained in detail in Chapter 3, when system upgrades are considered, no risk of overloading is considered, so renewable DG units can therefore not contribute to a reduction in the cost of upgrades. It is worth noting that, the connected DG units in this scenario are mainly dispatchable, and the PVDG units shown in outcomes affect only the system losses.

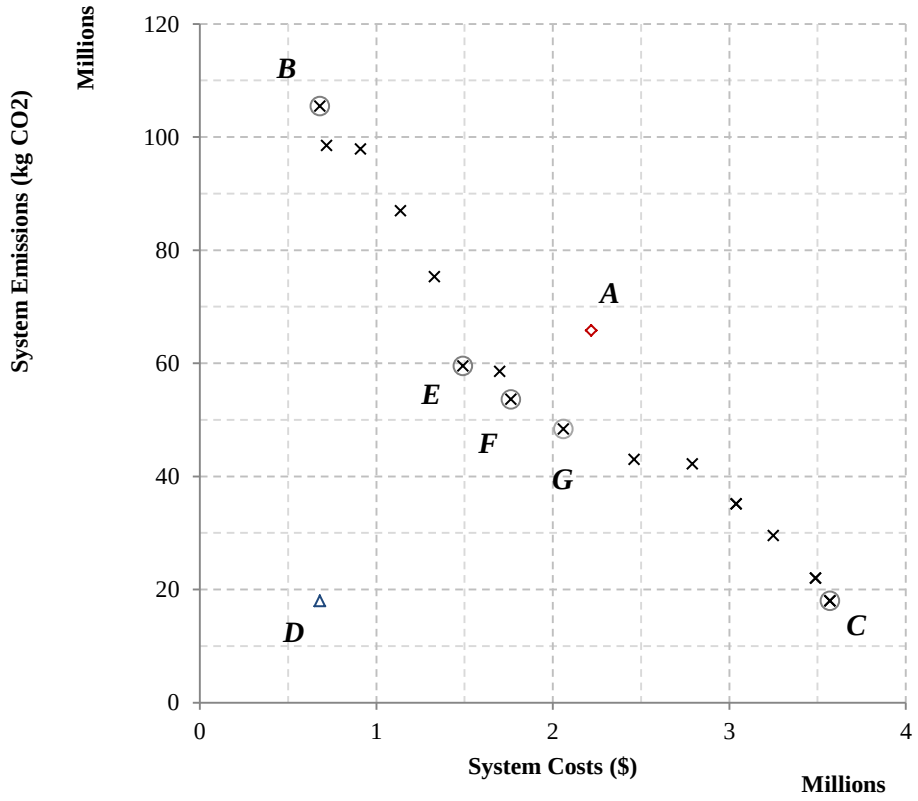

Figure 5.2 Pareto frontier results

On the other hand, scenario *C* represents minimum system emissions. As shown in Table 5.4, the system costs are 60.91 % higher than with the base case, and the system emissions are 72.64 % lower than the base case emissions. The outcome of the problem shows 0.6 MW WDG and almost 2.4 MW PVDG connected to the system. The benefit of this mix of renewable DG types is due to the advantages of each type relative to the other. PVDG has two advantages: the PVDG unit capacities can be almost any value (multiples of 75 W) compared to the discretized capacities of WDG (multiples of 100 kW), and PVDG can be connected to any bus in the system, while the WDG can be connected only to 5 buses. On the other hand, the WDG has two advantages: it is more appropriate for providing output power for the extra load imposed by PEV charging because most PEV charging occurs at evening and night when wind speeds are high and solar irradiance is negligible, and WDG has a higher capacity factor than PVDG. In this scenario, the target PEV penetration reaches 60 % in 20 years, as shown in Figure 5.3.

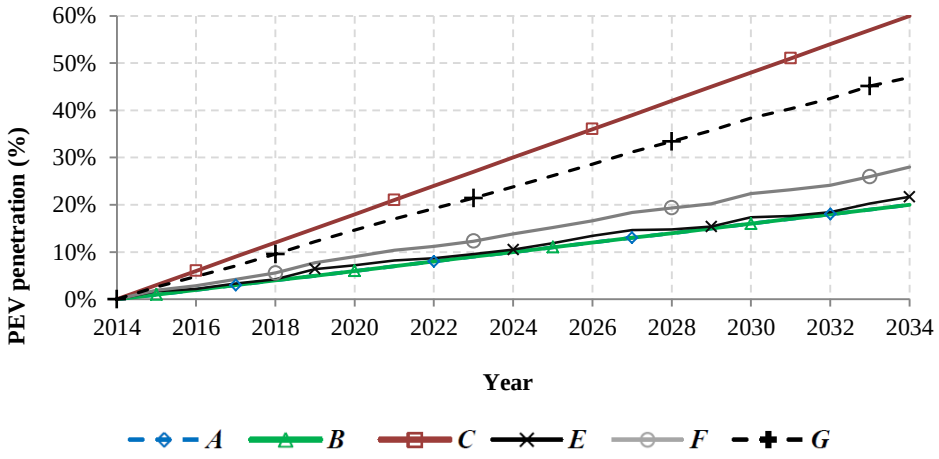

Figure 5.3 PEV target penetration levels for different scenarios

Table 5.3 Base case results

Results for scenario *A*			
System Costs ($)			
Upgrade	**Losses**		**Total**
1.790×10^6	4.287×10^5		2.219×10^6
System Emissions (kg CO_2 equivalent)			
Energy from grid	**DG units**	**Reduction due to PEV**	**Total**
8.379×10^7	0	1.797×10^7	6.582×10^7

Table 5.4 Results for boundary scenarios

Results for scenario *B*								
System Costs ($)								
Upgrade			**Losses**			**Total**		
4.752×10^5			2.049×10^5			6.801×10^5		
System Emissions (kg CO_2 equivalent)								
Energy from grid			**DG units**			**Reduction due to PEV**		**Total**
3.467×10^7			8.954×10^7			1.797×10^7		10.624×10^7
DG Units (kW)								
NGDG			**WDG**			**PVDG**		
Size	**Bus**	**Year**	**Size**	**Bus**	**Year**	**Size**	**Bus**	**Year**
200	13	1				63.88	13	1
100	18	1				2.78	18	1
900	24	1				126.67	24	2
200	31	1				1.883	31	1
200	33	2				26.65	33	1
Results for scenario *C*								
System Costs ($)								
Upgrade			**Losses**			**Total**		
3.196×10^6			0.374×10^6			3.570×10^6		
System Emissions (kg CO_2 equivalent)								
Energy from grid			**DG units**			**Reduction due to PEV**		**Total**
7.192×10^7			0			5.391×10^7		1.801×10^7
DG Units (kW)								
NGDG			**WDG**			**PVDG**		
Size	**Bus**	**Year**	**Size**	**Bus**	**Year**	**Size**	**Bus**	**Year**
			600	35	1	624.8	11	1
						1.66	13	1
						739.02	17	1
						2.22	18	1
						1032.23	29	1

5.6.3 Compromise Solution

Depending on the preferences of the DM, any point on the Pareto frontier can be chosen as an operating point if it conforms to their operational policies and reflects their emission/cost requirements. However, one of the widely used posteriori techniques for choosing a compromise solution for multi-objective problems is based on minimizing the distance between the Pareto frontier and an ideal solution called the utopia point [138]. This point is infeasible because it is impossible to minimize the two objectives simultaneously, i.e., it lies outside the feasible region. Thus, the utopia point, which represents the minimum system costs and the minimum system emissions, was defined as scenario *D*, as shown in Figure 5.2. The costs and emissions for the ideal scenario *D* are \$0.680 M and 1.801 × 10^7 kg CO_2, respectively. Assume $\mathcal{FS}$ is the set of feasible solution vectors and $\mathcal{OS} \subset \mathcal{FS}$ is the set of optimal solution vectors, which corresponds to the Pareto frontier. Thus, among the solution Pareto frontier vectors $\Omega^* \in \mathcal{OS}$, there is only one solution vector $\Omega_{(\sigma)}^{*MIN} \in \mathcal{OS}$ corresponds to the optimum value for each objective $OF_{(\sigma)}(\cdot)$. The dissatisfaction associated with any operating point $DS_{(\sigma)}(\Omega^*)$ is defined as the normalized distance to the ideal point $(\Omega_{(1)}^{*MIN}, \Omega_{(2)}^{*MIN}, \dots)$, as in [138]. Therefore, the compromise solution can be defined as in (5.43).

$$DS_{(\sigma)}(\Omega^*) = \sqrt{\frac{\left(OF_{(\sigma)}(\Omega^*) - OF_{(\sigma)}\left(\Omega_{(\sigma)}^{*MIN}\right)\right)^2}{\left(OF_{(\sigma)}\left(\Omega_{(\sigma)}^{*MAX}\right) - OF_{(\sigma)}\left(\Omega_{(\sigma)}^{*MIN}\right)\right)^2}} \tag{5.42}$$

$$\min_{\Omega^*}\left(\sqrt{\sum_{\sigma \in \mathcal{O}}\left(DS_{(\sigma)}(\Omega^*)\right)^2}\right) \tag{5.43}$$

where $\Omega_{(\sigma)}^{*MAX}$ is the solution vector on the Pareto frontier that corresponds to the maximum value for objective σ.

The point corresponding to the compromise solution is shown in Figure 5.2 as scenario *E*. The outcomes of this scenario are shown in Table 5.5 and Figure 5.3. For scenario *E*, the target PEV penetration reaches 21.7 % after 20 years, and the reductions in the system costs and emissions, compared to the base case, are 32.82 % and 9.55 %, respectively. This solution shows DG units with a total capacity of 1.689 MW connected to the system, involving 11.84 %, 5.92 %, and 82.2 % NGDG, WDG, and PVDG, respectively. This mix represents the optimal mix for the compromise solution *E* for the two objectives considered.

Table 5.5 Compromise solution results

Results for scenario *E*								
System Costs ($)								
Upgrade			**Losses**			**Total**		
1.184×10^6			0.306×10^6			1.491×10^6		
System Emissions (kg CO_2 equivalent)								
Energy from grid			**DG units**		**Reduction due to PEV**		**Total**	
6.776×10^7			1.126×10^7		1.949×10^7		5.953×10^7	
DG Units (kW)								
NGDG			**WDG**			**PVDG**		
Size	**Bus**	**Year**	**Size**	**Bus**	**Year**	**Size**	**Bus**	**Year**
100	15	1	100	35	1	16.91	13	1
100	18	1				27.99	17	1
						9.32	18	1
						347.05	24	1
						988.54	29	1
Results for scenario *F*								
System Costs ($)								
Upgrade			**Losses**			**Total**		
1.459×10^6			0.304×10^6			1.762×10^6		
System Emissions (kg CO_2 equivalent)								
Energy from grid			**DG units**		**Reduction due to PEV**		**Total**	
6.739×10^7			1.126×10^7		2.503×10^7		5.362×10^7	
DG Units (kW)								
NGDG			**WDG**			**PVDG**		
Size	**Bus**	**Year**	**Size**	**Bus**	**Year**	**Size**	**Bus**	**Year**
200	15	1	100	35	1	14.60	13	1
						141.00	17	1
						8.32	18	1
						392.35	24	1
						995.50	29	1

The second best solution is scenario *F*, in which the reduction in system costs and emissions are 20.57 % and 18.53 %, respectively, as shown in Table 5.5. The target PEV penetration for scenario *F* reaches 28.01 % after 20 years, as shown in Figure 5.3. This penetration level increases the total costs and reduces the total emissions as compared to scenario *E*. As shown in Table 5.5, scenario *F* is also characterized by a PVDG share of almost 91.83 % of the total DG installation in the system.

In summary, the two optimal solutions *E* and *F* represent the solutions closest to the ideal scenario, and each encompasses different percentages of DG types, years of DG installation, PEV penetration levels, emission reductions, and cost reductions. Based on operational preferences, the DM can choose either of these two optimal solutions or can select any other solution from the Pareto frontier as an operational point. For example, for higher PEV penetration, the DM can choose scenario G as an operating point, which is characterized by maximum penetration 46.98 %, as shown in Figure 5.3.

5.7 Conclusions

This chapter has presented a long-term dynamic planning approach to accommodate a rising penetration of uncoordinated PEV charging load in distribution networks. The presented method can help the LDCs to better assess the impacts of PEV charging load on their systems and enable them to gather additional information about the PEV charging demand before deploying charging coordination infrastructure.

The proposed work can also assist the LDC in evaluating DG connection proposals based on a determination of the optimal location, size, and year of installation of renewable and dispatchable DG units so that system costs and emissions are minimized while higher percentages of PEV integration are permitted in the system. The proposed method takes into consideration the stochastic nature of renewable DG, load variability, load types, and the technical constraints of the system. A probabilistic method is also proposed as a means of generating virtual scenarios of PEV charging patterns, while taking into account travel patterns, variable charging times, multiple charging events per day, and the effect of ambient temperature.

The planning problem is defined as multi-objective mixed-integer nonlinear programming, in which an NDSGA is used to obtain the Pareto frontier. The outcome of the planning problem shows the domination of dispatchable DG units with respect to system costs, while a mix of WDG and PVDG can effectively reduce system emissions. The results demonstrate that a significant reduction in either system costs or system emissions can be obtained. However, because system costs and

system emissions cannot both be minimized simultaneously, a compromise solution must be chosen based on the preferences of the DMs. Although the results are entirely system dependent, the proposed method is generalizable and can be applied to any distribution network.

Chapter 6
Real-time PEV Charging Coordination in Smart Distribution Systems

6.1 Introduction

Two categories of solutions have been proposed in the literature as a means of facilitating the accommodation of high PEV penetration. The first involves uncoordinated PEV charging, which is possible either through upgrades to the power system infrastructure or through the deployment of DG units to meet the excess power demand. The second category, which is addressed in this chapter, targets coordinated PEV charging or charging/discharging, which relies on a two-way communication infrastructure under the smart grid paradigm.

Smart charging/discharging coordination architecture consists of three main units: a data collection and storage unit, a prediction unit, and an optimization unit [7]. The data collection and storage unit governs the collection of information related to current power demands of PEVs and regular loads. In most cases, an aggregator is assumed to be in place to deal with PEV data collection and storage. The role of the aggregator is to collect information from the PEVs and send it to the control center, and to send charging/discharging decisions from the control center to the chargers. The prediction unit should provide accurate forecasts of future PEV power demands and regular loads in the system. Based on this information, the optimization unit should then make optimal coordinated charging and discharging decisions that guarantee service reliability, maximize operator profit, satisfy system constraints, and meet customer power demands.

As mentioned in section 2.6, one limitation of the solutions proposed in the literature is that most fail to address coordinated PEV charging and discharging decisions that are based on real-time measurements from the grid. As a result, the effect of current and future PEV charging and discharging decisions on the power grid is not considered. While some studies involve coordinated decisions based on PEV load forecast data, not many details are available with respect to the actual performance of the PEV load forecast, and perfect PEV load forecast data are usually assumed. The system response to short-term fluctuations in the PEV load is therefore not examined. As well, in most cases, the problem formulation fails to include consideration of electric power grid constraints and customer power demands. Customer satisfaction and the feasibility of the decisions are hence not guaranteed.

Motivated by the above deficiencies, a novel online coordination method for the charging of PEVs in smart distribution networks is proposed in this chapter. The goal of the proposed method is to optimally charge the PEVs in order to maximize the PEV owners' satisfaction and to minimize system operating costs without violating the grid constraints. Unlike the solutions reported in the literature, the proposed charging architecture guarantees the feasibility of the charging decisions by means of a novel prediction unit that can forecast future PEVs power demand and through an innovative two-stage optimization unit that ensures effective charging coordination.
In the next section an overview of the proposed PEV coordination architecture is introduced, followed by detailed descriptions of the proposed prediction unit and optimization unit.

6.2 Proposed PEV coordination architecture

The proposed smart real-time coordination system (SRTCS) architecture is shown in Figure 6.1. The smart distribution system has a set of buses $\mathcal{I}$. The smart distribution is also partitioned into sections, each served by one aggregator. The set of system aggregators is denoted by $\mathcal{A} = \{A_{(1)}, A_{(2)}, \cdots A_{(N_{AG})}\}$, where N_{AG} is the total number of aggregators in the system. Each bus $i \in \mathcal{I}_{(a)}^{AGG}$ has a set of parking lots $\mathcal{PL}_{(i,a)}$, where $\mathcal{I}_{(a)}^{AGG}$ is the set of buses under the jurisdiction of aggregator $a \in \mathcal{A}$. A set of chargers $\mathcal{CH}_{(i,p_{(i,a)})}$ is defined for each parking lot $p_{(i,a)} \in \mathcal{PL}_{(i,a)}$, which is connected to any bus $i \in \mathcal{I}_{(a)}^{AGG}$. A maximum of one PEV is connected per charger. The whole system is served by one central vehicle controller (CVC). The prediction and optimization units are located inside the aggregators and the CVC, respectively.

Each vehicle driver provides the system with the vehicle charging identity (ID), his/her parking duration, and the required SOC value, which should be less than or equal to a maximum value displayed on the charging panel. The driver-required SOC value can be less than the maximum SOC value because it is dependent on the driver's preferences, the current electricity price, and his/her daily trips. The maximum SOC value depends on the battery capacity, the battery characteristics, the charger capacity, and the parking duration. The current SOC value of the PEV is also made available to the aggregator through the physical measurement of the battery pack voltage. Three types of SOC values can therefore be defined: required, maximum, and current.

The operation of the CVC and the aggregator is illustrated in Figure 6.2, and is described as follows. The aggregator receives a request for information from the CVC at a time instant $t_{(r)}$, $r \in \mathcal{RQ}$ with $\mathcal{RQ}$ denoting the set for the CVC information request events.

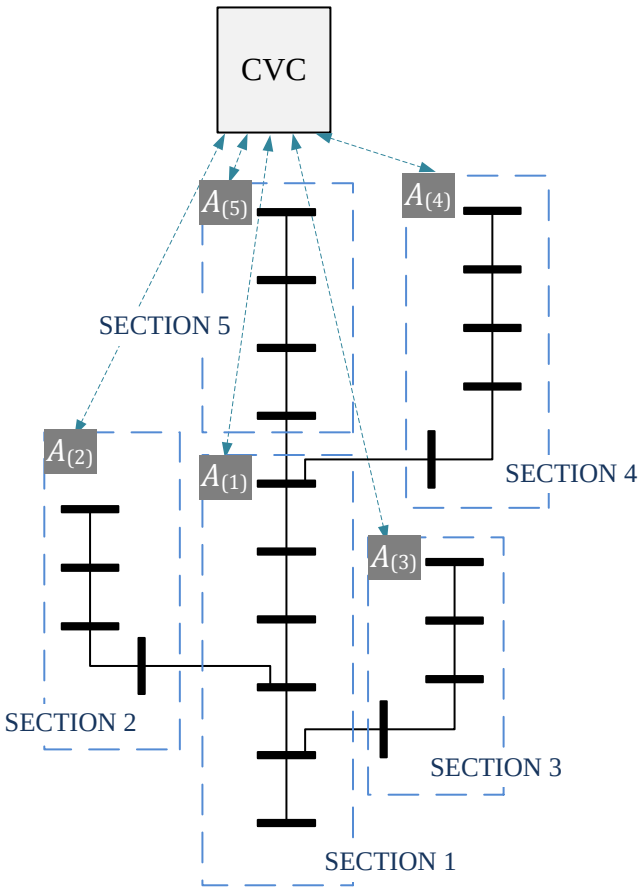

Figure 6.1 Proposed SRTCS architecture.

At $t_{(r)}$, the aggregator starts to process the vehicle data in all parking lots in the territory served by the aggregator. Using the processed data an individual prediction interval $\tau_{(a,r)}^{PRD}$ for each $a \in \mathcal{A}$ and $r \in \mathcal{RQ}$. The prediction interval $\tau_{(a,r)}^{PRD}$ can be defined as the maximum parking duration of all PEVs under the jurisdiction of the aggregator $a \in \mathcal{A}$.

Each aggregator sends its individual prediction duration $\tau_{(a,r)}^{PRD}$ to the CVC, which defines a unified prediction interval $\tau_{sys(r)}^{PRD}$ so that all aggregators can impose a synchronous operation. The choice of $\tau_{sys(r)}^{PRD}$ ensures that the CVC has information about the PEV load in the system sufficiently far ahead to enable optimal coordination decisions to be produced. Given $\tau_{sys(r)}^{PRD}$, which is sent back from the CVC, each aggregator runs its prediction unit in order to forecast the number of PEVs in the system during the next $\tau_{sys(r)}^{PRD}$ interval, given the current PEVs in the system.

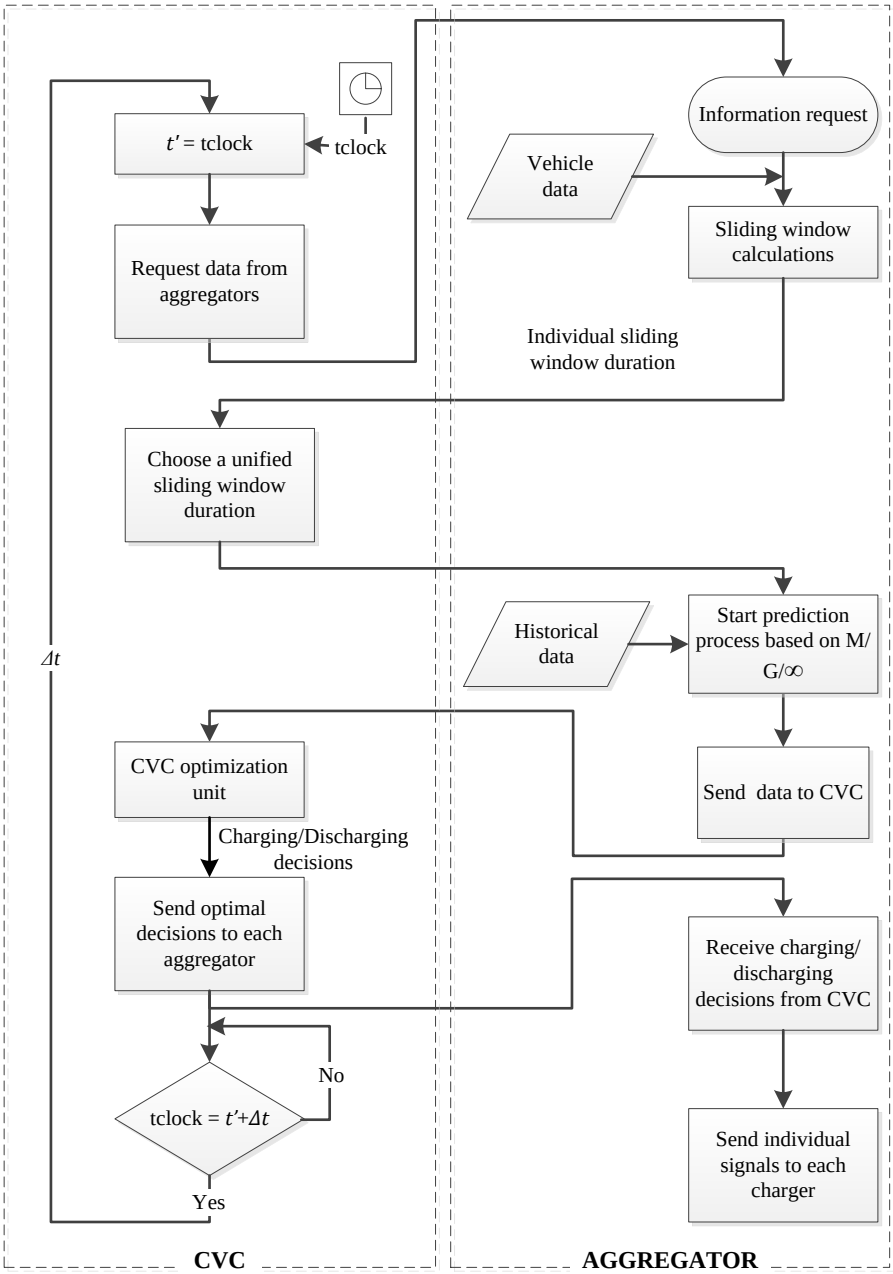

Figure 6.2 Flow chart of the CVC and aggregator operation [139].

Each aggregator then transmits to the CVC the information about currently connected PEVs along with the predicted number of PEVs. Once the CVC receives this information from all aggregators in the system, it runs its optimization unit. To produce its charging/discharging decisions, the optimization unit solves a two-stage optimization problem. The first stage is aimed at reaching a

feasible power allocation decision with respect to a target SOC value for each PEV connected, while including consideration of the electric grid constraints, customer demand (SOC required by the PEV), and current and future system power loads. Future power loads include both the PEV loads predicted by the aggregators for the next $\tau_{sys(r)}^{PRD}$ interval and the regular load forecast. The regular load forecast can follow any of the conventional techniques described in [140].

The first stage is referred to as the delivered energy maximization stage (DEMS). The second stage is designed to achieve the efficient utilization of the available resources in order to satisfy the target PEV SOC, as calculated in the DEMS, while minimizing system operating costs. The second optimization stage is referred to as the cost minimization stage (CMS). This sequential structure results in charging/discharging decisions that are guaranteed to be feasible, as will be explained later. The decisions are then transmitted from the CVC to the aggregators, which send an individual control signal to each charger under its jurisdiction. The entire process is repeated after a time duration Δt for a synchronous operation, $\Delta t \ll \tau_{sys(r)}^{PRD}$. The duration of Δt should be sufficiently long to allow for computation and communication delays. In the following two sections, the aggregator prediction unit and the CVC optimization unit are discussed in greater detail.

6.3 Aggregator PEV Prediction Unit

The aggregator PEV prediction unit predicts the number of PEVs that will be simultaneously present in the parking lots under the jurisdiction of that aggregator during the next $\tau_{sys(r)}^{PRD}$ interval.

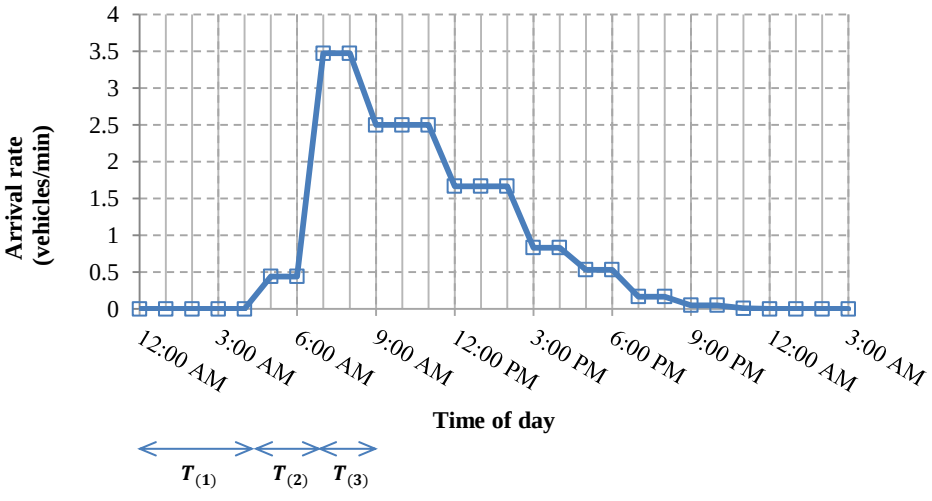

Figure 6.3 Temporal variation of the PEV arrival rates over the day.

The time is partitioned into a set of intervals $\mathcal{T} = \{T_{(1)}, T_{(2)}, \cdots, T_{(N_t)}\}$, where $\mathcal{T}$ covers 24 h of the day. The time intervals of $\mathcal{T}$ reflect temporal variations in the PEV arrival rates during the course of a day, as shown in Figure 6.3, which shows a typical weekday arrival pattern in a commercial parking lot in downtown Toronto, Canada. Within time interval $T_{(w)} \in \mathcal{T}$, PEV arrivals to parking lot $p_{(i,a)}$ under the jurisdiction of aggregator a are modeled as a Poisson process, with an arrival rate $\lambda_{(p_{(i,a)},w)}$. The durations of the PEVs' stay in the parking lot $t_{prk(p_{(i,a)},w)}$ follow a general distribution with pdf $f_{prk(p_{(i,a)},w)}(t)$ and mean time $t^{AVG}_{prk(p_{(i,a)},w)}$. The capacity of each parking lot $p_{(i,a)}$ under the jurisdiction of aggregator a is $H^{MAX}_{(p_{(i,a)})}$ PEVs.

The next operation takes place during each time interval $T_{(w)} \in \mathcal{T}$ and for each parking lot $p_{(i,a)}$ under the jurisdiction of each aggregator $a \in \mathcal{A}$. Once the aggregator receives the unified prediction interval value $\tau^{PRD}_{sys(r)}$ from the CVC, the prediction unit determines the number of PEVs that will be simultaneously present during $\tau^{PRD}_{sys(r)}$. The prediction interval is partitioned into a set of periods $\mathcal{D}_{(r)} = \left\{D_{(1_{(r)})}, D_{(2_{(r)})}, \cdots, D_{(B_{(r)})}\right\}$, each with an equal duration Δt, where $B_{(r)} = \frac{\tau^{PRD}_{sys(r)}}{\Delta t}$. This process is shown in Figure 6.4, with the end of period $D_{(b_{(r)})}$ being denoted by $t_{(b_{(r)})}$, where $b_{(r)} = 1,2,\cdots,B_{(r)}$.

Given the number of PEVs present at the time instant $H_{(p_{(i,a)})}\left(t_{(b_{(r)})}\right)$ and their parking durations, a simple calculation provides the number of PEVs that will stay until the end of each period in $\mathcal{D}_{(r)}$, which is denoted by $\widetilde{H}_{1(p_{(i,a)})}\left(t_{(b_{(r)})}\right)$. Since the PEV arrivals follow a Poisson process, the duration of each PEV's stay follows a general distribution, and since all PEVs are served without queueing, the transient analysis of an $M/G/\infty$ queueing model [141, 142] can be used to determine the number of PEVs that will arrive during $D_{(b_{(r)})} \in \mathcal{D}_{(r)}$ and stay in each parking lot until the end of each period $t_{(b_{(r)})}$. Specifically, assuming a stationary PEV arrival and departure process in $T_{(w)} \in \mathcal{T}$, PEV arrivals follow a Poisson process with a mean $\mu_{V(p_{(i,a)},w,b_{(r)})} = \lambda_{(p_{(i,a)},w)} \times b_{(r)} \times \Delta t \times \mathbb{p}_{T(p_{(i,a)},b_{(r)})}$ denotes the probability that a PEV arriving at a parking lot under the jurisdiction of aggregator a during $\left(t_{(r)}, t_{(b_{(r)})}\right]$ is still present in the same parking lot at time $t_{(b_{(r)})}$. The probability $\mathbb{p}_{T(p_{(i,a)},b_{(r)})}$ is given by the following [142]

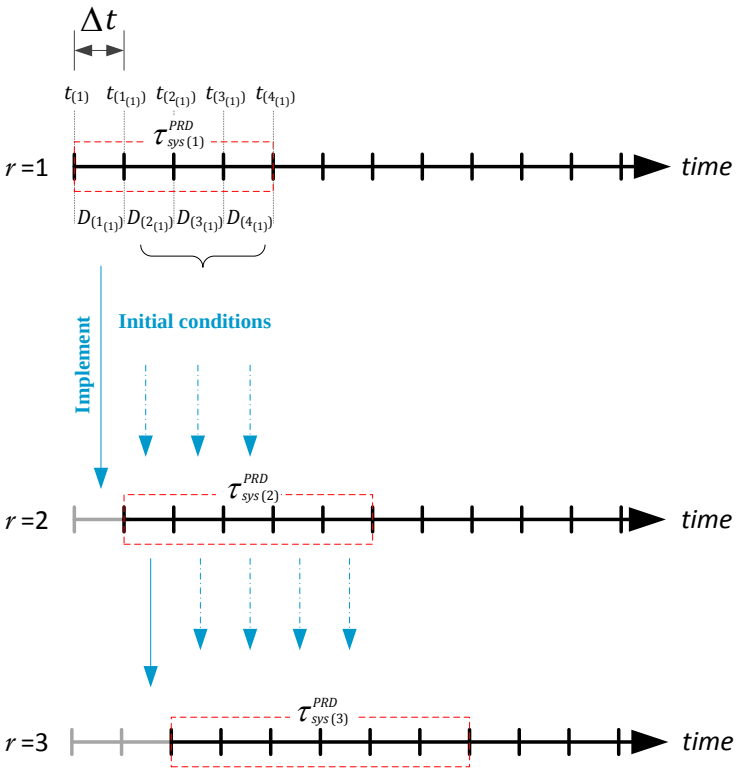

Figure 6.4 Prediction interval sliding window.

$$\mathbb{P}_{T(p_{(i,a)},b_{(r)})} = \int_0^{b_{(r)}\times\Delta t} \frac{1}{b_{(r)}\times\Delta t}\Pr(t_{prk(p_{(i,a)},w)} > t)\,dt$$
$$= \int_0^{b_{(r)}\times\Delta t} \frac{1}{b_{(r)}\times\Delta t}(1 - f_{prk(p_{(i,a)},w)}(t))\,dt \quad (6.1)$$

Hence, the predicted number of new PEV arrivals by the end of period $D_{(b_{(r)})}$, $\widetilde{H}_{2(p_{(i,a)})}\left(t_{(b_{(r)})}\right)$ is given as the minimum integer that satisfies

$$\sum_{n=0}^{\tilde{H}_{2(p_{(i,a)})}\left(t_{(b_{(r)})}\right)} \frac{\left(\mu_{V(p_{(i,a)},w,b_{(r)})}\right)^{n} \times \exp\left(-\mu_{V(p_{(i,a)},w,b_{(r)})}\right)}{n!} \geq (1-\epsilon) \tag{6.2}$$

where $\epsilon \in [0,1]$ is the prediction error probability.

As a result, the predicted number of PEVs that will be simultaneously present in the parking lots under the jurisdiction of aggregator a by the end of $t_{(b_{(r)})}$ is given by $\tilde{H}_{(p_{(i,a)})}\left(t_{(b_{(r)})}\right) = \tilde{H}_{1(p)}\left(t_{(b_{(r)})}\right) + \tilde{H}_{2(p_{(i,a)})}\left(t_{(b_{(r)})}\right)$. If $\tilde{H}_{(p_{(i,a)})}\left(t_{(b_{(r)})}\right) > H^{MAX}_{(p_{(i,a)})}$, then $\tilde{H}_{(p_{(i,a)})}\left(t_{(b_{(r)})}\right) = H^{MAX}_{(p_{(i,a)})}$ because additional PEVs will not have access to the parking lot chargers. All aggregators reply to the CVC request with their prediction of the number of PEVs under their jurisdiction during the next interval $\tau^{PRD}_{sys(r)}$.

Figure 6.5 presents sample results for short term prediction for a parking lot of 25 chargers capacity, where λ = 1.5 vehicle/min and ϵ = 0.01. As shown in Figure 6.5, the prediction unit successfully predicted the incoming PEVs to the parking lot. As shown in Figure 6.5, the actual PEVs in the parking lot are less than or equal the predicted PEVs with a probability of $1-\epsilon$, as stated in (6.2). It is assumed that satisfying this condition results in more robust operation. This is because the coordination decisions are based on a future predicted load that is higher than the future actual load.

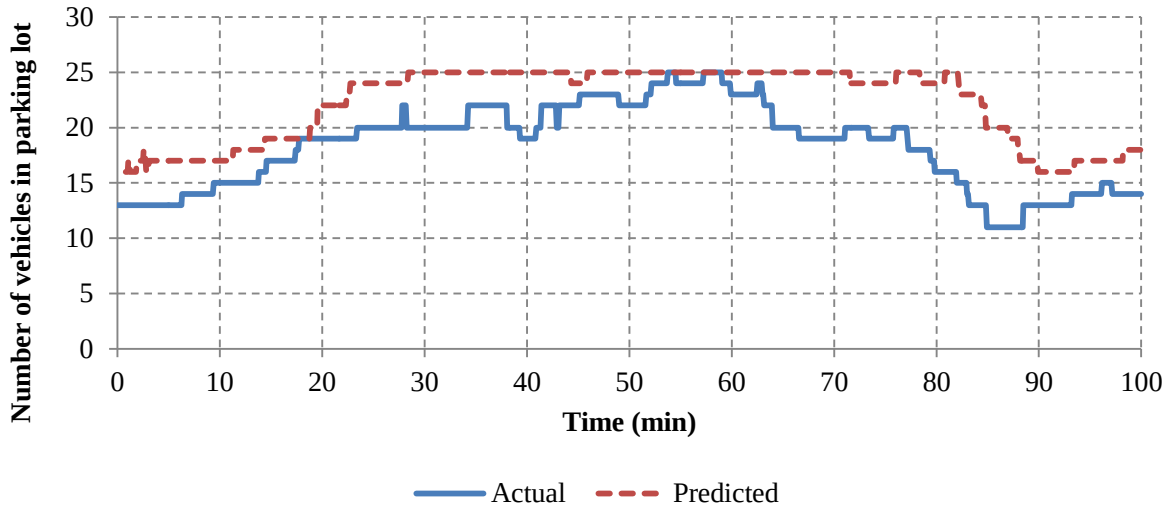

Figure 6.5 Sample results for the prediction units.

6.4 The CVC optimization unit

The CVC optimization unit makes coordinated charging/discharging decisions over a time duration $\tau_{sys(r)}^{PRD}$ for all chargers located under its jurisdiction. Two optimization units are proposed: the first does not allow PEV discharging, while the second does. Over the prediction interval $\tau_{sys(r)}^{PRD}$ and with consideration of the predicted PEV and regular load values, each unit solves two sequential optimization stages: DEMS and CMS. Although the two stages provide charging or charging/discharging decisions at every time instant $t_{(r)}$ and $t_{(b_{(r)})}$, during $\tau_{sys(r)}^{PRD}$, only the decisions at time instant $t_{(r)}$ are implemented. The decisions at the other time instants $t_{(b_{(r)})}$ during $\tau_{sys(r)}^{PRD}$ are used as initial conditions employed for the solution of the two stages for the next prediction interval $\tau_{sys(r+1)}^{PRD}$, as shown in Figure 6.4.

According to the distribution system code developed by the Ontario Energy Board, a local distribution company may disconnect loads for the following reasons: non-payment, emergency, safety, or technical limit violation [143]. In this work, it is therefore assumed that the utility will deliver the required amount of energy to customers unless there is a technical limit violation. Hence, as a first priority, the CVC unit satisfies PEV energy requirements subject to the technical limits of the system. As a second priority, the system then minimizes operating costs.

The flow charts of the proposed CVC optimization unit for the charging only and charging discharging modes of operation are shown in Figure 6.6. The detailed procedure and mathematical formulation are explained in the next two subsections.

6.4.1 Charging Only Optimization Unit

In this case, only charging decisions are allowed. The optimization unit solves the following two stages.

6.4.1.1 DEMS

The objective of this stage is to maximize the energy delivered to all PEV batteries, including both those already connected and those predicted. The energy delivered from $t_{(b_{(r)})}$ to $t_{(b_{(r)}+1)}$ is denoted for a PEV (actual or predicted) connected to charger $ch_{(p_{(i,a)})} \in \mathcal{CH}_{(p_{(i,a)})}$ in parking lot $p_{(i,a)} \in \mathcal{PL}_{(i,a)}$ at bus $i \in \mathcal{I}_{(a)}^{AGG}$, due to a decision taken at time instant $t_{(b_{(r)})}$ as $E_D\left(ch_{(p_{(i,a)})}, b_{(r)}\right)$. The charging decision $\mathbb{X}\left(ch_{(p_{(i,a)})}, b_{(r)}\right)$ is a percentage of the charging power permitted for charger

$ch_{(p_{(i,a)})}$ at time instant $t_{(b_{(r)})}$, i.e., $\mathbb{X}\left(ch_{(p_{(i,a)})}, b_{(r)}\right) \in [0,1]$. The objective of the DEMS can then be described as

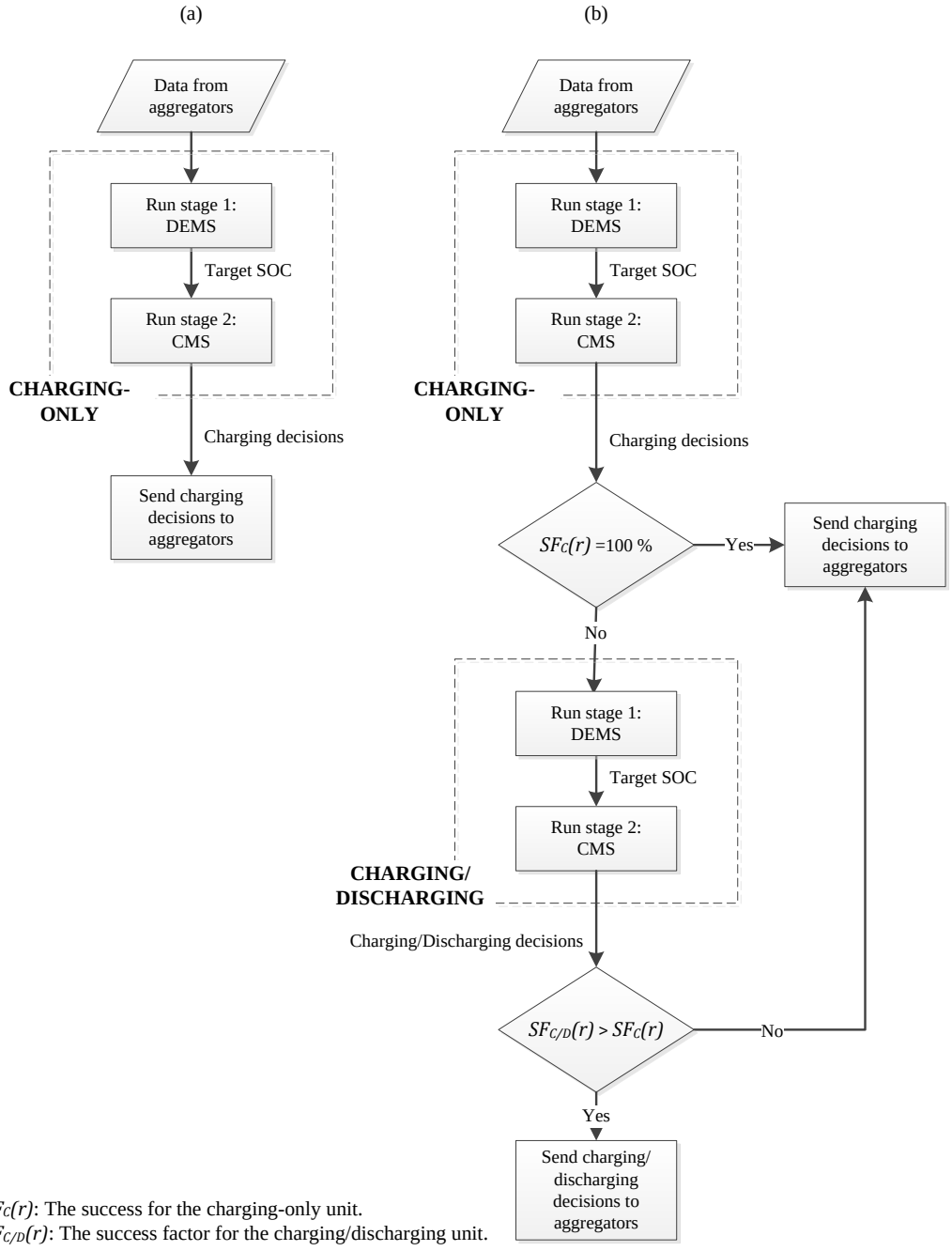

Figure 6.6 Proposed CVC optimization unit: (a) charging only and (b) charging/discharging

$$\max_{\mathbb{X}} \sum_{a\in\mathcal{A}} \sum_{i\in\mathcal{I}_{(a)}^{AGG}} \sum_{p} \sum_{ch} \sum_{b_{(r)}=1}^{B_{(r)}} E_D\left(ch, b_{(r)}\right)$$
$$: \mathbb{X} = \mathbb{X}\left(ch, b_{(r)}\right), ch = ch_{(p)} \in \mathcal{CH}_{(i,p)}, p = p_{(i,a)} \in \mathcal{PL}_{(i,a)} \tag{6.3}$$
$$s.t. \text{ (6.4)-(6.15)}$$

The DEMS should satisfy the power flow constraints, as given by

$$P_{G(i,b_{(r)})} - P_{L(i,b_{(r)})} = \sum_{j\in\mathcal{J}} V_{(i,b_{(r)})} V_{(j,b_{(r)})} Y_{(i,j)} \cos\left(\theta_{(i,j)} + \delta_{(j,b_{(r)})} - \delta_{(i,b_{(r)})}\right) \ \forall i, b_{(r)} \tag{6.4}$$

$$Q_{G(i,b_{(r)})} - Q_{L(i,b_{(r)})} = -\sum_{j\in\mathcal{J}} V_{(i,b_{(r)})} V_{(j,b_{(r)})} Y_{(i,j)} \sin\left(\theta_{(i,j)} + \delta_{(j,b_{(r)})} - \delta_{(i,b_{(r)})}\right) \ \forall i, b_{(r)} \tag{6.5}$$

where

$P_{G(i,b_{(r)})}$ and $Q_{G(i,b_{(r)})}$ denote the per unit active and reactive power generated at bus i for time instant $t_{(b_{(r)})}$;

$P_{L(i,b_{(r)})}$ and $Q_{L(i,b_{(r)})}$ denote the per unit active and reactive power demands at bus i for time instant $t_{(b_{(r)})}$;

$V_{(i,b_{(r)})}$ and $\delta_{(i,b_{(r)})}$ denote the per unit magnitude and the angle of the voltage at bus i for time instant $t_{(b_{(r)})}$;

$Y_{(i,j)}$ and $\theta_{(i,j)}$ are the per unit magnitude and angle of the Y-bus matrix admittance.

The voltage limits and thermal limits of the feeders should also hold, i.e.,

$$V_{min} \le V_{(i,b_{(r)})} \le V_{max} \quad \forall i, b_{(r)} \tag{6.6}$$

$$I_{(l,b_{(r)})} \le I_{(l)}^{CAP} \quad \forall l, b_{(r)} \tag{6.7}$$

where $I_{(l,b_{(r)})}$ denotes the per unit current through line $l \in \mathcal{L}$ for time instant $t_{(b_{(r)})}$.

The power generated at each bus is obtained from the DG connected to that bus:

$$P_{G(i,b_{(r)})} = P_{DG(i,b_{(r)})}\,, Q_{G(i,b_{(r)})} = Q_{DG(i,b_{(r)})} \quad \forall i \in \mathcal{I}_{DG}, b_{(r)} \tag{6.8}$$

where $P_{DG(i,b_{(r)})}$ and $Q_{DG(i,b_{(r)})}$ denote the per unit DG active and reactive power levels generated at bus i for time instant $t_{(b_{(r)})}$, which is based on current measurements and forecasted data.

The total active power consumed by load $P_{L(i,b_{(r)})}$ is the sum of the power consumed by the regular load $P_{NL(i,b_{(r)})}$ and the PEV load $P^{PEV}_{L(i,b_{(r)})}$:

$$P_{L(i,b_{(r)})} = P_{NL(i,b_{(r)})} + P^{PEV}_{L(i,b_{(r)})} \quad \forall i \in \mathcal{I}, b_{(r)} \tag{6.9}$$

The consumed power at each bus due to the PEV load depends on the charging decision $\mathbb{X}\left(ch_{(p_{(i,a)})}, b_{(r)}\right)$, the charger's power limit transferred to/from the battery in kW $P_{CH}\left(ch_{(p_{(i,a)})}, b_{(r)}\right)$, and the efficiency of the charger $\eta_{CH}\left(ch_{(p_{(i,a)})}\right)$, as given by

$$P^{PEV}_{L(i,b_{(r)})} = \sum_{p}\sum_{ch} \frac{\mathbb{X}(ch, b_{(r)})\, P_{CH}(ch, b_{(r)})}{\eta_{CH}(ch).S_{base}} \; : ch = ch_{(p)} \in \mathcal{CH}_{(i,p)}, p = p_{(i,a)} \in \mathcal{PL}_{(i,a)} \quad \forall i \in \mathcal{I}, b_{(r)} \tag{6.10}$$

where S_{base} is the base power for the per unit system in kW. The charger's power transfer limit P_{CH} is a function of the PEV battery SOC and is limited by the capacity of the charger, i.e. $P_{CH} \leq P^{Charger}_{rating}$. This function is dependent on the characteristics of the battery:

$$P_{CH}(ch, b_{(r)}) = f^{CH}_{(ch,b_{(r)})}\left(SOC^{Final}_{(ch,b_{(r)})}\right) \quad : \; ch = ch_{(p)} \in \mathcal{CH}_{(i,p)}, p = p_{(i,a)} \in \mathcal{PL}_{(i,a)} \quad \forall ch_{(p_{(i,a)})}, b_{(r)} \tag{6.11}$$

where

$f^{CH}_{(ch,b_{(r)})}$ is a function that represents the characteristics of the PEV battery connected to charger $ch = ch_{(p_{(i,a)})} \in \mathcal{CH}_{(i,p_{(i,a)})}$ at bus i for time $t_{(b_{(r)})}$;

$SOC^{Final}_{(ch,b_{(r)})}$ is the reached SOC at time instant $t_{(b_{(r)}+1)}$ for a PEV connected to charger $ch = ch_{(p_{(i,a)})} \in \mathcal{CH}_{(i,p_{(i,a)})}$ at bus i due to a decision taken at time $t_{(b_{(r)}+1)}$.

The relationship between the energy delivered to a PEV battery and the battery SOC is expressed as

$$E_D(ch, b_{(r)}) = E_{BAT}(ch) \sum_{b_{(r)}} \left(SOC^{Final}_{(ch,b_{(r)})} - SOC^{Initial}_{(ch,b_{(r)})}\right)/100 \; : \; ch = ch_{(p)} \in \mathcal{CH}_{(i,p)}, p = p_{(i,a)} \in \mathcal{PL}_{(i,a)} \quad \forall ch, b_{(r)} \tag{6.12}$$

where

$E_{BAT}(ch)$ is the battery capacity in kWh of the vehicle connected to charger ch;

$SOC^{Initial}_{(ch,b_{(r)})}$ denotes the initial SOC for the PEV connected to charger ch at $t_{(b_{(r)})}$.

The SOC of the connected PEVs to the set of active chargers $\mathcal{CH}^{ON}_{(i,p)} \subset \mathcal{CH}_{(i,p)}$ should be limited by the SOC desired by the user $SOC^{Desired}_{(ch,b_{(r)})}$:

$$SOC^{Final}_{(ch,b_{(r)})} \leq SOC^{Desired}_{(ch,b_{(r)})} \; : \; ch = ch_{(p)} \in \mathcal{CH}^{ON}_{(i,p)} \subset \mathcal{CH}_{(i,p)}, p = p_{(i,a)} \in \mathcal{PL}_{(i,a)} \quad \forall ch, b_{(r)} \tag{6.13}$$

On the other hand, the predicted incoming PEVs are assumed to require a final SOC of 100% and to arrive with a minimum SOC of SOC^{MIN}, which represent a worst case condition:

$$SOC^{Initial}_{(ch,b_{(r)})} = SOC^{MIN}, SOC^{Desired}_{(ch,b_{(r)})} = 100 \; : \; ch = ch_{(p)} \in \mathcal{CH}^{R}_{(i,p)} \subset \mathcal{CH}_{(i,p)}, p = p_{(i,a)} \in \mathcal{PL}_{(i,a)} \quad \forall ch, b_{(r)} \tag{6.14}$$

where $\mathcal{CH}^{R}_{(i,p)} \subset \mathcal{CH}_{(i,p)}$ denote the chargers reserved for the newly incoming PEVs.

The SOC of different PEVs are updated according to

$$SOC^{Final}_{(ch,b_{(r)}+1)} = SOC^{Final}_{(ch,b_{(r)})} + \frac{\mathbb{X}(ch,b_{(r)})\, P_{CH}(ch,b_{(r)})(\Delta t/60)}{E_{BAT}(ch)} \;:\; ch = ch_{(p)} \in \mathcal{CH}^{ON}_{(i,p)} \subset \mathcal{CH}_{(i,p)}, p = p_{(i,a)} \in \mathcal{PL}_{(i,a)} \quad \forall ch, 1 \le b_{(r)} \le B_{(r)} - 1 \tag{6.15}$$

6.4.1.2 CMS

Based on the charging decisions $\mathbb{X}$, a feasible target SOC $SOC^{Target}_{(ch,r)} = SOC^{Final}_{(ch,B_{(r)})}$ can be calculated for each PEV from the DEMS, given the power system constraints and the SOC required by customers. The target SOC will be the same as the customer-desired SOC as long as it does not violate the technical constraints of the system. The CMS is designed to find alternative charging decisions $\mathbb{X}$ that can satisfy the feasible target SOC $SOC^{Target}_{(ch,b_{(r)})}$ and system constraints, while at the same time minimizing either the charging costs for PEV owners or the system operating costs. It is assumed in this work that the system operating costs are minimized, and the utility charges the PEV owners with the minimum rate during their parking duration in return. During time interval $\tau^{PRD}_{sys(r)}$, the operating costs consist of two parts: the cost of losses $C_L(\tau^{PRD}_{sys(r)})$ and the peak demand charges $C_P(\tau^{PRD}_{sys(r)})$. The cost of losses is given by

$$C_L(\tau^{PRD}_{sys(r)}) = \sum_{b_{(r)}} c^{ENG}_{(b_{(r)})}\; S_{base}\; P_{Loss(b_{(r)})}\; \frac{\Delta t}{60} \tag{6.16}$$

where $c^{ENG}_{(b_{(r)})}$ is the price signal, which represents the cost of kWh during interval $t_{(b_{(r)})}$ and $P_{Loss(b_{(r)})}$ is the system power loss, which is given by

$$P_{Loss(b_{(r)})} = \frac{1}{2}\sum_{i\in\mathcal{J}}\sum_{j\in\mathcal{J}} G_{(i,j)}\left(V^2_{(i,b_{(r)})} + V^2_{(j,b_{(r)})} - 2V_{(i,b_{(r)})}V_{(j,b_{(r)})}\cos\left(\delta_{(j,b_{(r)})} - \delta_{(i,b_{(r)})}\right)\right) \quad \forall b_{(r)} \tag{6.17}$$

where $G_{(i,j)}$ is the per unit conductance of the line between buses i and j. The peak demand charges are calculated based on the peak load reached within one month, but the SRTCS operates in real time over time interval $\tau^{PRD}_{sys(r)}$. To incorporate the peak demand charges $C_P(\tau^{PRD}_{sys(r)})$ within the SRTCS, a

target peak value $\tilde{P}_{max}\left(\tau_{sys(r)}^{PRD}\right)$ is therefore used as in [144], which is updated to the maximum incurred total load power during $\tau_{sys(r)}^{PRD}$, $P_{max}\left(\tau_{sys(r)}^{PRD}\right)$, but only if this maximum power exceeds $\tilde{P}_{max}\left(\tau_{sys(r)}^{PRD}\right)$:

$$\tilde{P}_{max}\left(\tau_{sys(r)}^{PRD}\right) = \max\left(\tilde{P}_{max}\left(\tau_{sys(r-1)}^{PRD}\right), P_{max}\left(\tau_{sys(r-1)}^{PRD}\right)\right) \tag{6.18}$$

The CMS minimizes the peak demand charges only if the maximum power incurred during $\tau_{sys(r)}^{PRD}$ is greater than the target peak value:

$$C_P\left(\tau_{sys(r)}^{PRD}\right) = \begin{cases} c_d\, S_{base}\, \left(P_{max}\left(\tau_{sys(r)}^{PRD}\right) - \tilde{P}_{max}\left(\tau_{sys(r)}^{PRD}\right)\right) & \forall\, P_{max}\left(\tau_{sys(r)}^{PRD}\right) > \tilde{P}_{max}\left(\tau_{sys(r)}^{PRD}\right) \\ 0 & elsewhere \end{cases} \tag{6.19}$$

where c_d is the peak demand charges in \$/kW. By definition,

$$P_{max}\left(\tau_{sys(r)}^{PRD}\right) = \max_{b_{(r)}}\left(\sum_{i\in\mathcal{I}} P_{L(i,b_{(r)})}\right) \tag{6.20}$$

The CMS is hence given by

$$\begin{aligned} \min_{\mathbb{X}}\left(C_L\left(\tau_{sys(r)}^{PRD}\right) + C_P\left(\tau_{sys(r)}^{PRD}\right)\right) :\ \mathbb{X} = \mathbb{X}\left(ch, b_{(r)}\right) \in [0,1], ch = ch_{(p)} \in \mathcal{CH}_{(i,p)}, p \\ = p_{(i,a)} \in \mathcal{PL}_{(i,a)} \\ s.t.\ \ (6.4)\text{-}(6.7), (6.14), (6.15), (6.20)¢ \\ SOC_{(ch,B_{(r)})}^{Final} = SOC_{(ch,r)}^{Target} \quad \forall ch \end{aligned} \tag{6.21}$$

6.4.2 Charging/Discharging Optimization Unit

In this case, discharging decisions are allowed. However, charging/discharging decisions are not implemented unless the charging-only decisions cannot satisfy the customer needs, as shown in Figure 6.6. In other words, decisions from the charging-only unit are checked first, and if they satisfy

all of the customers' needs (100 % success), the charging decision is implemented. If the charging decisions cannot achieve 100 % success, the charging/discharging unit is enabled, and its results are implemented only if they would achieve greater success than those produced by the charging-only unit, as shown in Figure 6.6. The charging/discharging optimization unit has the same structure as the charging-only one, including the objective functions and constraints of the DEMS and CMS, with the exception of constraints (6.10) and (6.11), and the $\mathbb{X}$ range, as discussed next.

Since discharging is permitted, $\mathbb{X} \in [-1,1]$, in which positive decisions denote charging and negative ones indicate discharging. The power delivered or consumed by each charger is given by

$$P^{CH/DCH}_{(ch,b_{(r)})} = \begin{cases} \dfrac{\mathbb{X}\, P_{CH}\left(ch, b_{(r)}\right)}{\eta_{CH}(ch)\, S_{base}} & \forall \mathbb{X} \geq 0 \\ \dfrac{\mathbb{X}\, P_{CH}\left(ch, b_{(r)}\right) \eta_{DCH}(ch)}{S_{base}} & \forall \mathbb{X} < 0 \end{cases} : \mathbb{X} = \mathbb{X}\left(ch, b_{(r)}\right), ch = ch_{(p)} \in \mathcal{CH}_{(i,p)}, p = p_{(i,a)} \in \mathcal{PL}_{(i,a)}\ \forall ch_{(p_{(i,a)})}, i \in \mathcal{I} \tag{6.22}$$

The total PEV delivered or consumed power by at any bus i at $t_{(b_{(r)})}$ is given by

$$P^{PEV}_{L(i,b_{(r)})} = \sum_{p}\sum_{ch} P^{CH/DCH}_{(ch,b_{(r)})} : ch = ch_{(p)} \in \mathcal{CH}_{(i,p)}, p = p_{(i,a)} \in \mathcal{PL}_{(i,a)}\ \ \forall i \in \mathcal{I}, b_{(r)} \tag{6.23}$$

The power transfer limit of the charger $P_{CH}\left(ch, b_{(r)}\right)$ has different characteristics for charging and discharging:

$$P_{CH}\left(ch, b_{(r)}\right) = \begin{cases} f^{CH}_{(ch,b_{(r)})}\left(SOC^{Final}_{(ch,b_{(r)})}\right) & \forall\, \mathbb{X} \geq 0 \\ f^{DCH}_{(ch,b_{(r)})}\left(SOC^{Final}_{(ch,b_{(r)})}\right) & \forall\, \mathbb{X} < 0 \end{cases} : ch = ch_{(p)} \in \mathcal{CH}_{(i,p)}, p = p_{(i,a)} \in \mathcal{PL}_{(i,a)}\ \forall ch_{(p_{(i,a)})}, b_{(r)} \tag{6.24}$$

The charge/discharge optimization unit uses discharging only to increase the PEV charging success rate, through vehicle to vehicle (V2V) scheme, i.e., no power is delivered to the grid. Hence,

the constraint in (6.26) is included to ensure that power is exchanged only among PEVs within the same parking lot; i.e., no power is delivered to the grid[3].

$$P^{PEV}_{L(i,b_{(r)})} \geq 0 \quad \forall i \in \mathcal{I}, b_{(r)} \tag{6.25}$$

To ensure that whenever the vehicle owner unplugs his/her PEV before the declared departure time the SOC is not lower than its initial value, the discharging scheme should satisfy the following constraint:

$$SOC^{Final}_{(ch,b_{(r)})} \geq SOC^{Initial}_{(ch,b_{(r)})} \tag{6.26}$$

6.5 Simulation Results and Discussion

To evaluate the performance of the proposed SRTCS, two case studies were examined using a 38-bus system [113] that contains a mix of residential, commercial, and industrial customers and PEV parking lots, all of which are supplied from the main substation, as shown in Figure 6.7. The total system peak load is 4.37 MVA. The system line data, and load point demand are as given in Appendix A. Three profiles were used to model the regular load in the system, as shown in Figure 6.8 [145]. The system under study, including aggregators and prediction units, was modeled in a MATLAB software tool. The CVC optimization unit was modeled in a General Algebraic Modeling System (GAMS) software tool. To update the SOC of the PEV batteries, charging/discharging decisions are sent from the GAMS to the MATLAB environment. For the simulation, $\Delta t = 10$ min, and the simulation covers 24 h of one day. The maximum computation times for the prediction and optimization units in the system under study are 1.1 sec and 75 sec, respectively. The computer utilized for simulation was a quad core 2.8 GHz processor with 6 GB of RAM. The error probability for the prediction unit is $\epsilon = 0.1$. The peak demand charge is 3 \$/kW [146], and the energy price is assumed to be proportional to the regular load demand of the system with an average of 50 \$/MW. The initial moving peak value for the day under study is set to the maximum regular load demand: 3.55 MW.

The system contains four parking lots on buses 25, 29, 34, and 36, as shown in Figure 6.7. For simplicity, all chargers are assumed to be second-level chargers with a 7.2 kW rating. All PEVs

[3] For V2G scheme, this constraint is removed from the SRTCS

are assumed to have an AER of 50 miles. All PEV batteries have the same charging characteristics, as given in [147] and shown in Figure 6.9 with adjustment to match the ratings of the PEV chargers and the AER. These characteristics are approximated as in [122] , while the discharging power limit for all PEV batteries is set to the maximum limit of the charger. To encounter for the initial and the desired SOCs variability, their randomness is assumed to follow a uniform distribution between a 30 % to 50 % for the initial SOC and 80 % to 100 % for desired SOC.

Two case studies were examined. The first investigated the performance of the SRTCS with charging-only (SRTCS-C) decisions for a low PEV penetration level. The second case study evaluated the performance of the SRTCS for a high PEV penetration level with both charging-only and charging/discharging (SRTCS-C/D) decisions. In both cases, the proposed SRTCS was compared to first-come, first-served (FCFS) benchmark for coordinated charging decisions [148]. In the FCFS approach, PEV charging decisions are based on allocating priority to vehicles that arrive at the parking lot earlier. The SRTCS was also compared to an uncoordinated charging approach, whereby all PEVs connected to the grid are charged without consideration of the technical limitations of the system and in the absence of communication between the grid operators and the PEVs. A success factor SF was introduced as a figure of merit related to customer's satisfaction. The success factor is defined as the average success of PEV charging for all vehicles in the system over the 24 h period under study and is given by

$$SF = \frac{1}{H_{total}} \sum_{vh=1}^{H_{total}} \frac{E_{D(vh)}}{E_{R(vh)}} \tag{6.27}$$

where

H_{total} denotes the total number of PEVs served during the 24 h of the day;

$E_{D(vh)}$ and $E_{R(vh)}$ denote the delivered and required energy for PEV vh, respectively.

6.5.1 Smart PEV charging with low PEV penetration

In this case study, the total PEV demand represents 12 % of the regular load. The total regular load of the system over the 24 h period is shown in Figure 6.10 (a). As shown in Figure 6.10 (b), both the uncoordinated (UNCR) and FCFS approaches yield the same performance, which is attributable to

the low PEV penetration level, which enables the system to charge all connected PEVs without violating the technical limitations.

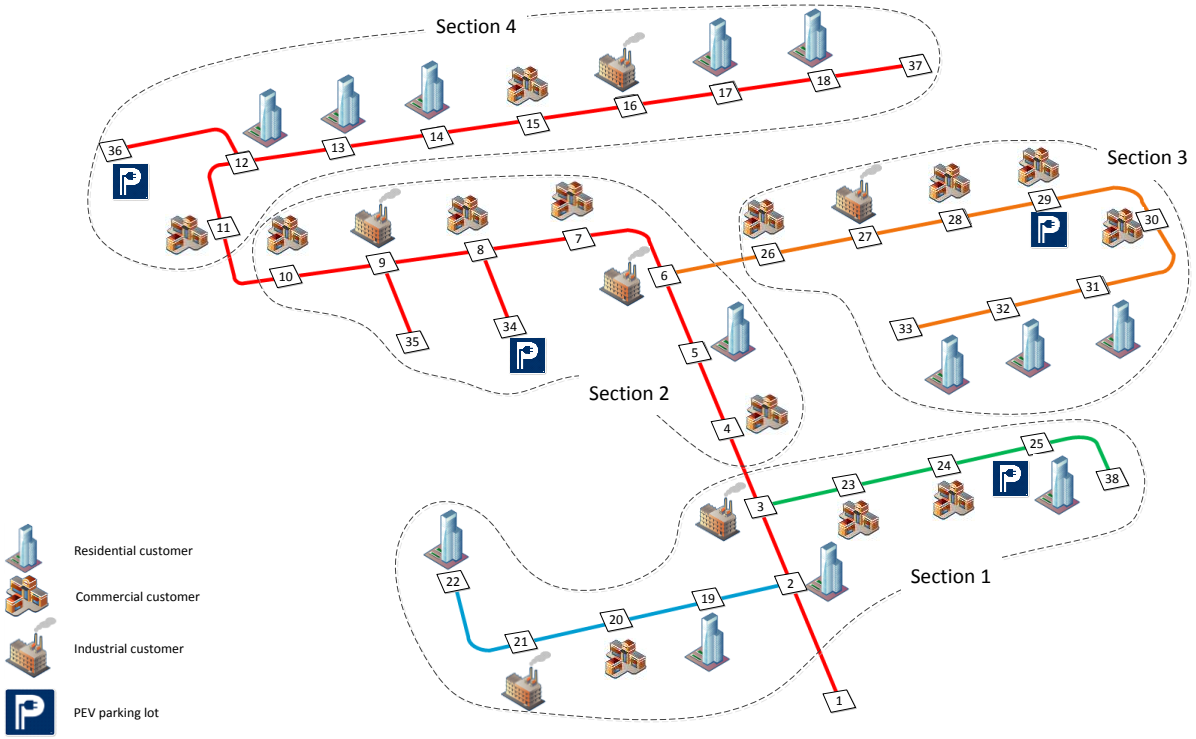

Figure 6.7 38-bus distribution test feeder.

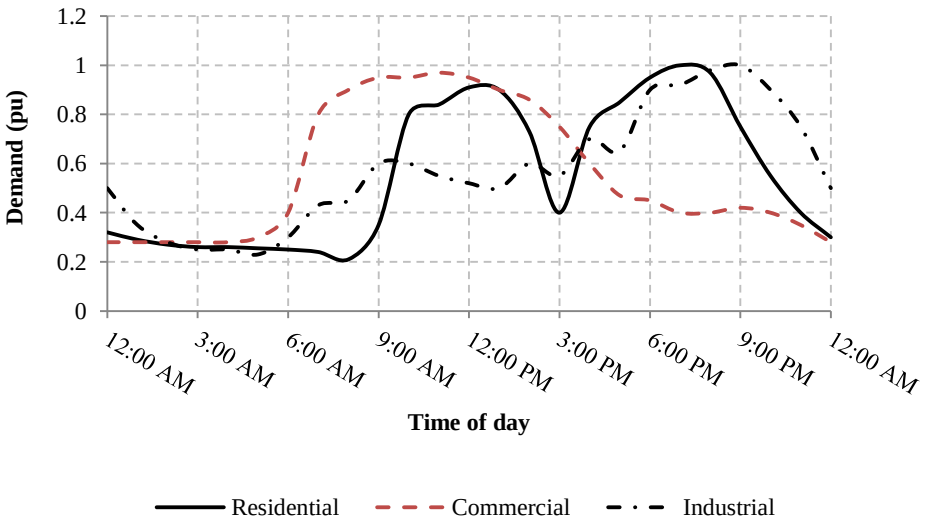

Figure 6.8 Regular load profiles [145].

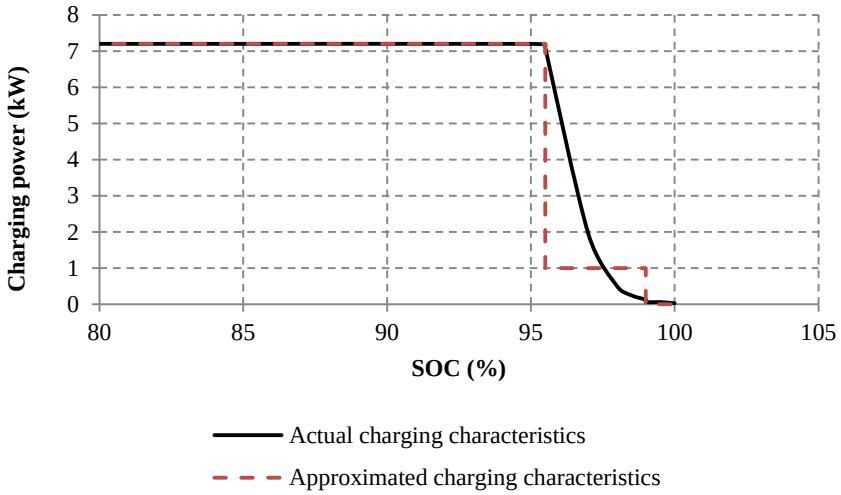

Figure 6.9 Li-ion battery characteristics [147].

On the other hand, the proposed SRTCS can significantly reshape the charging requirement of the PEVs connected to the system. With the use of the SRTCS, during the normal load peak, PEV charging is limited and is performed either before or after the peak load interval, thanks to the prediction unit. In contrast to the uncoordinated and FCFS approaches, with the SRTCS, the PEV charging peaks occur at the troughs of normal load: around 3:00 pm, and after midnight. With low PEV penetration, all three charging approaches can achieve a success factor of $SF = 100\%$. Table 6.1 shows the percentage increase in operating costs compared to the case without PEV. Because the PEV charging load is shifted to the off-peak periods, the SRTCS results in a significant reduction in the peak demand charges compared to the FCFS approach. It can be inferred from Figure 6.10 (b) that the system peak without PEV, which occurs at 12:00 pm, is not affected by the SRTCS, which reduces the charging load of the PEVs to zero during this period. On the other hand, the FCFS approach results in 8 % increase in the system peak. The increase in the cost of the system losses for the SRTCS are also 6 % lower compared to the FCFS approach due to the ability of the SRTCS to allocate the PEV charging energy during low price periods.

6.5.2 Smart PEV charging/discharging with high PEV penetration

In the second case study, the total PEV demand represents 50 % of the regular load. For uncoordinated vehicle charging, such a penetration level is beyond the technical limitations of the system. The PEV parking lots on buses 25 and 29 are assumed to be residential, while those on buses

34 and 36 are assumed to be commercial. For the commercial parking lots, arrival and departure data are provided by Toronto Parking Authority. The PEV load results are shown in Figure 6.10 (c) and

Table 6.2. While the uncoordinated approach can achieve a success factor of $SF = 100$ %, the charging decisions are infeasible because they violate the system constraints. On the other hand, the FCFS approach delivered 90.37 % of the required energy to the PEV, i.e., $SF = 90.37$ %.

Using the predictions for the normal and PEV loads, the SRTCS can shift the PEV load so that a higher success factor is achieved than with the FCFS approach, at a lower cost of losses and same peak load, as shown in Table 6.2. The SRTCS achieves a significantly higher success factor of 93.4% and 95.3 % for the charging-only and charging/discharging, respectively. The results demonstrate that the SRTCS is more reliable than the other approaches with respect to addressing the PEV charging requirements through the efficient utilization of system resources.

The performance of the SRTCS-C/D is very close to the SRTCS-C, which is dependent on several factors: PEV arrivals, parking durations, system configuration, and regular load. A higher SF is achieved when discharging is enabled; however, this result is obtained at the expense of a higher operating cost than in the charging-only case. The higher cost with respect to losses is due to excess charging energy, which correlates with the higher success factor. Although the discharging operation results in an improvement in the SF compared to the charging only operation, a number of related technical issues present challenges, such as its impact on battery life and appropriate compensation for PEV owners who adopt such a strategy. For the presented case study, the discharging effectiveness is questionable, due to the mentioned challenges, and the minor effect on the system compared to the charging only approach. However, as the parking lots dynamics increase, the charging/discharging may lead to significantly better results compared to the charging-only operation.

Table 6.1 System operating costs and success factors for the low penetration case

Scheme	SF (%)	Percentage increase in C_L (%)	Percentage increase in C_P (%)	Feasibility
UNCR	100.0	12.76	7.97	feasible
FCFS	100.0	12.76	7.97	feasible
SRTCS-C	100.0	6.81	0	feasible

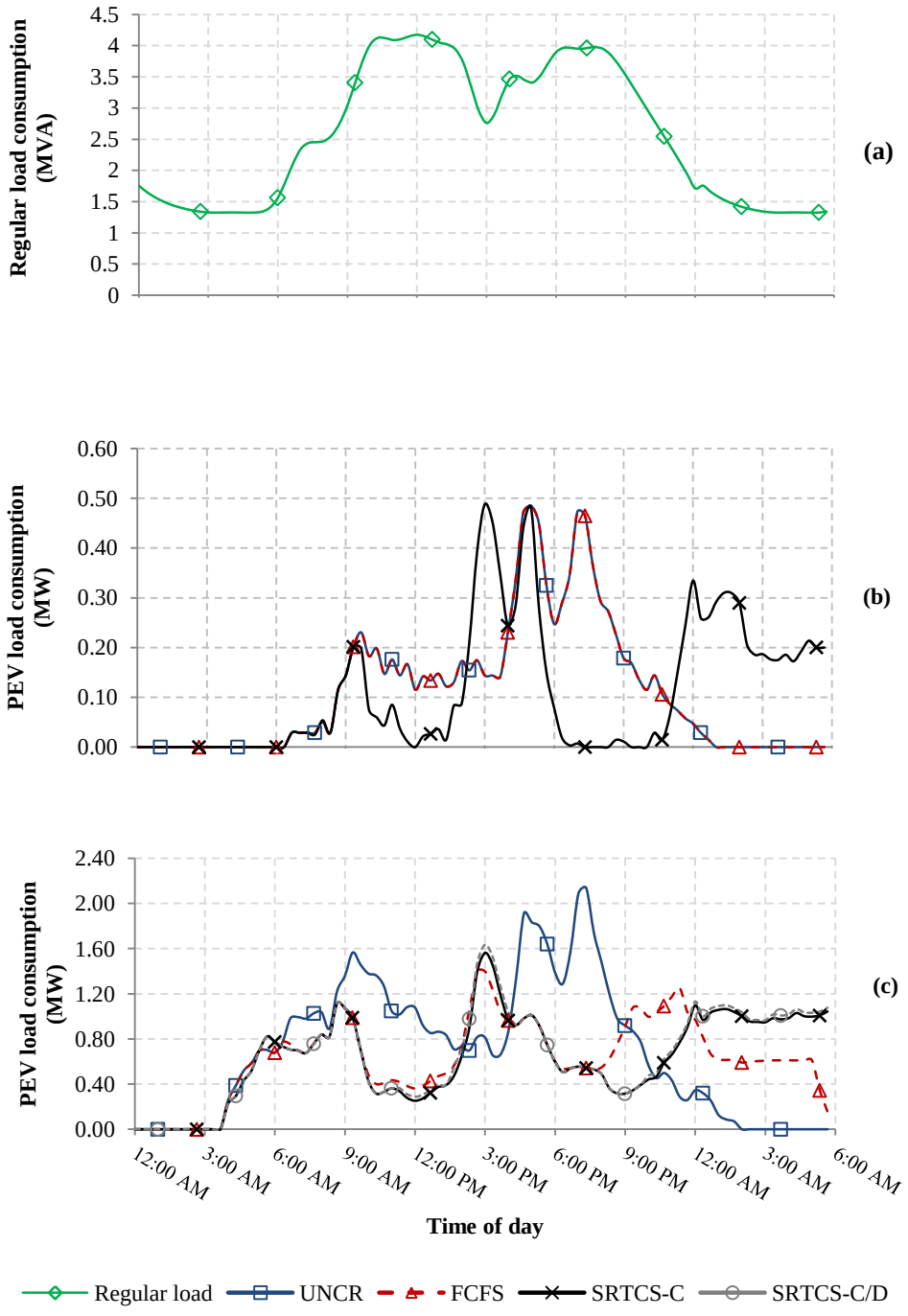

Figure 6.10 Power demands for normal and PEV loads for different scenarios: (a) Normal load demand; (b) PEV demand at low penetration; and (c) PEV demand at high penetration.

Therefore, the application of charging/discharging strategy for V2V has not yet been proved. Future research should thus include the investigation of the impacts on battery life and appropriate compensation. For compensation that is too low would discourage the PEV owners from embracing the discharging strategy, while compensation that is too high would motivate utilities to deploy other options such as DG or storage devices. The establishment of an appropriate compensation value that balances the benefits for both PEV owners and utilities needs further study.

Table 6.2 System operating costs and success factor for the high penetration case

Scheme	SF (%)	Percentage increase in C_L (%)	Percentage increase in C_P (%)	Feasibility
UNCR	100.0	82.48	55.11	infeasible
FCFS	90.37	56.54	10.18	feasible
SRTCS-C	93.38	47.45	10.18	feasible
SRTCS-C/D	95.33	49.75	10.18	feasible

6.6 Conclusions

In this chapter, a proposed real-time system was developed for managing the dynamics associated with coordinated charging/discharging decisions for PEVs in a smart grid. The SRTCS incorporates two novel prediction and optimization units. The prediction unit provides information regarding the future PEV load in the system for better coordination of vehicle charging. The two-stage optimization unit guarantees the feasibility of the charging/discharging decisions by first maximizing PEV owner satisfaction and then minimizing system operating costs. The performance of the SRTCS has been investigated for both low and high PEV penetration levels and for charging-only and charging/discharging decisions. The simulation results demonstrate the robust performance of the proposed SRTCS with respect to its ability to address the dynamics of multiple parking lots in a timely manner. The findings also reveal the effectiveness of the SRTCS architecture in providing a higher PEV charging success than other charging approaches. The advantages of the proposed SRTCS can thus be summarized as providing immunity to extreme loading conditions, robustness, and an acceptable computation time, all of which make it suitable for practical implementation. The results also reveal that the improvement in the SRTCS is minor when discharging is enabled. Given

the challenges accompanied with the implementation of the charging/discharging coordination strategy, further research is required to investigate its effectiveness.

Chapter 7
Concluding remarks

7.1 Summary and Conclusions

The research in this thesis presents new approaches to accommodate high PEV penetration in distribution networks. Two main scenarios were presented, namely the uncontrolled charging scenario considering the current situation of the grid (without communication) and the coordinated charging under the smart grid paradigm (with two way communication).

Under the uncontrolled charging, three stages were presented in chapters 3, 4, and 5. In chapter 3, an approach to evaluate the economic benefits of renewable DG was developed. Moreover, a GA based approach was proposed for long-term multi-objective optimal DG allocation. Three economic benefits associated with DG allocation are considered in this chapter: deferral of system upgrade investments, reduced cost of energy losses, and reduced cost of interruptions. The proposed planning technique has been applied to different scenarios for a typical distribution system. The results reveal the effectiveness of the proposed approach in significantly reducing the mentioned costs, which benefits both the LDC and the consumers. It is concluded in this chapter that the cost of upgrades is the most effective economic benefit, which is highly affected by the intermittent nature of renewable DG units. It has been shown that for the renewable DG units to contribute to the cost of upgrade, a risk has to be taken, which depends mainly on the output power patterns of the renewable DG units. On the other hand, the cost of interruption was found to be of least significance due to the limitations on the islanded mode of operation in distribution networks.

In chapter 4, a novel uncontrolled PEV charging load model was developed. The model incorporates different aspects, such as driver behaviour and ambient temperature effect, to reflect the variations and uncertainty of the PEV charging. Moreover, the developed model has been applied to different scenarios for two configurations of a typical distribution system. It is concluded in this chapter that including the driving habits and ambient temperature in the energy consumption pattern in the PEV load model affects the results significantly. Moreover, it is concluded that the effects of high penetration of PEVs are not significant on systems with commercial and industrial dominant loads assuming charging at home, where the vehicles are parked most of the time. On the other hand, the lines loading levels for systems with dominant residential loads are significantly affected with high penetration of PEV charging.

In chapter 5, a multi-objective long-term dynamic planning approach was proposed to accommodate the high penetration of PEV uncontrolled charging utilizing renewable DG units. In this chapter, the different models and approaches developed in chapters 3 and 4 are utilized. It can be concluded that the dispatchable DG units are dominant with respect to system costs, while a mix of WDG and PVDG can effectively reduce system emissions. The results demonstrate that a significant reduction in either system costs or system emissions can be obtained. However, because system costs and system emissions cannot both be minimized simultaneously, a compromised solution can be chosen based on the preferences of the LDC. Moreover, neither the WDG nor the PVDG can be superior to each other, and the mix of these renewable DG types is the optimal installation due to the advantages of each type.

Under the coordinated charging scenario, a real-time coordinated PEV charging architecture is presented in chapter 6, which consists of three units, namely data collection and storage unit, prediction unit, and optimization unit. The proposed architecture was developed in two stages. In the first stage, a novel PEV prediction unit was developed. The unit predicts the number of PEVs that will be simultaneously present in the parking lots under the aggregator jurisdiction. In the second stage, a central multi-stage optimization unit which makes the charging/discharging coordinated decisions was developed. The provided simulation results prove that the proposed charging mechanism gives immunity to extreme loading conditions, robustness, and acceptable computational time. These advantages make it adequate for practical implementation. It was concluded in this chapter that for high PEV penetration, the uncontrolled charging can impose potential risk on the system equipment. On the other hand, the proposed coordinated charging can efficiently maximize the PEV owner satisfaction and minimize the system operating costs without jeopardizing system equipment. Moreover, it was concluded that the effectiveness of V2V discharging scheme requires further investigation.

8.2 Contributions

The main contribution of this thesis is the development of different approaches to accommodate high PEV penetration in distribution networks. Under the main contribution, two sub-contributions can be highlighted as follows:

- The development of a long-term multi-objective dynamic planning approach to accommodate high penetration of uncontrolled PEV charging in distribution networks utilizing renewable and dispatchable DG units.

- The development of a new real-time charging/discharging architecture to manage the dynamics of coordinated charging of PEVs in smart distribution networks.

8.3 Directions for Future Work

In continuation of this work, the following subjects are suggested for future studies:

- Investigating the ancillary services that can be offered by discharging of PEVs in smart distribution systems: These ancillary services can be described as active or reactive power support. For example, during outages events, the PEVs stored energy can be used to supply critical loads through vehicle-to-grid active power support (V2GP) strategy. Also, the PEVs can be used to improve the system voltage profile and relax the tap operation of the on-load tap changers through vehicle-to-grid reactive power support (V2GQ) strategy. In this work, the coordination methodology developed in chapter 6 will be modified to perform the required V2G strategy.
- Developing planning approaches for smart buildings with smart parking lots: The objective of this research work is to determine the investment decisions for smart buildings whose owners may consider making benefit from selling electricity to PEVs in there parking lots. Moreover, the work can consider other investment decisions that can be integrated to facilitate accommodating the PEV charging units, such as PVDG units and battery storage systems.
- Developing planning approach for fast PEV charging stations: In fast charging stations, the PEV batteries are charged with high current and high voltage leading to the recovery of 50 % battery charge within less than 20 min. Planning the locations, capacities, and control strategies of these charging stations requires investigating several aspects, such as PEV arrival rates in this charging stations, queueing strategies, clusters of PEVs in the market, and the impacts of this sudden load on the existing grid.

Appendix A

The 38-bus test system data

Table A.1 38-bus test system data [113]

F	T	Ln	Line impedance in pu	To node - load	
				P	Q
1	2	1	0.000574+0.000293j	0.1	0.06
2	3	6	0.00307+0.001564j	0.09	0.04
3	4	11	0.002279+0.001161j	0.12	0.08
4	5	12	0.002373+0.001209j	0.06	0.03
5	6	13	0.0051+0.004402j	0.06	0.02
6	7	22	0.001166+0.003853j	0.2	0.1
7	8	23	0.00443+0.001464j	0.2	0.1
8	9	25	0.006413+0.004608j	0.06	0.02
9	10	27	0.006501+0.004608j	0.06	0.02
10	11	28	0.001224+0.000405j	0.045	0.03
11	12	29	0.002331+0.000771j	0.06	0.035
12	13	31	0.009141+0.007192j	0.06	0.035
13	14	32	0.003372+0.004439j	0.12	0.08
14	15	33	0.00368+0.003275j	0.06	0.01
15	16	34	0.004647+0.003394j	0.06	0.02
16	17	35	0.008026+0.010716j	0.06	0.02
17	18	36	0.004558+0.003574j	0.09	0.04
2	19	2	0.001021+0.000974j	0.09	0.04
19	20	3	0.009366+0.00844j	0.09	0.04
20	21	4	0.00255+0.002979j	0.09	0.04
21	22	5	0.004414+0.005836j	0.09	0.04
3	23	7	0.002809+0.00192j	0.09	0.05
23	24	8	0.005592+0.004415j	0.42	0.2
24	25	9	0.005579+0.004366j	0.42	0.2
6	26	14	0.001264+0.000644j	0.06	0.025
26	27	15	0.00177+0.000901j	0.06	0.025
27	28	16	0.006594+0.005814j	0.06	0.02
28	29	17	0.005007+0.004362j	0.12	0.07
29	30	18	0.00316+0.00161j	0.2	0.6
30	31	19	0.006067+0.005996j	0.15	0.07
31	32	20	0.001933+0.002253j	0.21	0.1
32	33	21	0.002123+0.003301j	0.06	0.04
8	34	24	0.012453+0.012453j	0	0
9	35	26	0.012453+0.012453j	0	0
12	36	30	0.012453+0.012453j	0	0
18	37	37	0.003113+0.003113j	0	0
25	38	10	0.003113+0.003113j	0	0

Bibliography

[1] J. Arrillaga and B. Smith, *AC-DC Power Systems Analysis*. IET, 1998.

[2] Environment Canada, "National inventory report 1990-2011: Greenhouse gas sources and sinks in Canada - executive summary," Tech. Rep. ISSN: 1910-7064, 2013.

[3] N. Tanaka, "Technology roadmap: Electric and plug-in hybrid electric vehicles," International Energy Agency, Tech. Rep., 2011.

[4] R. Liu, L. Dow and E. Liu, "A survey of PEV impacts on electric utilities," in *Innovative Smart Grid Technologies (ISGT), IEEE PES*, pp. 1-8, 2011.

[5] M. F. Shaaban, Y. M. Atwa and E. F. El-Saadany, "PEVs Modeling and Impacts Mitigation in Distribution Networks," *IEEE Trans. Power Syst.*, no. 2 vol. 28, pp. 1122-1131, 2013.

[6] H. Khayyam, H. Ranjbarzadeh and V. Marano, "Intelligent control of vehicle to grid power," *Journal of Power Sources*, vol. 201, pp. 1-9, 2012.

[7] O. Sundstrom and C. Binding, "Flexible charging optimization for electric vehicles considering distribution grid constraints," *IEEE Trans. on Smart Grid*, vol. 3, pp. 26-37, 2012.

[8] W. El-Khattam and M. Salama, "Distributed generation technologies, definitions and benefits," *Electr. Power Syst. Res.*, vol. 71, pp. 119-128, 2004.

[9] A. Soroudi, M. Ehsan and H. Zareipour, "A practical eco-environmental distribution network planning model including fuel cells and non-renewable distributed energy resources," *Renewable Energy*, vol. 36, pp. 179-188, 2011.

[10] A. Piccolo and P. Siano, "Evaluating the impact of network investment deferral on distributed generation expansion," *IEEE Trans. Power Syst.*, vol. 24, pp. 1559-1567, 2009.

[11] C. Wang and M. H. Nehrir, "Analytical approaches for optimal placement of distributed generation sources in power systems," IEEE Trans. Power Syst., vol. 19, pp. 2068-2076, 2004.

[12] Y. Hegazy, M. Salama and A. Chikhani, "Adequacy assessment of distributed generation systems using Monte Carlo simulation," *IEEE Trans. Power Syst.*, vol. 18, pp. 48-52, 2003.

[13] R. Billinton, H. Chen and R. Ghajar, "A sequential simulation technique for adequacy evaluation of generating systems including wind energy," *IEEE Trans. Energy Conversion*, vol. 11, pp. 728-734, 1996.

[14] R. Karki, P. Hu and R. Billinton, "A simplified wind power generation model for reliability evaluation," *IEEE Trans. Energy Conversion*, vol. 21, pp. 533-540, 2006.

[15] R. Billinton and Y. Gao, "Multistate wind energy conversion system models for adequacy assessment of generating systems incorporating wind energy," *IEEE Trans. Energy Conversion*, vol. 23, pp. 163-170, 2008.

[16] R. Billinton, B. Karki, R. Karki and G. Ramakrishna, "Unit commitment risk analysis of wind integrated power systems," *IEEE Trans. Power Syst.*, vol. 24, pp. 930-939, 2009.

[17] R. Billinton, H. Chen and R. Ghajar, "Time-series models for reliability evaluation of power systems including wind energy," *Microelectronics Reliability*, vol. 36, pp. 1253-1261, 1996.

[18] Y. Atwa, E. El-Saadany, M. Salama and R. Seethapathy, "Optimal renewable resources mix for distribution system energy loss minimization," *IEEE Trans. Power Syst.*, vol. 25, pp. 360-370, 2010.

[19] S. H. Jangamshetti and V. G. Rau, "Site matching of wind turbine generators: a case study," *IEEE Trans. Energy Conversion*, vol. 14, pp. 1537-1543, 1999.

[20] S. H. Jangamshetti and V. Ran, "Optimum siting of wind turbine generators," *IEEE Trans. Energy Conversion*, vol. 16, pp. 8-13, 2001.

[21] Y. Atwa, E. El-Saadany and A. Guise, "Supply adequacy assessment of distribution system including wind-based DG during different modes of operation," *IEEE Trans. Power Syst.*, vol. 25, pp. 78-86, 2010.

[22] G. Desrochers, M. Blanchard and S. Sud, "A Monte-Carlo simulation method for the economic assessment of the contribution of wind energy to power systems," *IEEE Trans. Energy Conversion*, pp. 50-56, 1986.

[23] M. G. Ippolito, F. Massaro and M. Mustacciolo, "Application of monte carlo technique to evaluate the power injectable on electrical grid by wind farms," in *Universities Power Engineering Conference, 2008, UPEC 43rd International*, 2008, pp. 1-5.

[24] W. Li, *Reliability Assessment of Electrical Power Systems using Monte Carlo Methods*. Springer, 1994.

[25] R. E. Brown and L. Freeman, "Analyzing the reliability impact of distributed generation," in *Power Engineering Society Summer Meeting, 2001*, 2001, pp. 1013-1018.

[26] R. E. Brown, J. Pan, X. Feng and K. Koutlev, "Siting distributed generation to defer T&D expansion," in *Transmission and Distribution Conference and Exposition, 2001 IEEE/PES*, 2001, pp. 622-627.

[27] P. Chiradeja and R. Ramakumar, "An approach to quantify the technical benefits of distributed generation," *IEEE Trans. Energy Conversion*, vol. 19, pp. 764-773, 2004.

[28] H. A. Gil and G. Joos, "Models for quantifying the economic benefits of distributed generation," *IEEE Trans. Power Syst.*, vol. 23, pp. 327-335, 2008.

[29] A. Alarcon-Rodriguez, G. Ault and S. Galloway, "Multi-objective planning of distributed energy resources: A review of the state-of-the-art," *Renewable and Sustainable Energy Reviews*, vol. 14, pp. 1353-1366, 2010.

[30] H. A. Gil and G. Joos, "On the quantification of the network capacity deferral value of distributed generation," *IEEE Trans. Power Syst.*, vol. 21, pp. 1592-1599, 2006.

[31] G. Pudaruth and F. Li, "Costs and benefits assessment considering deferral of assets expansion in distribution systems," in *Universities Power Engineering Conference, UPEC 42nd International*, 2007, pp. 872-878.

[32] Y. Zhang, C. Gu and F. Li, "Evaluation of investment deferral resulting from microgeneration for EHV distribution networks," in *Power and Energy Society General Meeting*, 2010 IEEE, 2010, pp. 1-5.

[33] G. Celli and F. Pilo, "Optimal distributed generation allocation in MV distribution networks," in *22nd IEEE Power Engineering Society International Conference on Power Industry Computer Applications*, , 2001, pp. 81-86.

[34] D. Wang, L. F. Ochoa and G. P. Harrison, "DG impact on investment deferral: network planning and security of supply," *IEEE Trans. Power Syst.*, vol. 25, pp. 1134-1141, 2010.

[35] G. Celli, S. Mocci, F. Pilo and G. Soma, "A multi-objective approach for the optimal distributed generation allocation with environmental constraints," in, *Proceedings of the 10th International Conference on Probabilistic Methods Applied to Power Systems, PMAPS'08*, 2008, pp. 1-8.

[36] H. Khan and M. A. Choudhry, "Implementation of Distributed Generation (IDG) algorithm for performance enhancement of distribution feeder under extreme load growth," *International Journal of Electrical Power & Energy Systems*, vol. 32, pp. 985-997, 2010.

[37] M. Kashem, A. D. Le, M. Negnevitsky and G. Ledwich, "Distributed generation for minimization of power losses in distribution systems," in *IEEE Power Engineering Society General Meeting*, 2006, pp. 8 pp.

[38] D. Q. Hung, N. Mithulananthan and R. Bansal, "Analytical expressions for DG allocation in primary distribution networks," *IEEE Trans. Energy Conversion*, vol. 25, pp. 814-820, 2010.

[39] A. Abou El-Ela, S. Allam and M. Shatla, "Maximal optimal benefits of distributed generation using genetic algorithms," *Electr. Power Syst. Res.*, vol. 80, pp. 869-877, 2010.

[40] W. El-Khattam, K. Bhattacharya, Y. Hegazy and M. Salama, "Optimal investment planning for distributed generation in a competitive electricity market," *IEEE Trans. Power Syst.*, vol. 19, pp. 1674-1684, 2004.

[41] F. S. Abu-Mouti and M. El-Hawary, "Optimal distributed generation allocation and sizing in distribution systems via artificial bee colony algorithm," *IEEE Trans. on Power Delivery*, vol. 26, pp. 2090-2101, 2011.

[42] L. F. Ochoa, A. Padilha-Feltrin and G. P. Harrison, "Evaluating distributed generation impacts with a multiobjective index," *IEEE Trans. on Power Delivery*, vol. 21, pp. 1452-1458, 2006.

[43] V. M. Quezada, J. R. Abbad and T. G. S. Roman, "Assessment of energy distribution losses for increasing penetration of distributed generation," *IEEE Trans. Power Syst.*, vol. 21, pp. 533-540, 2006.

[44] L. F. Ochoa and G. P. Harrison, "Minimizing energy losses: Optimal accommodation and smart operation of renewable distributed generation," *IEEE Trans. Power Syst.*, vol. 26, pp. 198-205, 2011.

[45] A. Alarcon-Rodriguez, E. Haesen, G. Ault, J. Driesen and R. Belmans, "Multi-objective planning framework for stochastic and controllable distributed energy resources," *IET Renewable Power Generation*, vol. 3, pp. 227-238, 2009.

[46] L. F. Ochoa, A. Padilha-Feltrin and G. P. Harrison, "Time-series-based maximization of distributed wind power generation integration," *IEEE Trans. Energy Conversion*, vol. 23, pp. 968-974, 2008.

[47] G. Celli, E. Ghiani, S. Mocci and F. Pilo, "A multiobjective evolutionary algorithm for the sizing and siting of distributed generation," *IEEE Trans. Power Syst.*, vol. 20, pp. 750-757, 2005.

[48] I. Bae, J. Kim, J. Kim and C. Singh, "Optimal operating strategy for distributed generation considering hourly reliability worth," *IEEE Trans. Power Syst.*, vol. 19, pp. 287-292, 2004.

[49] Y. M. Atwa and E. F. El-Saadany, "Reliability evaluation for distribution system with renewable distributed generation during islanded mode of operation," *IEEE Trans. Power Syst.*, vol. 24, pp. 572-581, 2009.

[50] D. Wu, D. C. Aliprantis and K. Gkritza, "Electric energy and power consumption by light-duty plug-in electric vehicles," *IEEE Trans. Power Syst.*, vol. 26, pp. 738-746, 2011.

[51] U. Eberle and R. von Helmolt, "Sustainable transportation based on electric vehicle concepts: a brief overview," *Energy & Environmental Science*, vol. 3, pp. 689-699, 2010.

[52] EV CANADA. Canadian national campaign for electric vehicles. [Online]. Available: http:// www.evcanada.org/Default.aspx

[53] Government of Ontario. Ontario Paves The Way For Electric Vehicles. [Online]. Available: http:// www.ontario.ca/

[54] White house official website. FACT SHEET: President Obama's plan to make the U.S. the first country to put 1 million advanced technology vehicles on the road. [Online]. Available: http:// www.whitehouse.gov/sites/default/files/other/fact-sheet-one-million-advanced-technology-vehicles.pdf

[55] C. Chan, "The state of the art of electric, hybrid, and fuel cell vehicles," *Proc IEEE*, vol. 95, pp. 704-718, 2007.

[56] Commonwealth Edison Company, "Initial assessment of the impact of the introduction of plug-in electric vehicles on the distribution system," *ILLINOIS COMMERCE COMMISSION*, Tech. Rep., 2010.

[57] Chevrolet. Chevrolet electric vehicle specifications. [Online]. Available: http://www. chevrolet.com

[58] C. Roe, A. Meliopoulos, J. Meisel and T. Overbye, "Power system level impacts of plug-in hybrid electric vehicles using simulation data," in *IEEE Energy 2030 Conference, ENERGY 2008*, 2008, pp. 1-6.

[59] H.L. Busch. ARGONNE National Laboratory, Vehicle to Grid Interaction in the Smart Grid. [Online]. Available:http://www.gaccmidwest.org/fileadmin/ahk_chicago/Dokumente

[60] T. Bohn (Argonne National Laboratory, U.S. Department of Energy), "Codes and standards support for vehicle electrification," 2011 *DOE Hydrogen Program and Vehicle Technologies, Annual Merit Review*, Tech. Rep. Project ID #VSS053, 2011.

[61] W. Su, H. Eichi, W. Zeng and M. Chow, "A survey on the electrification of transportation in a smart grid environment," *IEEE Trans. on Ind. Informat.*, vol. 8, pp. 1-10, 2012.

[62] A. Majumder and J. Caffery Jr, "Power line communications," *IEEE Potentials*, vol. 23, pp. 4-8, 2004.

[63] J. T. Salihi, "Energy requirements for electric cars and their impact on electric power generation and distribution systems," *IEEE Trans. on Ind. Applicat.*, pp. 516-532, 1973.

[64] M. Kintner-Meyer, K. Schneider and R. Pratt, "Impacts assessment of plug-in hybrid vehicles on electric utilities and regional US power grids, Part 1: Technical analysis," *Pacific Northwest National Laboratory* (a), Tech. Rep., 2007.

[65] J. C. Gomez and M. M. Morcos, "Impact of EV battery chargers on the power quality of distribution systems," *IEEE Trans. on Power Delivery*, vol. 18, pp. 975-981, 2003.

[66] S. W. Hadley and A. A. Tsvetkova, "Potential impacts of plug-in hybrid electric vehicles on regional power generation," *The Electricity Journal*, vol. 22, pp. 56-68, 2009.

[67] S. Letendre and R. A. Watts, "Effects of plug-in hybrid electric vehicles on the vermont electric transmission system," in *Transportation Research Board Annual Meeting*, Washington DC, 2009, pp. 11-15.

[68] A. Hajimiragha, C. Caizares, M. W. Fowler and A. Elkamel, "Optimal transition to plug-in hybrid electric vehicles in Ontario, Canada, considering the electricity-grid limitations," *IEEE Trans. on Ind. Electron.*, vol. 57, pp. 690-701, 2010.

[69] P. Denholm and W. Short, "An Evaluation of Utility System Impacts and Benefits of Optimally Dispatched," National Renewable Energy Laboratory, Tech. Rep. NREL/TP-620-40293, 2006.

[70] G. Strbac, C. Gan, M. Aunedi, V. Stanojevic, P. Djapic, J. Dejvises, P. Mancarella, A. Hawkes, D. Pudjianto and S. Le Vine, "Benefits of advanced smart metering for demand response based control of distribution networks," *Summary Report*, Version 2, Tech. Rep., 2010.

[71] K. Qian, C. Zhou, M. Allan and Y. Yuan, "Modeling of load demand due to EV battery charging in distribution systems," *IEEE Trans. Power Syst.*, vol. 26, pp. 802-810, 2011.

[72] J. Wang, C. Liu, D. Ton, Y. Zhou, J. Kim and A. Vyas, "Impact of plug-in hybrid electric vehicles on power systems with demand response and wind power," *Energy Policy*, vol. 39, pp. 4016-4021, 2011.

[73] K. Clement-Nyns, E. Haesen and J. Driesen, "The impact of charging plug-in hybrid electric vehicles on a residential distribution grid," *IEEE Trans. Power Syst.*, vol. 25, pp. 371-380, 2010.

[74] C. Roe, A. Meliopoulos, J. Meisel and T. Overbye, "Power system level impacts of plug-in hybrid electric vehicles using simulation data," in *Energy 2030 Conference, ENERGY 2008, IEEE*, pp. 1-6, 2008.

[75] D. Lemoine, D. Kammen and A. Farrell, "Effects of plug-in hybrid electric vehicles in california energy markets," in *86th Annual Meeting of the Transportation Research Board*, Washington, DC, 2007, .

[76] K. Parks, P. Denholm and A. J. Markel, *Costs and Emissions Associated with Plug-in Hybrid Electric Vehicle Charging in the Xcel Energy Colorado Service Territory*. National Renewable Energy Laboratory Golden, CO, 2007.

[77] J. P. Lopes, F. J. Soares and P. R. Almeida, "Identifying management procedures to deal with connection of electric vehicles in the grid," in *PowerTech, 2009 IEEE Bucharest*, pp. 1-8, 2009.

[78] M. F. Shaaban and E. El-Saadany, "Accommodating High Penetrations of PEVs and Renewable DG Considering Uncertainties in Distribution Systems," *IEEE Trans. Power Syst.*, vol.29, no.1, pp.259,270, Jan. 2014 .

[79] R. A. Verzijlbergh, M. O. Grond, Z. Lukszo, J. G. Slootweg and M. D. Ilic, "Network impacts and cost savings of controlled EV charging," *IEEE Trans. on Smart Grid*, vol. 3, pp. 1203-1212, 2012.

[80] S. Deilami, A. S. Masoum, P. S. Moses and M. A. Masoum, "Real-time coordination of plug-in electric vehicle charging in smart grids to minimize power losses and improve voltage profile," *IEEE Trans. on Smart Grid*, vol. 2, pp. 456-467, 2011.

[81] C. Pang, P. Dutta and M. Kezunovic, "BEVs/PHEVs as dispersed energy storage for V2B uses in the smart grid," *IEEE Trans. on Smart Grid*, vol. 3, pp. 473-482, 2012.

[82] Y. Ota, H. Taniguchi, T. Nakajima, K. M. Liyanage, J. Baba and A. Yokoyama, "Autonomous distributed V2G (vehicle-to-grid) satisfying scheduled charging," *IEEE Trans. on Smart Grid*, vol. 3, pp. 559-564, 2012.

[83] C. Quinn, D. Zimmerle and T. H. Bradley, "An Evaluation of State-of-Charge Limitations and Actuation Signal Energy Content on Plug-in Hybrid Electric Vehicle, Vehicle-to-Grid Reliability, and Economics," *IEEE Trans. on Smart Grid*, vol. 3, pp. 483-491, 2012.

[84] Y. Cao, S. Tang, C. Li, P. Zhang, Y. Tan, Z. Zhang and J. Li, "An optimized EV charging model considering TOU price and SOC curve," *IEEE Trans. on Smart Grid*, vol. 3, pp. 388-393, 2012.

[85] S. Han, S. Han and K. Sezaki, "Estimation of achievable power capacity from plug-in electric vehicles for v2g frequency regulation: Case studies for market participation," *IEEE Trans. on Smart Grid*, vol. 2, pp. 632-641, 2011.

[86] Y. He, B. Venkatesh and L. Guan, "Optimal scheduling for charging and discharging of electric vehicles," *IEEE Trans. on Smart Grid*, vol. 3, pp. 1095-1105, 2012.

[87] R. J. Bessa, M. A. Matos, F. J. Soares and J. A. P. Lopes, "Optimized bidding of a EV aggregation agent in the electricity market," *IEEE Trans. on Smart Grid*, vol. 3, pp. 443-452, 2012.

[88] A. Y. Saber and G. K. Venayagamoorthy, "Intelligent unit commitment with vehicle-to-grid—A cost-emission optimization," *J. Power Sources*, vol. 195, pp. 898-911, 2010.

[89] M. E. Khodayar, L. Wu and M. Shahidehpour, "Hourly coordination of electric vehicle operation and volatile wind power generation in SCUC," *IEEE Trans. on Smart Grid*, vol. 3, pp. 1271-1279, 2012.

[90] C. Liu, J. Wang, A. Botterud, Y. Zhou and A. Vyas, "Assessment of impacts of PHEV charging patterns on wind-thermal scheduling by stochastic unit commitment," *IEEE Trans. on Smart Grid*, vol. 3, pp. 675-683, 2012.

[91] H. Khayyam, J. Abawajy, B. Javadi, A. Goscinski, A. Stojcevski and A. Bab-Hadiashar, "Intelligent battery energy management and control for vehicle-to-grid via cloud computing network," *Appl. Energy*, vol. 111, pp. 971-981, 2013.

[92] M. Singh, K. Thirugnanam, P. Kumar and I. Kar, "Real-Time Coordination of Electric Vehicles to Support the Grid at the Distribution Substation Level," *IEEE Systems Journal*, *to be published*.

[93] K. De Craemer, S. Vandael, B. Claessens and G. Deconinck, "An Event-Driven Dual Coordination Mechanism for Demand Side Management of PHEVs," *IEEE Trans. on Smart Grid*, vol.5, no.2, pp.751,760, March 2014

[94] R. A. Barnitt, A. D. Brooker, L. Ramroth, J. Rugh and K. A. Smith, "Analysis of off-board powered thermal preconditioning in electric drive vehicles," National Renewable Energy Laboratory, *Proc. 25th WorldBattery, Hybrid and Fuel Cell Electric Vehicle Symp. Expo. (EVS-25)*, 2010.

[95] Canadian Electricity Association. [Online]. Available: http://www. electricity.ca.

[96] "IEEE Std. 1547.4", "IEEE Guide for Design, Operation, and Integration of Distributed Resource Island Systems with Electric Power Systems," 2011.

[97] R. Karki and R. Billinton, "Cost-effective wind energy utilization for reliable power supply," *IEEE Trans. Energy Conversion*, vol. 19, pp. 435-440, 2004.

[98] W. El-Khattam, Y. Hegazy and M. Salama, "An integrated distributed generation optimization model for distribution system planning," IEEE Trans. Power Syst., vol. 20, pp. 1158-1165, 2005.

[99] Royal Netherlands meteorological institute. Potential wind in Netherlands. [Online]. Available: http://www.knmi.nl /klimatologie /onderzoeksgegevens /potentiele_wind/.

[100] J. Hetzer, D. C. Yu and K. Bhattarai, "An economic dispatch model incorporating wind power," *IEEE Trans. Energy Conversion*, vol. 23, pp. 603-611, 2008.

[101] World meteorological organization (Geneva). *Guide to meterological instruments and methods of observation*. Secretariat of the World Meteorological Organization, 1996.

[102] M. F. Shaaban, Y. M. Atwa and E. F. El-Saadany, "DG allocation for benefit maximization in distribution networks," *IEEE Trans. Power Syst.*, vol.28, no.2, pp.639,649, May 2013

[103] C. Singh and Y. Kim, "An efficient technique for reliability analysis of power systems including time dependent sources," *IEEE Trans. Power Syst.*, vol. 3, pp. 1090-1096, 1988.

[104] Vestas. V80-2.0 MW: Technical specifications. [Online]. Available: http://www.vestas.com/en/

[105] C. Grigg, P. Wong, P. Albrecht, R. Allan, M. Bhavaraju, R. Billinton, Q. Chen, C. Fong, S. Haddad and S. Kuruganty, "The IEEE reliability test system-1996. A report prepared by the reliability test system task force of the application of probability methods subcommittee," *IEEE Trans. Power Syst.*, vol. 14, pp. 1010-1020, 1999.

[106] G. M. Masters, *Renewable and Efficient Electric Power Systems*. John Wiley & Sons, 2005.

[107] Ontario Independent Electricity System Operator (IESO). [Online]. Available: http://www.ieso.ca.

[108] G. Tollefson, R. Billinton, G. Wacker, E. Chan and J. Aweya, "A Canadian customer survey to assess power system reliability worth," *IEEE Trans. Power Syst.*, vol. 9, pp. 443-450, 1994.

[109] Y. Attwa and E. El-Saadany, "Reliability based analysis for optimum allocation of DG," in *Electrical Power Conference, EPC 2007, IEEE Canada*, 2007, pp. 25-30.

[110] HydroOne. Technical DG interconnection requirements of HydroOne. [Online]. Available: http://www.hydroone.com.

[111] S. A. Kazarlis, A. Bakirtzis and V. Petridis, "A genetic algorithm solution to the unit commitment problem," *IEEE Trans. Power Syst.*, vol. 11, pp. 83-92, 1996.

[112] C. Chiang, "Genetic-based algorithm for power economic load dispatch," *IET Generation, Transmission & Distribution*, vol. 1, pp. 261-269, 2007.

[113] D. Singh and R. Misra, "Effect of load models in distributed generation planning," *IEEE Trans. Power Syst.*, vol. 22, pp. 2204-2212, 2007.

[114] Bank of Canada. [Online]. Available: http://www.bankofcanada.ca/rates/.

[115] S. W. Hadley and A. A. Tsvetkova, "Potential impacts of plug-in hybrid electric vehicles on regional power generation," *The Electricity Journal*, vol. 22, pp. 56-68, 2009.

[116] P. Richardson, D. Flynn and A. Keane, "Impact assessment of varying penetrations of electric vehicles on low voltage distribution systems," in *Proc. IEEE Power and Energy Society General Meeting*, 2010, pp. 1-6.

[117] G. Putrus, P. Suwanapingkarl, D. Johnston, E. Bentley and M. Narayana, "Impact of electric vehicles on power distribution networks," in *IEEE Vehicle Power and Propulsion Conference, VPPC'09*, pp. 827-831.

[118] I. Sharma, C. A. Cañizares and K. Bhattacharya, "Modeling and impacts of smart charging PEVs in residential distribution systems," in *2012 IEEE Power and Energy Society General Meeting*, , 2012, pp. 1-8.

[119] V. Monteiro, H. Gonçalves, J. C. Ferreira and J. L. Afonso, "Batteries charging systems for electric and plug-in hybrid electric vehicles," 2012.

[120] S. J. Prince, *Computer Vision: Models, Learning, and Inference*. Cambridge University Press, 2012.

[121] Z. Darabi and M. Ferdowsi, "Aggregated impact of plug-in hybrid electric vehicles on electricity demand profile," *IEEE Trans. on Sustainable Energy*, vol. 2, pp. 501-508, 2011.

[122] P. Richardson, D. Flynn and A. Keane, "Optimal charging of electric vehicles in low-voltage distribution systems," *IEEE Trans. on Power System*,, vol. 27, pp. 268-279, 2012.

[123] Department of Transportation, "National travel survey," London, United Kingdom, Tech. Rep., 2009.

[124] National Household Travel Survey, "Summary of travel trends: 2009," U.S. Department of Transportation, Tech. Rep., 2010.

[125] M. Uzunoglu and M. Alam, "Dynamic modeling, design, and simulation of a combined PEM fuel cell and ultracapacitor system for stand-alone residential applications," *IEEE Trans. Energy Conversion*, vol. 21, pp. 767-775, 2006.

[126] P. Subcommittee, "IEEE reliability test system," *IEEE Trans. on Power App. and Syst.*, pp. 2047-2054, 1979.

[127] S. Deilami, A. S. Masoum, P. S. Moses and M. A. Masoum, "Real-time coordination of plug-in electric vehicle charging in smart grids to minimize power losses and improve voltage profile," *IEEE Trans. on Smart Grid*, vol. 2, pp. 456-467, 2011.

[128] E. Sortomme, M. M. Hindi, S. J. MacPherson and S. Venkata, "Coordinated charging of plug-in hybrid electric vehicles to minimize distribution system losses," *IEEE Trans. on Smart Grid*, vol. 2, pp. 198-205, 2011.

[129] J. Koski, "Defectiveness of weighting method in multicriterion optimization of structures," *Communications in Applied Numerical Methods*, vol. 1, pp. 333-337, 1985.

[130] C. A. C. Coello, D. A. Van Veldhuizen and G. B. Lamont, *Evolutionary Algorithms for Solving Multi-Objective Problems*. Springer, 2002.

[131] R. T. Marler and J. S. Arora, "Survey of multi-objective optimization methods for engineering," *Structural and Multidisciplinary Optimization*, vol. 26, pp. 369-395, 2004.

[132] Z. M. Salameh, B. S. Borowy and A. R. Amin, "Photovoltaic module-site matching based on the capacity factors," *IEEE Trans. Energy Conversion*, vol. 10, pp. 326-332, 1995.

[133] C. A. Coello Coello, "Evolutionary multi-objective optimization: a historical view of the field," *IEEE Computational Intelligence Magazine*, vol. 1, pp. 28-36, 2006.

[134] K. Deb, A. Pratap, S. Agarwal and T. Meyarivan, "A fast and elitist multiobjective genetic algorithm: NSGA-II," *IEEE Trans. on Evol. Comput.*, vol. 6, pp. 182-197, 2002.

[135] Ontario Power Generation, "Sustainable development report," Toronto, Ontario, Tech. Rep., 2010.

[136] A. Zangeneh, S. Jadid and A. Rahimi-Kian, "A hierarchical decision making model for the prioritization of distributed generation technologies: A case study for Iran," *Energy Policy*, vol. 37, pp. 5752-5763, 2009.

[137] A. Y. Saber and G. K. Venayagamoorthy, "Plug-in vehicles and renewable energy sources for cost and emission reductions," *IEEE Trans. on Ind. Electron.*, vol. 58, pp. 1229-1238, 2011.

[138] H. Eschenauer, J. Koski, E. Osyczka, Eds., *Multicriteria Design Optimization: Procedures and Applications*. Berlin, Germany: Springer-Verlag, 1990.

[139] M. F. Shaaban, Muhammad Ismail, E. F. El-Saadany, Weihua Zhuang, "Real-Time PEV Charging/Discharging Coordination in Smart Distribution Systems," *IEEE Trans. on Smart Grid*, to be published, 2014.

[140] I. Moghram and S. Rahman, "Analysis and evaluation of five short-term load forecasting techniques," *IEEE Trans. Power Syst.*, vol. 4, pp. 1484-1491, 1989.

[141] D. Gross, J. Shortle, J. Thompson and C. Harris, *Fundamentals of Queueing Theory*. 4th Edition, John Wiley & Sons, 2008.

[142] M. Mandjes and P. Zuraniewski, "M/G/infinity transience, and its applications to overload detection," *Centrum Wiskunde & Informatica (CWI) Probability, Networks and Algorithms [PNA]*, pp. 1-22, 2009.

[143] Ontario energy board. Distribution system code. [Online]. Available: http://www.ontarioenergyboard.ca/OEB / Documents/Regulatory/ Distribution System Code.pdf

[144] T. Logenthiran, D. Srinivasan and T. Z. Shun, "Demand side management in smart grid using heuristic optimization," *IEEE Trans. on Smart Grid*, vol. 3, pp. 1244-1252, 2012.

[145] E. Lopez, H. Opazo, L. Garcia and P. Bastard, "Online reconfiguration considering variability demand: Applications to real networks," *IEEE Trans. Power Syst.*, vol. 19, pp. 549-553, 2004.

[146] HydroOne. Delivery Rates. [Online]. Available: http://www.hydroone.com/RegulatoryAffairs/ RatesPrices/ Pages/SmallBusinessDeliveryRates.aspx.

[147] F. Marra, G. Y. Yang, C. Traholt, E. Larsen, C. N. Rasmussen and S. You, "Demand profile study of battery electric vehicle under different charging options," in *2012 IEEE Power and Energy Society General Meeting*, 2012, pp. 1-7.

[148] J. Huang, V. Gupta and Y. Huang, "Scheduling algorithms for PHEV charging in shared parking lots," in *American Control Conference (ACC) 2012*, 2012, pp. 276-281.